The Role of ASC Specks as Essential Cofactor in Amyloid β-induced Pathophysiology

Doctoral thesis

to obtain a doctorate

from the Faculty of Medicine

of the University of Bonn

Katharina Olivia Schuler

from Mainz

2024

Written with authorization of

the Faculty of Medicine of the University of Bonn

First reviewer: Prof. Dr. med. Michael T. Heneka

Second reviewer: Prof. Dr. Matthias Geyer

Day of oral examination: 21.08.2024

From the Klinik für Neurodegenerative Erkrankungen und Gerontopsychiatrie Bonn

Director: Prof. Dr. med. Michael T. Heneka

Table of Contents

List of Abbreviations

Aβ	Amyloid β
$Aβ_{1-42}$	42-aminoacid form of Amyloid β
AD	Alzheimer's Disease
AEBSF	4-(2-aminoethyl)benzenesulfonyl fluoride hydrochloride
ANOVA	Analysis of variance
APP	Amyloid precursor protein
APP/PS1$^{wt/tg}$	AD mouse model genotype, (B6.CgTg(APPswe,PSEN1dE9) 85Dbo/Mmjaxmice)
APP/PS1$^{wt/tg}$;ASC$^{-/-}$	Genotype of AD mice crossed with ASC-deficient mice
approx.	Approximately
ASC	Apoptosis-associated speck-like protein containing a CARD
α6β1 integrin	Cell surface receptor on platelets, leukocytes, epithelial cells triggering different signal transduction pathways
BACE1	β-site APP cleaving enzyme 1
BCA	Bicinchoninic acid
BDNF	Brain-derived neurotrophic factor
Bis	Bisamino-trismethan
BSA	Bovine serum albumin
C	Celsius
CA	Cornu ammonis
cDNA	Complementary deoxyribonucleic acid
CD	Cluster of Differentiation
cf.	Confer
CI	Confidence interval
Co-IP	Co-Immunoprecipitation

DAMP	Danger-associated molecular pattern
DAPI	4′,6-diamidino-2-phenylindole
DNA	Deoxyribonucleic acid
E. coli	*Escherichia coli*
e.g.	Example given
EtOH	Ethanol
ε	Extinction coefficient
Fig.	Figure
G	Gauge
g	Gravity
GmbH	Gesellschaft mit beschränkter Haftung
GSDMD	Gasdermin D
h	Hour
HFIP	1,1,1,3,3,3-hexafluoro-2-propanol
H_2O_2	Hydrogen peroxide
IB	Immunoblot
Iba-1	Ionized calcium-binding adaptor molecule 1
i.e.	Id est, that is
IHC	Immunohistochemistry
IL-1β and IL-18	Interleukin 1 β and interleukin 18
Ig	Immunglobulin
i.p.	intraperitoneal
IP	Immunoprecipitation
l	Liter
kDa	Kilo Dalton
kg	Kilogramme

LANUV NRW	Landesamt für Natur, Umwelt und Verbraucherschutz Nordrhein-Westfalen
mA	Milliampere
MES	2-(N-morpholino)ethanesulfonic acid
MetOH	Methanol
mg	Milligram
min	Minute
ml	Milliliter
mM	Millimole
µg	Microgram
µl	Microliter
µm	Micrometer
NaCl	Sodium chloride
NaF	Sodium fluoride
NaVO3	Sodium metavanadate
NFκB	Nuclear factor kappa B, signal transduction pathway
NLR/NOD-like-receptor	Nucleotide-binding and oligomerization domain-like receptor
NLRP3	NACHT-, LRR-, and pyrin domain (PYD)-containing protein 3
NP-40	Nonoxinol 40
ns	Not significant
N-terminus	Amino-terminus
OD_{600}	Optical density at a wavelength of 600 nm
p	P-value of statistical probability
PAMP	Pathogen-associated molecular pattern
PBS	Phosphate-buffered saline
PBS-T	PBS + Tween

PCR	Polymerase chain reaction
PRR	Pattern recognition receptors
PSEN1 / PSEN2	Presenilin 1 / 2
px	Pixel
Pycard	PYD and CARD domain containing
RawIntDen	Raw integrated intensity
ROS	Reactive oxygen species
RT	Room temperature
R^2	Coefficient of determination
s. c.	Subcutaneous
sec	Second
SEM	Standard error of the mean
shRNA	Short hairpin ribonucleic acid
TBS	Tris-buffered saline
Tab.	Table
TEV	Tobacco Etch Virus
TLR	Toll-like-receptor
TNFα	Tumor Necrosis Factor α
Tris	Trishydroxymethylaminomethan
TVA	Tierversuchsantrag
V	Volt
W	Watt
2^{nd}	Second
%	Percent

1. Introduction

1.1 Alzheimer's Disease

Due to the demographic ageing of most developed societies neurodegenerative diseases, particularly Alzheimer's Disease (AD), are becoming increasingly prevalent. Despite its clinical and societal importance and decades of intense research, the underlying pathogenesis of AD still is poorly understood and there is still no curative treatment. Based on novel findings from basic and clinical research the perception of classical Alzheimer's disease (AD) has evolved throughout recent years. In more than 95% of all cases AD occurs sporadically, while the remaining cases can be attributed to inherited autosomal dominant mutations affecting the genes *APP*, *PSEN1* or *PSEN2* (Reitz und Mayeux, 2014). The onset of clinical symptoms follows certain patterns, in which the trajectories of tau and Aβ aggregate spreading differ dramatically and thus characterize different subtypes (Vogel et al., 2021). It is proposed that histopathological changes in the brain tissue can be detected decades before the onset of clinical symptoms (Braak et al., 2011). Central to the clinical manifestation of AD is a progressive loss of memory function in addition to non-cognitive symptoms. In early stages of AD, short-term memory is impaired, concentration incapacity and time- and place-related disorientation develop. Throughout this stage, AD patients are able to conceal their loss of brain function surprisingly well keeping a proper "facade". Typical non-cognitive manifestations of AD include hyposmia, depressive symptoms, loss of activity and general motivation. With the progression of AD, the replicability of long-term memory deteriorates, coming along with situative and person-related disorientation, semantic paraphrasing, apraxia, alexia, agnosia, acalculia and "logopenic aphasia". Productive ("positive") manifestations of advanced AD can be activation of primitive reflexes, hyperreflexia, hyperactivity, delusion and hallucinations. "Negative" symptoms include Parkinson's syndrome, apathy and mutism. Commonly, the sleep-wake rhythm as well as urinal and fecal continence are impaired (Soria Lopez et al., 2019; 231–255). The progressive loss of independency over time leads to total care dependency. Most end stage AD patients succumb to infections (Ryman et al., 2014). Concluding, AD usually is not a rapidly lethal disease. However, the cognitive dying causes utterly devastating morbidity, which occurs many years before the biological death of the patient.

The underlying pathophysiology of all clinical symptoms of AD is a complex synopsis of brain atrophy, extracellular amyloid plaques, neurofibrillary tau aggregates and inflammatory processes.

1.2 Brain Atrophy in Alzheimer's Disease

Atrophy of grey and white brain matter occurs during progression of AD, which follows typical trajectories. The shrinking of the hippocampal area is the most characteristic feature, which correlates best with the clinical presentation of the disease stage. It is coming along with atrophy of additional brain regions, such as the amygdala, entorhinal, inferior parietal and medial temporal thickness. An enlargement of the volume of the inferior lateral ventricle is also characteristic (Koenig et al., 2020). Most of these (sub-) cortical structures affected in AD are directly linked to hippocampal functioning. Normal brain aging as well comprises white matter lesions. However, these have far lower levels of impact on cognitive functioning than the cognitive decline observed in AD caused by neurodegeneration (Pini et al., 2016).

1.3 Amyloid β in Alzheimer's Disease

Neurodegeneration in AD is accompanied by extracellular aggregates of amyloid β (Aβ). Aβ is a product of cleavage of the amyloid precursor membrane protein (APP) by aspartate proteases: β-site APP cleaving enzyme 1 (BACE1) and the γ-secretase complex, including among others presenilin 1 and 2 (Fig. 1). The composition of the C-terminal end of the Aβ cleavage products determines the likelihood to form complexes such as monomers, dimers, oligomers, protofibrils and fibrils. Particularly the 42-amino acid form ($A\beta_{1-42}$) assembles to larger compounds. The largest form of these compounds is called senile or amyloid plaques. In any aggregation form amyloid binds to microglial cell surface receptors (e.g. Toll-like-receptors) to induce an inflammatory reaction of the innate immune system. Ongoing inflammation enhances the output of Aβ and thus enters a vicious cycle (Heneka et al., 2015).

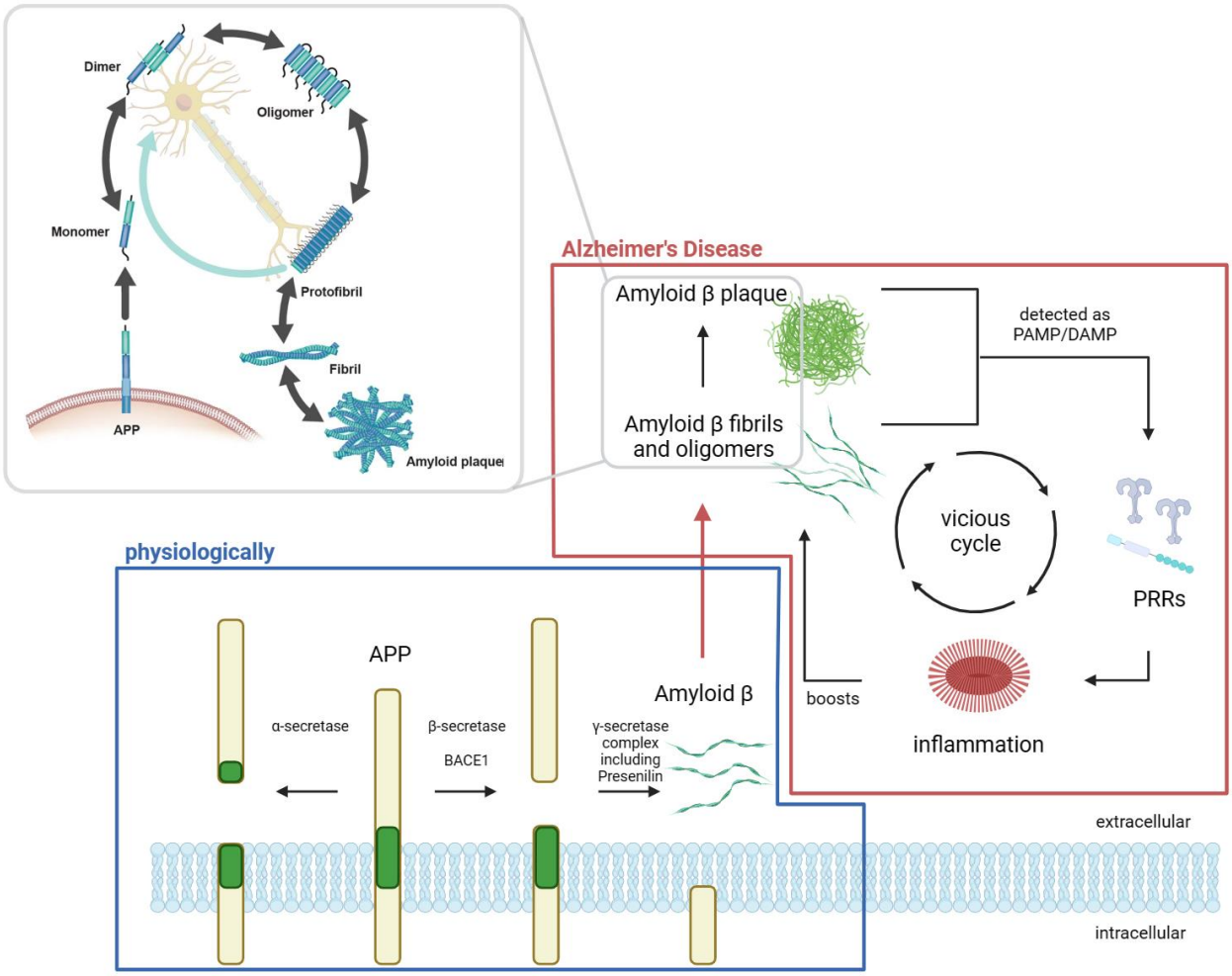

Fig. 1: Amyloid β Development. Physiologically (blue frame), amyloid precursor protein (APP), a transmembrane protein, is cleaved by different proteases. The α-secretase produces neuroprotective proteins, whereas cleavage by the β-side cleaving enzyme 1 (BACE1) and by γ-secretases presenilin 1 and 2 results in neurotoxic amyloid β (Aβ). In Alzheimer's disease (AD, red frame) the Aβ fibers cluster to form oligomers, fibrils and finally plaques. In detail (Hampel et al., 2021), Aβ peptides are first secreted as monomers, form dimers and oligomers afterwards, then up to protofibrils, fibrils and plaques. Any amyloid formation is reversible, meaning that a plaque can go back to a dimer or any other developmental stage spontaneously. All these amyloid aggregations are detected as pathogen-associated molecular patterns (PAMPs) and host-derived danger-associated molecular patterns (DAMPs) by microglial pattern recognition receptors (PRRs). Consequently, an inflammatory reaction is induced, which reinforces the assembly of Aβ fibrils to plaques. This vicious cycle maintains constant neuroinflammation in AD. Stages of amyloid plaque development in grey frame adopted (Hampel et al., 2021), the rest of the figure was created with BioRender.com

1.4 Tau in Alzheimer's Disease

AD belongs to the disease group of tauopathies, which come along with aberrantly hyperphosphorylated intracellular tau protein, which assembles into neurofibrillary tangles (Ye et al., 2017; Ising et al., 2019). Physiologically, tau is localized in neuronal axons where it contributes to the assembly of microtubules, stabilizes axons and regulates the microtubular transport. Upon hyperphosphorylation tau moves to the neuronal cell body together with additional AD-typical proteins (Dickson et al., 2021). Cognitively normal people also develop tau assemblies with increasing age. There is evidence that Aβ aggregation is a prerequisite for the spreading of tau pathology. The amount of tau accumulation rather than the amount of Aβ accumulation corresponds with the clinical disease presentation of AD (Long und Holtzman, 2019).

1.5 Microglia

Microglial cells represent the major part of the innate immune system in the central nervous system (CNS). Physiologically, these immune cells are motile within their designated brain areas, which they survey for pathogens or cellular debris. In addition, the microglia produce factors necessary for the preservation of the tissue homeostasis (e.g. brain-derived neurotrophic factor (BDNF)), the protection and remodelling of synapses and thus neuronal plasticity. Once microglial cells detect cell death, protein aggregates or pathogens, they cluster around the pathogen/aggregate and mount an innate immune response (Fig. 2). Recent studies suggest a pivotal role of neuroinflammation in AD pathophysiology (Labzin et al., 2018). Physiologically, Aβ and tau are constantly produced and degraded by brain-resident microglia. Once this homeostasis is disturbed towards amyloid accumulation, it leads to neurodegeneration with devastating consequences (Sarlus und Heneka, 2017). At a molecular level this is triggered by pathogen-associated molecular patterns (PAMPs) and host-derived danger-associated molecular patterns (DAMPs), which interact with extracellular pattern recognition receptors (PRRs) expressed by microglial cells leading to signal transduction and activation of inflammatory pathways. Subsequently, the formation of supramolecular complexes called inflammasomes is initiated. The NACHT-, LRR-, and pyrin domain (PYD)-containing

protein 3 (NLRP3) inflammasome complex is formed by NLRP3, caspase-1 and apoptosis-associated speck-like protein containing a CARD (ASC protein).

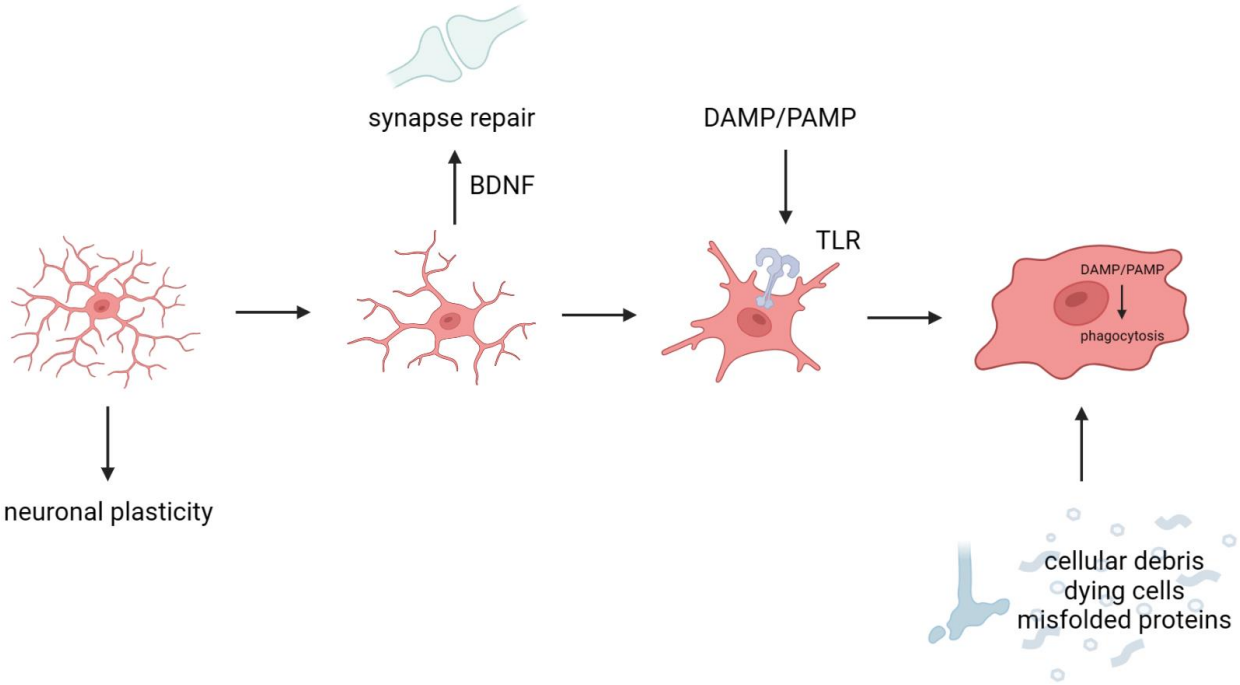

Fig. 2: Functionalities of Microglia. Under physiological conditions, microglia have a surveying role and preserve homeostasis of the brain tissue. In their resting state, which is morphologically characterized by wide-spreading branches, microglia produce brain-derived neurotrophic factor (BDNF), contribute to synapse repair and neuronal plasticity. Furthermore, they also dispose cellular debris, dying cells or misfolded proteins. Once microglia detect danger signals (DAMP/PAMP) through their pattern recognition receptors (PRR), e.g. Toll-like receptor (TLR), they transform into an ameboid cell state and phagocytose the intruder or debris. Figure created with BioRender.com

1.6 NLRP3 Inflammasome

In AD, oligomeric or fibrillar Aβ, among others, are identified by microglial cells as PAMPs and DAMPs. The relevant PRRs comprise Toll-like receptors (TLR2, TLR4, TLR6, TLR9), CD36, CD47, CD14, scavenger receptor A1, α6β1 integrin, and nucleotide-binding and oligomerization domain-like receptors (NOD-like-receptors). Ligand-binding of these receptors triggers intramicroglial signal transduction cascades (Heneka et al., 2015; Castro-Gomez et al., 2019). Since NOD-like-receptors (NLRs) are located in the cytosol, DAMPs and PAMPs also have to penetrate the microglial cells in order to bind to the N-termini of NLRs. Combined with a pyrin domain the NLRs form NACHT-, LRR-, and pyrin

domain (PYD)-containing protein 3 (NLRP3), which is essential for the development of AD pathophysiology. NLRP3 is central to the formation of supramolecular complexes called inflammasomes, which activate signalling events. The NLRP3 inflammasome of AD is composed of NLRP3, the Apoptosis-associated speck-like protein containing a CARD (ASC), and pro-caspase-1. Activation of this inflammasome complex requires two steps: priming and licensing (Fig. 3). In the priming step, extracellular microglial TLRs recognize PAMPs or DAMPs, such as Aβ aggregates. This induces nuclear factor kappa B (NFκB)-mediated intracellular signalling which stimulates transcription of inflammasome-related components, including inactive NLRP3, pro-IL-1β and pro-IL-18. Secondly, the inflammasome assembles by oligomerization of NLRP3 with ASC protein and procaspase-1 to form the active NLRP3 inflammasome complex. In this complex procaspase-1 is activated by cleavage to caspase-1, which induces the conversion of proinflammatory cytokines such as IL-1β and IL-18 into their active forms (Venegas et al., 2017; Shao et al., 2015). Other NLRPs contain a CARD domain themselves. Therefore, they are able to directly induce activation of caspase-1 and pro-inflammatory cytokines. NLRP3, however, requires ASC protein (containing a CARD domain) as co-factor to recruit procaspase-1 into the inflammasome resulting in the activation of inflammatory cytokines. Additional triggers of formation of the NLRP3 inflammasome include reactive oxygen species (ROS), destabilized ionic concentrations, mitochondrial damage, and phagocytosis of abnormal proteins. Activated microglia are characterized by such generation of pro-inflammatory cytokines like IL-1β, IL-18 and TNFα (Tejera et al., 2019). The result of active microglia is pyroptosis, a lytic form of cell death, and the alerting of the environment to pathogens. When pro-caspase-1 is autocatalytically cleaved in the inflammasome complex, mature caspase-1 and gasdermin D (GSDMD) are formed. The N-terminus of cleaved GSDMD oligomerizes after phospholipid-binding to fuse with the cell membrane. This opens a membrane pore channel resulting in the efflux of inflammatory factors and additional cellular contents into the extracellular space, cell swelling due to influx of water and ultimately bursting. $A\beta_{1-42}$ alone is not sufficient to induce pyroptosis. Caspases and GSDMD are essential cofactors (Han et al., 2020).

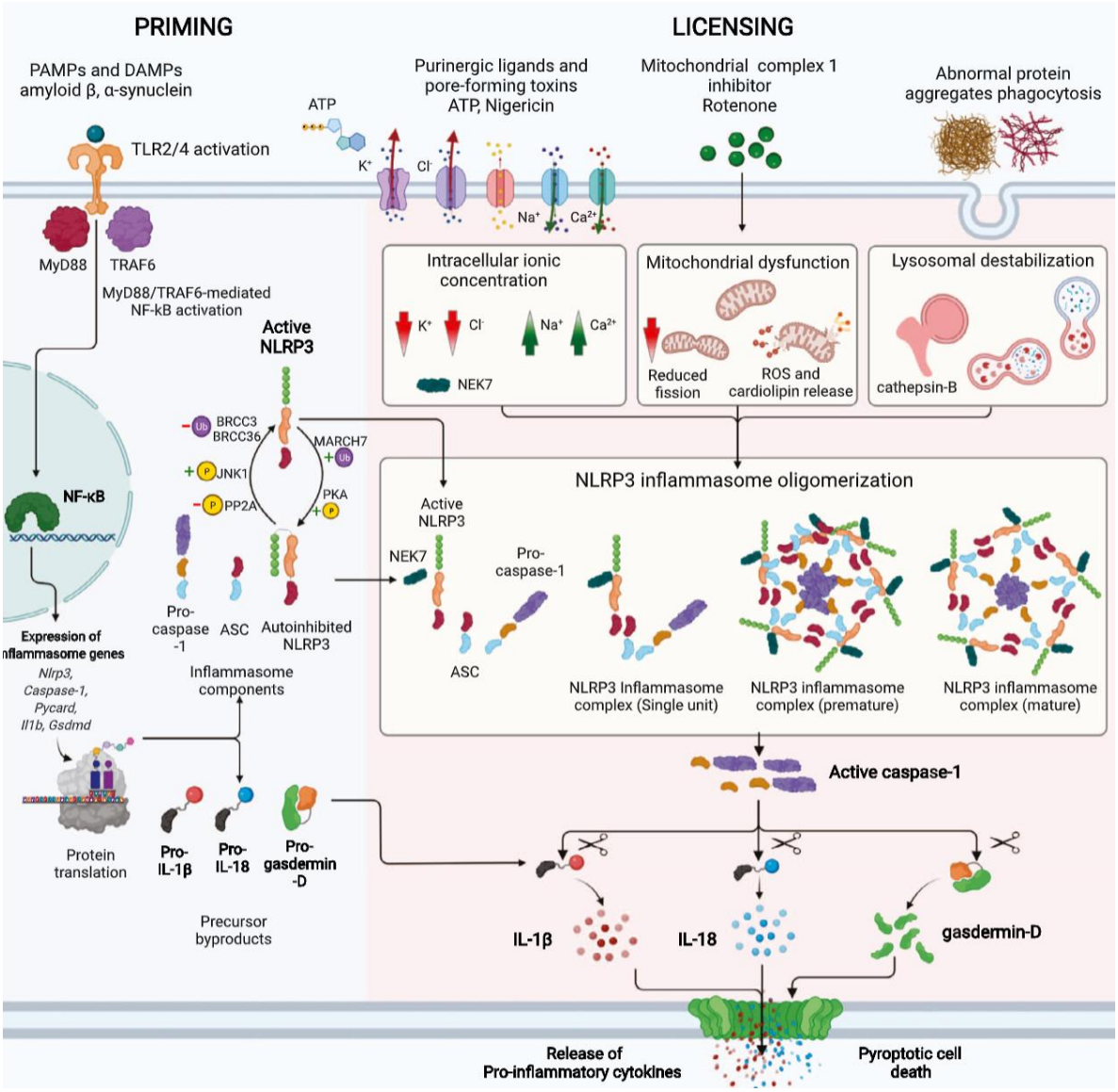

Fig. 3 (Ravichandran und Heneka, 2023): Formation of Active NLRP3 Inflammasome. Aβ aggregates, among others, serve as pathogen-associated molecular patterns (PAMPs) and host-derived danger-associated molecular patterns (DAMPs) leading to activation of the microglia. Firstly, pattern recognition receptors (PRRs), such as Toll-like receptors (TLR), interact with DAMPs/PAMPS, triggering NFκB-mediated signal transduction that leads to the transcriptional upregulation of NLRP3, caspase-1, gasdermin-D, etc. Protein translation then results in production of the inflammasome components pro-caspase-1, ASC and inactive NLRP3 with pro-IL1β, pro-IL18 and pro-gasdermin-D as by-products. The inflammasome components assembly to oligomerize into active NLRP3 inflammasome. Oligomerization is initiated by instable intracellular ionic concentrations, mitochondrial dysfunction or lysosomal destabilization. These instabilities are caused by toxins, cell inhibitors or phagocytosis of abnormal proteins. The active inflammasome facilitates maturation of IL1β, IL18 and gasdermin-D from their inactive forms through activating cleavage of pro-caspase-1 into caspase-1. This triggers the release of pro-inflammatory cytokines and pyroptosis, a lytic form of cell death.

1.7 Apoptosis-associated Speck-like Protein Containing a CARD (ASC)

NLRP3 serves as “molecular sensor” (Ravichandran und Heneka, 2021) of microglial cells. On the one side, NLRP3 promotes the onset and progression of various inflammatory states and diseases as described above. On the other side, NLRP3 protects the brain from aberrant patterns (Fusco et al., 2020; Kelley et al., 2019). This multifunctionality is based on complex molecular mechanisms of activating, deactivating and regulating the NLRP3 inflammasome, which depends on co-factors. ASC is one of these essential co-factors, serving as an adaptor for recruitment of pro-caspase-1 into the inflammasome, in which it matures into its activated, pro-inflammatory cytokine-activating state. The ASC protein contains a PYD-domain on the N-terminus and a CARD domain on the C-terminus, which are linked by 23 amino acids. The PYD and CARD domains belong to the death-fold superfamily containing six helices. Based on this structure, ASC assembles into various molecular structures via different interacting mechanisms including homotypic interactions. Once the NLRP3 inflammasome is activated, ASC proteins quickly assemble into aggregates with caspase-1 and NLRP3 called ASC specks (Hochheiser et al., 2022), which propagate the ongoing innate immune response to the neighbouring environment. ASC specks can be found intracellularly in microglia as well as extracellularly attached to Aβ. The generation of ASC specks involves ASC protein as well as caspase-1, which are both constituents of the NLRP3 inflammasome (Fig. 4). ASC specks thus serve as co-activators in terms of promoting and maintaining the pathological inflammatory reaction and aggregation of the pathogenic Aβ fibrils in AD (Sahillioglu et al., 2014). This work aims to put emphasis on the to date highly underestimated ASC as a promising future point of attack in AD treatment.

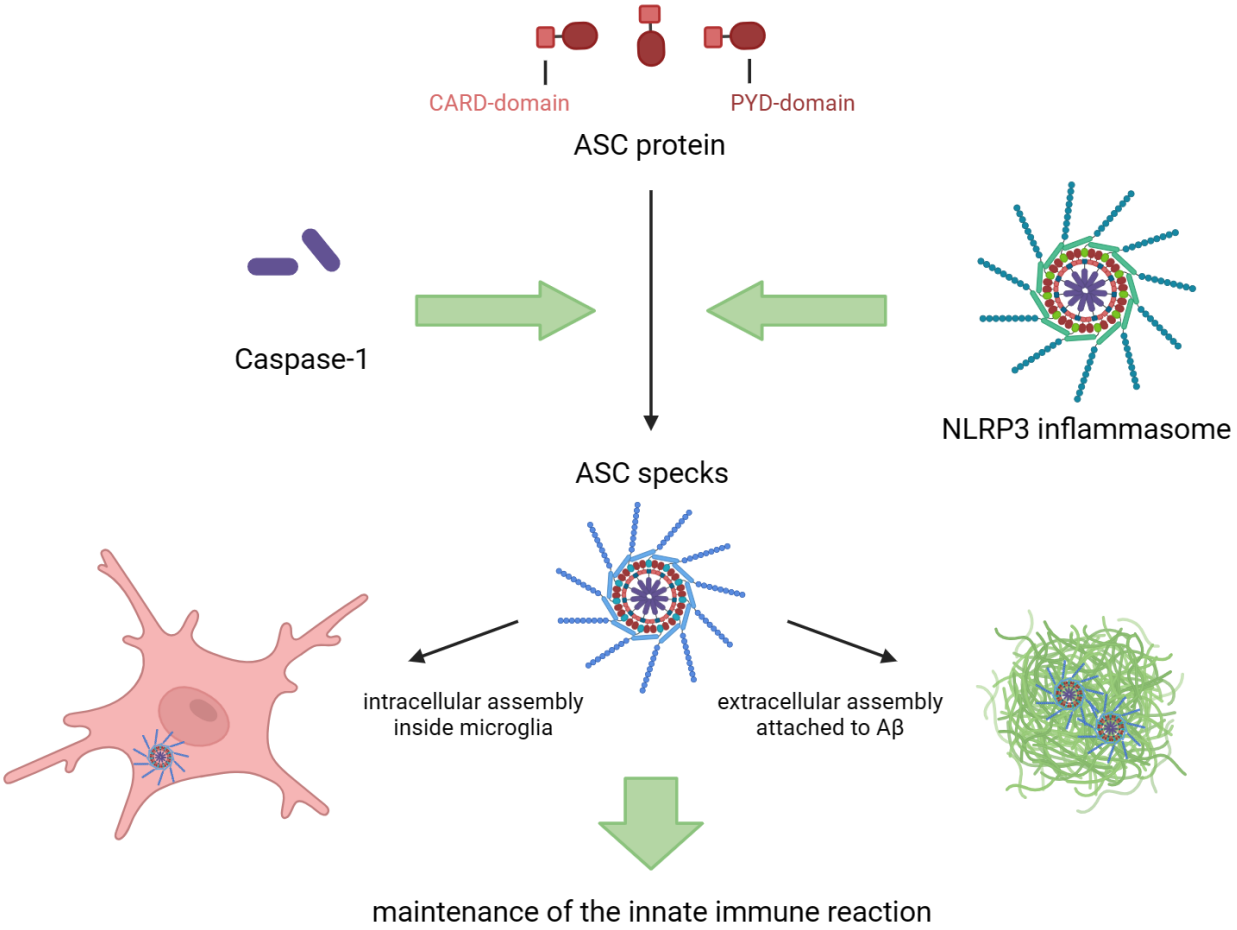

Fig. 4: ASC Speck Formation. The apoptosis-associated speck-like protein containing a CARD (ASC) is an essential part of the NLRP3 inflammasome. It contains a PYD-domain on the N-terminus and a CARD domain on the C-terminus, which are linked by 23 amino acids. Caspase-1 activated in the NLRP3 inflammasome triggers the assembly of ASC protein together with caspase-1 and NLRP3 into speck-like formations. The specks can be found intracellularly in microglia as well as extracellularly attached to amyloid β aggregates. ASC specks fulfil the task to maintain the ongoing innate immune response. Figure created with BioRender.com

1.8 Background and Aim of the Thesis

In AD, amyloid β begins to accumulate in the hippocampal area and afterwards spreads throughout the entire brain following specific trajectories. In experimental models, the injection of synthetic Aβ into the hippocampi of *wildtype* mice failed to seed and therefore did not lead to spreading of amyloid with the subsequent development of AD pathologies. From this observation it was concluded that additional factor(s) are required to trigger Aβ-seeding and inflammation-dependent spreading events (Marzesco et al., 2016). This

hypothesis was further explored by experiments in transgenic *APP/PS1*$^{wt/tg}$ C57/BL6 mice, which spontaneously form amyloid plaques. Crossing these mice with *ASC*-deficient C57/BL6 mice (*APP/PS1*$^{wt/tg}$*;ASC*$^{-/-}$) resulted in reduced Aβ plaque development. Aβ pathology was significantly dampened in *APP/PS1*$^{wt/tg}$*;ASC*$^{-/-}$ mice injected with brain homogenate of *APP/PS1*$^{wt/tg}$ animals (Venegas et al., 2017; Tejera et al., 2019). Hence, although Aβ aggregates are pathognomonic for AD, in the absence of ASC they are not sufficient to induce the neuroinflammatory reaction and subsequent spreading mechanisms of amyloid aggregates. Recent work from our group has described a central role of ASC in NLRP3 activation in microglial cells *in vitro* (Friker et al., 2020). Given this background, the aim of this thesis was to investigate *in vivo* whether ASC aggregates are necessary and sufficient co-factors to induce seeding and spreading of synthetic Aβ injected in murine brains.

2. Materials and Methods

This thesis is based on complex experimental setups that required structural training particularly to perform brain surgeries in murine models. In the following, the applied methods are described and illustrated.

2.1 Murine Models of Alzheimer's Disease

The Alzheimer phenotype was represented by *APP/PS1*$^{wt/tg}$ (B6.CgTg(APPswe,PSEN1dE9)85Dbo/Mmjaxmice) transgenic mice which were used as positive controls, whereas *wildtype* mice were used as main model for readout of the experiments. All mice were on a C57BL/6N genetic background, the *APP/PS1*$^{wt/tg}$ transgenic (The Jackson Laboratory, 2022) and non-*APP/PS1*$^{wt/tg}$-transgenic littermates as *wildtype* mice. *APP/PS1*$^{wt/tg}$ express a chimeric mouse/human APP with the familial Swedish mutation and a mutant human presenilin 1, which are both associated with the early-onset genetic form of patients with AD. *Pycard*-knockout mice, called *Asc*$^{-/-}$, (Millenium Pharmaceuticals) were used as control animals (Ising et al., 2019). The analysis included 41 male (57 %) and 31 female (43 %) mice. Animal husbandry was performed under standard conditions, including an ambient temperature of 21 ± 1 °C, light–dark cycles of 12 h each, and relative humidity of 50 ± 10 %. The animals had free access to food and water and were checked on a daily basis. Following the Declaration of Helsinki and the requirements of the approval of the state authority (LANUV NRW TVA 84-02.04.2017.A226 and 81-02.04.2019.A435) reassured appropriate animal care and handling.

Power analysis (G*Power, 3.1.9.6, Düsseldorf) was used to predetermine the sample size for *in vivo* studies (Venegas et al., 2017). In total, 50 *wildtype* and 22 *APP/PS1*$^{wt/tg}$ transgenic mice underwent intrahippocampal injection of peptides or brain homogenates (Fig. 5). Additionally, an *Asc*$^{-/-}$ mouse, 2 *APP/PS1*$^{wt/tg}$ transgenic mice and 2 *wildtype* mice served as non-injected controls for immunohistochemical staining and microscopy. Mice underwent brain surgery for injection of peptides/brain homogenates at an age of 3 months. The experiments were terminated after another 3 months and brain tissue was

harvested from *APP/PS1*$^{wt/tg}$ and *wildtype* mice for further analyses. Following surgery, the animals were placed in a pre-heated cage and received anaesthesia with buprenorphine, 0.1 mg/kg bodyweight thrice daily, for 3 days. The phase of anaesthesia was followed by daily inspections. All experiments were performed blinded for treatment groups throughout the surgeries and image analysis, wherever possible.

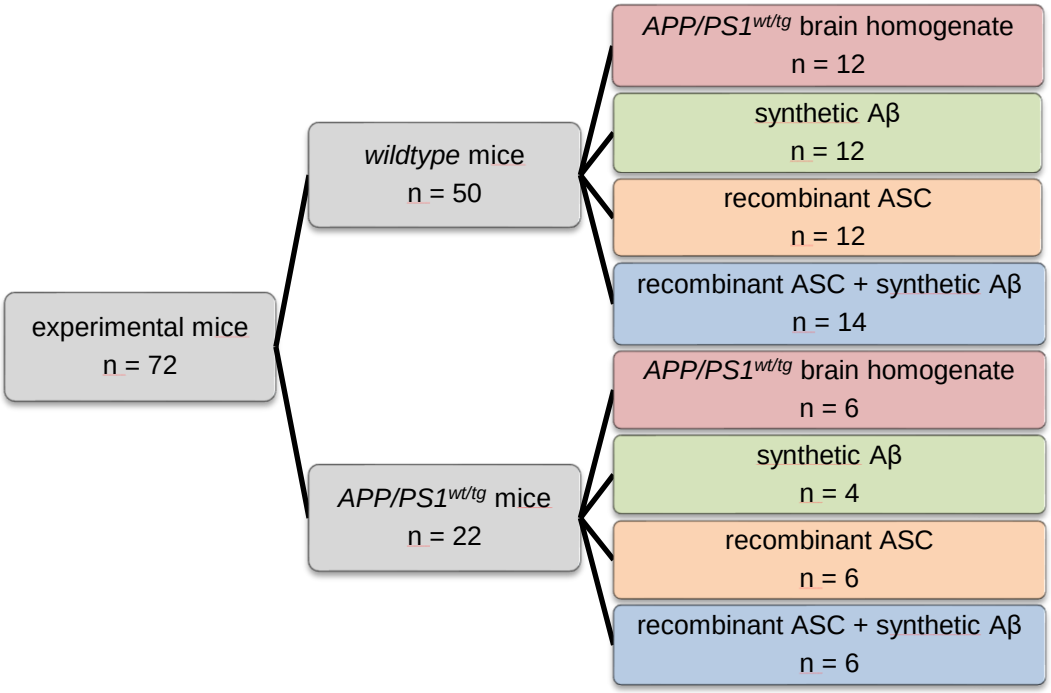

Fig. 5: Overview of the Injection Groups. The study comprised a total of 72 mice that underwent intrahippocampal injections, including 57 % male and 43 % female mice. 50 mice had a *wildtype* genotype and 22 were from an *APP/PS1*$^{wt/tg}$ genetic background. Mice were treated by intrahippocampal injection of either *APP/PS1*$^{wt/tg}$ brain homogenate (red), synthetic Aβ (green), recombinant ASC (orange) or with the combination of recombinant ASC and synthetic Aβ (blue). Required group sizes were determined by G*Power analysis (Venegas et al., 2017).

2.2 Genotyping by Polymerase Chain Reaction and Gel Electrophoresis

Genotypes of all genetically modified mice were determined by polymerase chain reaction (PCR) and gel electrophoresis of DNA extracted from tail clippings using a specific set of primers. Genotypes of each mouse were confirmed twice, first at an age of three weeks, and repeated at termination of the experiment at an age of 6 months. Tail clippings at a length of 1 - 5 mm were obtained, lysed overnight in 200 µL lysis buffer (diluted at a ratio

of 1:6 with H_2O) at 55 °C, followed by boiling at 95 °C for 10 min to obtain a DNA template. EconoTaq Plus Mastermix (19 µL) and corresponding primers were added to 1 µL of lysed DNA and subjected to PCR. The standard PCR program consisted of a denaturation cycle at 95 °C for 3 min, followed by 35 cycles of 95 °C for 30 sec, 65 °C for 75 sec and 72 °C for 60 sec. After the last cycle, the probes were cooled down to 4 °C. For analysis of PCR products, the probes were pipetted into the pockets of an agarose gel for electrophoresis at 120 V until separation of the bands was noted. Double bands indicated the *APP/PS1*$^{wt/tg}$ genotype (white arrows in Fig. 6), whereas single bands indicated the *wildtype* genotype (Fig. 6). All the genotypes defined at the first genotyping time points were confirmed at the second time point at termination of the experiment. As planned, a total of 22 *APP/PS1*$^{wt/tg}$ and 40 *wildtype* mice underwent surgery at the first round of our experiments, and another 10 *wildtype* mice were treated in the second round of experiments (Fig 5).

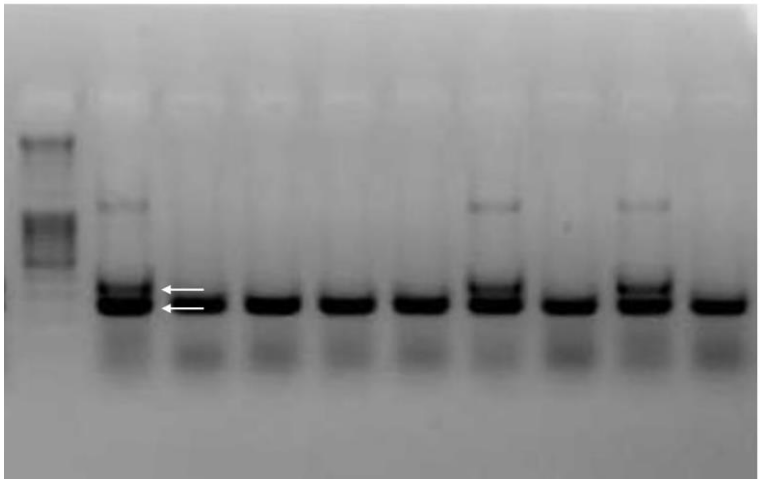

Fig. 6: Exemplary Genotyping Results. The lane 1 was loaded with a DNA marker. Lanes 2, 7 and 9 were loaded with PCR products from *APP/PS1*$^{wt/tg}$ mice (confirmed by double bands, exemplarily indicated with 2 white arrows), the remaining lanes were loaded with PCR products from *wildtype* mice.

2.3 Stereotaxic Surgery

Stereotaxic surgery was performed to inject mixed peptides or brain homogenates into mouse brains to mimic the seeding mechanism of Alzheimer's disease pathology in the most realistic manner. Since the amyloid-induced and inflammatory pathologies early in AD affect the hippocampus formation (Braak, 1991), this brain region was targeted with

the tip of the injection syringe to directly apply the experimental peptides or brain homogenates. Murine brains were measured accurately to defined coordinates with electronical read out rulers (Stoelting, Wood Dale, IL, USA) attached to the stereotaxic frame in all three dimensions.

In preparation of surgery each mouse was weighed in order to determine the accurate dose of buprenorphine (Temgesic®), which was administered subcutaneously (s. c.). To reach the full drug level on time, buprenorphine was dosed at 0.1 µg/g bodyweight 30 min before the start of the surgery. General anaesthesia of mice was performed in a special chamber filled with a mixture of ambient air, oxygen and isoflurane (3 % isoflurane, 2 l oxygen/min). Immediately after the induction of anaesthesia, the mouse was placed in the stereotaxic frame under continuous application of 2 l oxygen/min mixed with 1 - 2 % of isoflurane via a respiratory mask (Fig. 7). The surgery was started when the toe reflex could no longer be released using a surgical forceps. Further precautionary measures included application of dexpanthenol (Bepanthen®) on the mouse's eyes and placement on a heating blanket. The fur of the head was removed with an electrical shaver and a depilatory creme to eliminate all left-over hair. The skin was disinfected by generously applying povidone iodine solvent.

The first step of surgery was central incision of the skin of the head with a scalpel, which was stretched to the lateral sides. The periosteum of the skull was removed manually after application of hydrogen peroxide (H_2O_2). A mouse brain atlas guided the localization of Bregma and the coordinates for the intrahippocampal injections (Paxinos und Franklin, 2013). Bregma is described as the crossing point of the sagittal and the coronary suture and was set as 0/0/0 (x-/y-/z-axis). In order to reach the hippocampal tissue for the injection, the coordinates - 2.5 mm rostro-caudal, 2.0 mm latero-lateral and 1.8 mm dorso-ventral were applied. Small holes with a diameter of 0.4 mm and a depth of 1 mm were drilled into the skull above the corresponding coordinates using an electric surgical driller (Schick C2 Master, Wanzek, Mönchengladbach, Germany) adapted to the stereotaxic frame. Afterwards, the peptides or brain homogenates were injected bilaterally with a Hamilton syringe (2.5 µl volume, 45° 33 G-canula) using an automatic stereotaxic injector (Stoelting Instruments, Wood Dale, IL, USA). In each experiment, a volume of 2 µl was injected at a velocity of 0.5 µl/min, applying the experimental mixture into the left

hemisphere, and the control mixture into the right hemisphere. The syringe was not removed until 10 min past the end of the injection, in order to avoid reflux. During the waiting time, the amount of isoflurane was decreased step by step to allow a gentle wake-up of the mice. After careful vertical removal of the syringe, the wound was closed with surgical suturing techniques and the surgical situs was cleaned with sterile isotonic NaCl solution.

After the surgery, each mouse was placed in a clean preheated cage and some food soaked in water was provided. Afterwards the mouse was monitored until full recovery from general anaesthesia. Postoperative analgesia was applied for three days by s. c. injections of buprenorphine (0.1 mg/kg) every 4 hours (in total 3 times over 12 h). During the nights, buprenorphine (1 µg/ml) was added to the drinking water. Each mouse was checked and scored at least once daily for the following three months.

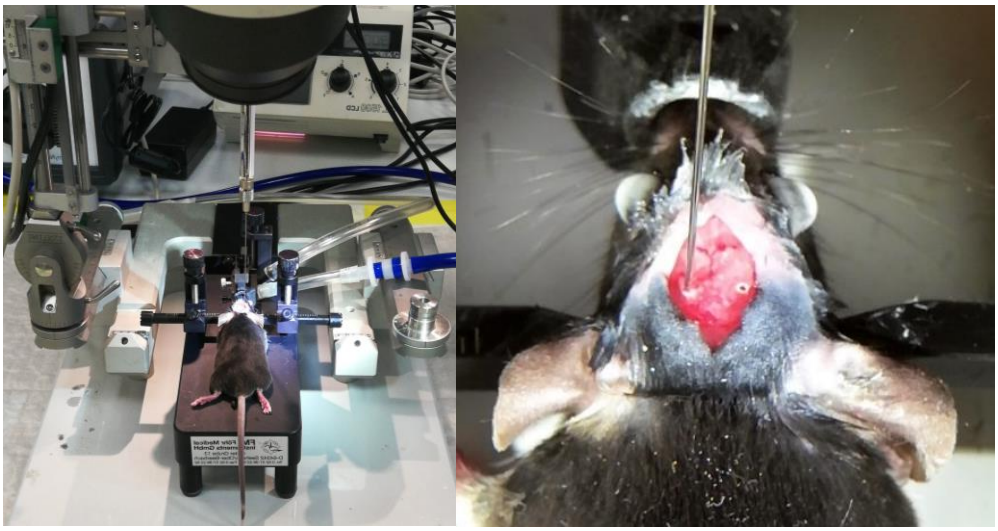

Fig. 7: Setup for Stereotactic Surgeries. After induction of general anaesthesia and analgesia each mouse was fixed in a stereotaxic frame, in order to reach the exact injection sites. To expose the skull, the fur was removed followed by a skin incision. Next, a hole was drilled in each hemisphere just above the injection site, all under microscopic visualisation. The tissue homogenates or protein suspensions were injected slowly (0.5 µl/min, total volume 2 µl). After a waiting time of 10 min, the canula and syringe were removed and the skin was sutured precisely. All mice received monitoring and pain medication for 3 postoperative days, which was followed by daily monitoring for 3 months. Pictures taken by Katharina Schuler.

2.4 Production of Recombinant ASC

Recombinant ASC protein was produced in *Escherichia coli* (*E. coli*) bacteria. The cDNA encoding full-length human ASC, the Tobacco Etch Virus (TEV) protease cleavage site and the mCherry coding sequence were cloned into the pET-28a expression vector, which provides a C-terminal hexa-histidine tag. The resulting plasmid was transformed into *E. coli* BL21 (DE3) bacteria. The transformed *E. coli* bacteria were cultured at 37 °C to an OD_{600} (optical density at a wavelength of 600 nm) of 0.8 and induced with 0.1 mM isopropyl beta-D-1-thiogalactopyranoside for 4 h at 37 °C. After centrifugation, the bacteria were collected, followed by sonication in lysis buffer A (20 mM Tris (pH 8.0), 500 mM NaCl and 5 mM imidazole). Next, the bacterial lysates were centrifuged at 20,000 x g for 30 min, and subsequently the pellet was resuspended in buffer A supplemented with 2 M Gdn-HCl for 1 h at 4 °C. Following another centrifugation step (20,000 x g for 30 min) the supernatant was dialyzed against buffer A overnight at 4 °C under constant stirring. The next day started with centrifuging the sample at 20,000 x g for 30 min. The supernatant was applied to a pre-equilibrated His-Trap™ column using an Äkta Prime FPLC system (GE Healthcare GmbH, Solingen, Germany). Subsequently, the sample was washed inside the column with 10 column volumes of lysis buffer A, and the recombinant protein was eluted using buffer A supplemented with 200 mM imidazole. The purified protein was dialysed against buffer B (20 mM Tris (pH 8.0), 300 mM NaCl) overnight at 4 °C under constant stirring. In order to determine the endotoxin level, the Pierce™ LAL Chromogenic Endotoxin Quantification Kit (Thermo Fischer Scientific, Waltham, Massachusetts, USA) was used according to the manufacturer's protocol. A final centrifugation step (100,000 x g) in a TLA-55 rotor and Beckmann Coulter Optima™ MAX-XP ultracentrifuge for 1 h at 4 °C, separated soluble ASC monomers from insoluble aggregated forms. Transferring the ASC-containing solution to LoBind Tubes (Eppendorf) and incubating for 1 h at 37 °C triggers ASC fibrillation. With the help of the NanoDrop 1000 Spectrophotometer (Thermo Scientific, Waltham, Massachusetts, USA), the final ASC concentration was determined, using the extinction coefficient $\varepsilon = 61.31$. ASC fibrils were stored at 4 °C for no longer than 3 weeks (Friker et al., 2020). The ASC protein was injected into the brain at a concentration of 0.5 µg/µl. The control injection into the right hemisphere for the ASC-group contained sodium-chloride.

2.5 Synthetic Amyloid β

Purified $A\beta_{1-42}$ monomers were used (1,1,1,3,3,3-Hexafluoro-2-propanol/HFIP-treated, Bachem AG, Bubendorf, Switzerland). 1 mg protein was dissolved in 1 ml sterile 10 x PBS and filtered manually. Synthetic Aβ was injected at a concentration of 1 µg/µl. Sham-injection into the right hemisphere contained PBS only.

2.6 Recombinant ASC and Amyloid β

1 µl of fibrillary ASC (concentration 0.5 µg/µl) and 1 µl of synthetic Aβ 1-42 monomers (concentration 1 µg/µl) were co-incubated overnight at 37 °C under constant stirring. The next day, ASC and Aβ were co-injected into the mouse brains (Friker et al., 2020). Right hemispheres were injected with PBS only.

2.7 Brain Homogenates

As positive and negative controls, brain homogenates from *APP/PS1*$^{wt/tg}$ mice as well as from *wildtype* mice were injected respectively into mouse brains. For production of this homogenate, 16-month-old mice were anaesthetised and transcardially perfused with cold phosphate buffer saline (PBS). The brains were removed, frozen on dry ice and homogenized in sterile PBS (5500 x g, 2 x 10 sec, 10 sec break) using a Precellys™ Control Device (Bertin Technologies, Montigny-le-Bretonneux, France). Afterwards, the homogenates were sonicated and centrifuged at 3,000 x g for 5 min at 4 °C. The resulting supernatant was aliquoted, immediately frozen on dry ice and stored at - 80 °C. The left hemispheres of the experimental mice were injected with 2 µl of the *APP/PS1*$^{wt/tg}$ brain homogenate, whereas the right hemispheres were injected with 2 µl of *wildtype* brain homogenate.

2.8 Brain Harvesting

In order to remove the brains for further analyses, the experimental mice were deeply anaesthetised (100 mg/kg ketamine and 16 mg/kg xylazine, respectively) at an age of 6 months. When full anaesthesia was achieved the chest was cut open and a butterfly needle was placed into the left cardiac ventricle to perfuse the mouse with 30 ml ice-cold PBS.

Mouse brains foreseen for histological analyses were removed and stored in 4 % paraformaldehyde (PFA) solution at 4 °C for 24 h. Subsequently, PFA was removed and the brains were washed 3x with PBS. For dehydration, the fixed brains were incubated in 10 % saccharose solution overnight. The next day, 10 % saccharose was replaced with 20 % saccharose solution until the brains sank to the bottom (approx. 24 h). The tissue then was shock frozen in isopentane (- 20 °C), cooled in dry ice and stored at - 80 °C until further analysis.

Mouse brains dedicated to immunoblot analyses were separated into cortical and hippocampal tissue samples. Samples were immediately shock frozen in liquid nitrogen and stored at - 80 °C until further use.

2.9 Cryosections

Brains were cut into slices of 8 - 10 µm thickness using the Leica CM3050 S Cryostat at a constant temperature of - 20 °C and placed on histo-bond microscope slides. Main area of interest was the hippocampal formation in proximity to the injection site. Some slides from the frontal cortex were kept for establishing the staining with new antibodies as well as for controls.

2.10 Immunohistochemistry

A standardized protocol for different immunohistochemical stainings was established. The general conditions were kept consistent throughout the various primary antibodies applied for immunohistochemistry in this work.

In brief, the cut brain slices were first surrounded with a fat barrier pen and dried overnight. Next, the slides were washed with PBS 3 x 10 min while shaking. Slides were incubated in Blocking Buffer (5 % BSA in PBS) for 1 h at room temperature in a humidified chamber. Afterwards, the primary antibodies dissolved in Blocking Buffer (diluted 1:10 in PBS) were applied overnight at 4 °C in a dark humidified chamber, and additionally for 1 h at room temperature on the following day. After washing step with PBS (3 x 5 min while constantly shaking), the secondary (detection) antibodies (diluted 1:10 in Blocking Buffer) were applied for 1 h at room temperature in the humidified chamber. Next, the Blocking Buffer was washed off with PBS (2 x 5 min) and subsequently Methoxy-X04 was applied for 15 min at room temperature, all in the dark humidified chamber. Methoxy-X04 was washed off with PBS (3 x 5 min), and stained slides were fixed with 50 % methanol (MetOH) for 15 min without shaking. After a further washing (2 x 5 min) with 50 % ethanol (EtOH), the sections were incubated with 4′,6-Diamidin-2-phenylindol (DAPI) fluorescent marker of DNA in cellular nuclei (1:10,000, dissolved in PBS) for 5 - 10 min. This was followed by a final washing step with PBS (3 x 5 min while shaking). The stained slides were covered with Immunomount (Epredia™ Immu-Mount™, Thermo Fisher Scientific, Pittsburgh, Pennsylvania, USA) and a coverslip, dried and stored at 4 °C protected from light.

2.11 List of Primary and Secondary Antibodies and Immunofluorescence Reagents

Tab. 1: List of Antibodies and Immunofluorescence Reagents. Compilation of all antibodies and immunofluorescence reagents used during the experiments with corresponding dilutions.

Name	Company	Catalogue Number	Dilution	Antigen	Appli-cation
DAPI (4',6-Diamidino-2′-phenylindol-dihydrochloride)	Thermo Fisher Scientific	62248	1:10000	DNA stain (nuclei)	IHC
Donkey anti-mouse IgG Alexa Fluor 488	Invitrogen	A21202	1:500	2nd antibody, anti-mouse Ig	IHC
Donkey anti-mouse IgG Alexa Fluor 488	Invitrogen	A32766	1:1000	2nd antibody, anti-mouse Ig	IHC
Donkey anti-rabbit IgG Alexa Fluor 594	Invitrogen	A21207	1:500	2nd antibody, anti-rabbit Ig	IHC
Donkey anti-rabbit IgG Alexa Fluor 647	Invitrogen	A32795	1:1000	2nd antibody, anti-rabbit Ig	IHC
Donkey anti-rat IgG Alexa Fluor Plus 568	Invitrogen	A78946	1:1000	2nd antibody, anti-rat Ig	IHC
Methoxy X04	TOCRIS Bioscience	863918-78-9	1:1000	Amyloid β plaques	IHC
Mouse anti-Aβ (6E10)	Sigma	39320-500	1:2000 (IHC) 1:1000 (WB)	Amyloid β monomers, fibrils, plaques (human)	IHC, IB, Co-IP
Rabbit anti-ASC (AL177)	AdipoGen	AG-25B-0006	1:1000	Cross-reacting with human and murine ASC	IHC, IB, Co-IP
Rabbit anti-ASC/TMS1 (D2W8U)	Cell Signaling Technology	67824	1:400	Murine ASC	IHC, IB, Co-IP
Rabbit anti-ASC/TMS1 (E1E3I)	Cell Signaling Technology	13833	1:1000 – 1:24000	Human ASC	IHC
Rabbit anti-ASC/TMS1 (polyclonal)	Proteintech	10500-1-AP	1:250	Human ASC	IHC
Rabbit anti-β-actin antibody	Cell Signaling Technology	4967	1:2000	β-actin protein	IB
Rabbit anti-Iba1	Wako	019-19741	1:1000	Activated microglia unspecific	IHC

2.12 List of Reagents

Tab. 2: List of Reagents. Compilation of all other reagents used for the experiments.

Name	Company	Catalogue Number	Application
Amyloid β protein$_{1-42}$ (HFIP-treated)	Bachem AG	4090148	Intrahippocampal injection
Bepanthen® (Dexpanthenol)	Bayer Vital GmbH	01578847	
Bovine serum albumin (BSA)	Rockland Immunochemicals, Inc.	BSA-1000	IHC, IB, Co-IP
EconoTaq® Plus Mastermix (Taq DNA Polymerase, reaction buffer, dATP, dGTP, dCTP, dTTP, MgCl, PCR enhancer)	Sigma-Aldrich	LUC30035-0	PCR
Ethanol, 50 %	Merck	107017	IHC, prepared from a ≥99.9% stock solution
Epredia™ Immu-Mount™	Thermo Fisher Scientific	1062268	IHC
Hydrogen peroxide 3%	P. W. Beyvers GmbH	04652515	Surgery
Isopentane	Sigma-Aldrich	78-78-4	Shock freezing
Ketamin 100 mg/ml	CP Pharma		Anaesthesia before the surgery, i.p. injection
Laemmli buffer (65.8 mM Tris-HCl, pH 6.8, 2.1 % SDS, 26.3 % glycerol, 0.01 % bromophenol blue)	Bio-Rad	1610747	Co-IP
Methanol, 50 %	Sigma-Aldrich	67-56-1	IHC, prepared from a ≥99.9% stock solution
Normal donkey serum	Abcam	ab7475	IHC
Normal goat serum	Abcam	ab7481	IHC
NP-40 lysis buffer	Thermo Fisher Scientific	J60766.AP	Co-IP
NuPAGE® 4-12 % Bis-Tris gel	Invitrogen	NP0323BOX	IB
NuPAGE MES SDS running buffer (20X)	Thermo Fisher Scientific	NP0002	IB
Paraformaldehyde (PFA), 4 %	Sigma-Aldrich	P6148	Perfusion

Phosphate-buffered saline (PBS)			Permanent use in all assays and mouse surgery
Pierce™ BCA Protein Assay kit	Thermo Fisher Scientific	23225	Determination of Protein Concentration
Protease/Phosphatase Inhibitor Cocktail (100X)	Cell Signaling Technology	5872	Protease inhibition in cell extracts
Protein LoBind Tubes	Eppendorf	00301081 16	
Saccharose 10 %, 20 %	Merck	57-50-1	Prepared in distilled water
Sodium chloride 0.9 %, sterile	B. Braun Melsungen AG	06173569	Surgery
SureBeadsTM Protein G Magnetic beads	Bio-Rad Laboratories	1614023	Co-IP
Temgesic® 0.3 mg/ml	Reckit Benckiser, Wallisellen, Switzerland		Surgery
Trans-Blot® Turbo Mini Nitrocellulose Transfer Packs	Bio-Rad Laboratories	1704158	IB
Tris buffered saline (TBS)	Sigma-Aldrich	T6664	IB
Triton™ X-100	Sigma-Aldrich	9036-19-5	IHC
Xylazine 16 mg/kg			Anaesthesia before the surgery, i.p. injection

2.13 Light and Fluorescence Microscopy

Immunofluorescence acquisitions of the stained brain slices were conducted using an epifluorescence and transmitted wide-field light microscope (Olympus BX61) with the cellSens Dimension software (Olympus Life Science) and for higher resolution with a confocal laser scanning microscope (Leica TCS SP8 X) with LAS X software (3.5.7.23225 Leica Microsystems CMS GmbH). To obtain an initial overview of the slide, the 4x objective was used and the images for quantitative analysis were taken with the epifluorescence microscope with a 20x objective. In order to analyse comparable regions of interest (ROI) in each slide, predefined 0.145 mm^2 ROIs were selected, 2 medial (yellow) and 1 lateral to the injection site (blue), all in CA1 region of the hippocampus (Fig.

8). For each mouse, 6 8-10 µm-thick slices were selected and imaged, with a 50 µm-spacing interval between them. The fluorescent signals were acquired sequentially, using identical microscopic settings. Each image has a resolution of 1344 x 1024 px. The exposure time varied depending on the chosen channel: DAPI signals were visible after an exposure time of 0.3 sec, whereas to receive adequate 6E10 and Iba1 signals, the slides had to be exposed to light for 1.3 sec.

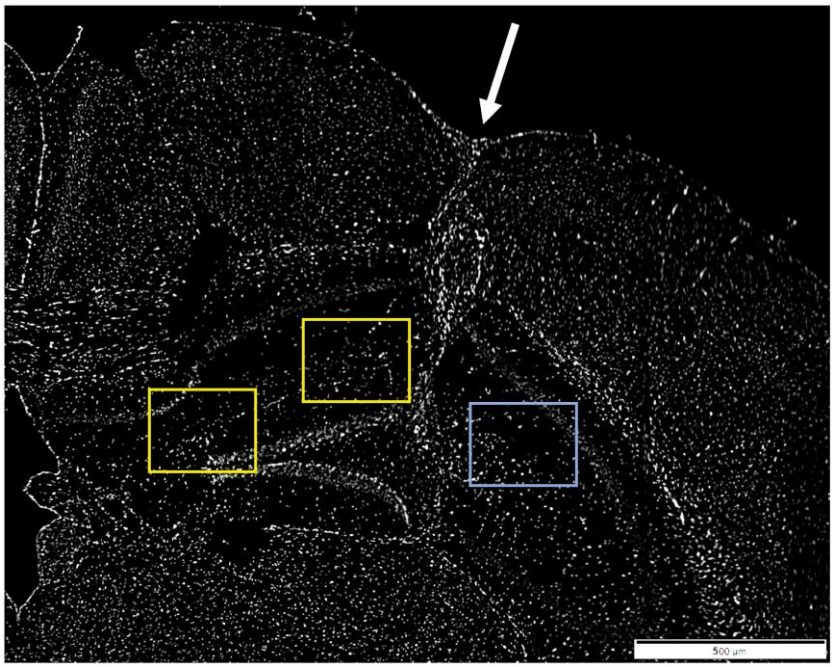

Fig. 8: Selected Hippocampal Regions of Interest. For immunohistochemical analyses 3 intrahippocampal regions of interest (ROIs) in close proximity to the injection site (two medially, one laterally) were selected in each brain hemisphere. Chosen ROIs medially to the injection site are marked by yellow boxes in a representative microphotograph, the ROI laterally to the injection site by a blue box. The injection site can be detected in the extension of the white arrow. All ROIs are located in hippocampal CA1 region, in which amyloid plaques are found already at an early age. The image was captured on an Olympus light microscope with a 4x objective.

For high magnification images, Z-stacks with an interval of one picture per 0.5 µm of selected ROIs were captured via the confocal laser scanning fluorescence microscope (Leica TCS SP8 X) with 40x and 63x oil-immersion objectives. Image processing of high-magnification images was accomplished with Fiji software by ImageJ (ESO/J

Emerson/VISTA Cambridge Astronomical Survey Unit ver. 2.1.0/1.53t) and 3D-reconstruction with Imaris (Version 9.9.1).

2.14 Quantitative Image Analysis

Fiji software by ImageJ (ESO/J Emerson/VISTA Cambridge Astronomical Survey Unit ver. 2.1.0/1.53c) was used to quantify and measure Aβ signals and microglia. For image acquisition, contrast, resolution and threshold were set at the identical level for all microscopy images to be analysed. The total number of signals per ROI was automatically acquired using a self-coded bot recorded by MurGaa Recorder (Daanav Softwares, Panaji, Goa, India). This bot also measured the sizes of the signals. Detection was set at a highly sensitive level to acquire as many single Aβ signals as possible with the consequence that larger amyloid clusters and plaques (particularly developing in *APP/PS1*$^{wt/tg}$ control animals) were counted as multiple single Aβ signals. In addition, the intensities of Aβ signals were automatically acquired. Results were reported as counts per ROI and a mean value of 3 ROIs per mouse was calculated.

2.15 Determination of Protein Concentration in Cell Lysates

Protein concentrations of cell lysates were determined using a commercial bicinchoninic acid assay (Pierce™ BCA Protein assay, Thermo Fischer Scientific, Waltham, Massachusetts, USA) according to the manufacturer's instructions.

2.16 Immunoblotting

Cell lysates were diluted in purified water in a total volume of 24 µl to obtain the required concentration. Next, 4 x Loading Buffer was added, followed by vortexing and short centrifugation. The samples were boiled at 95 °C for 5 min, again centrifuged, and 20 µl of sample were loaded into the pockets of 4 – 12 % Bis-Tris NuPAGE® gradient gels (Invitrogen). Electrophoresis was carried out in MES buffer-filled vertical gel electrophoresis system at 150 V, 300 W (up to 300 mA) for 90 minutes. After removal of

the stacking gel, the gel was plotted on a nitrocellulose membrane using a Trans-Blot Turbo Transfer (Bio-Rad) at a standardized program for 7 minutes (Manabe et al., 2021; Friker et al., 2020).

Blotted membranes were placed in TBS. In addition, the primary antibody clone 6E10 (against amyloid β) required a quick boiling step in the microwave. Membranes were incubated in Blocking Buffer (3 % BSA in TBS) for 30 min while shaking. After preparation of the primary antibody solution in 3 % BSA TBST (TBS supplemented with Tween 0.1 %) in a 50 ml Falcon tube, membranes were placed in the tube and incubated overnight at 4 °C on a rotor. The following day, membranes were washed in TBST (3 x 5 min while shaking), and the secondary antibodies (dissolved in TBST) were incubated for 30 min while shaking. This was followed by additional washing with TBST (3 x 5 min while shaking). Protein signals were acquired with the Odyssey Fc or CLx Imaging System (LI-COR Biosciences) using the Licor Image Studios Software version 5.2.5 (LI-COR Biosciences).

2.17 Co-immunoprecipitation

Brain samples were homogenized in NP-40 lysis buffer supplemented with protease inhibitors (AEBSF, protease inhibitor cocktail, Sigma-Aldrich), NaF and $NaVO_3$.

Immunoprecipitation (IP) was carried out using a commercially available protocol from Bio-Rad Laboratories (Bio-Rad, 2023). SureBeads™ Protein G Magnetic Beads were resuspended in the respective buffer, and 50 µl were transferred into 1.5 ml tubes. The beads were magnetized in magnetic racks and the supernatant was discarded. Next, the solution was washed with 1,000 µl PBS-T (PBS + 0.1 % Tween 20). After centrifugation, the beads were resuspended by vortexing and spun down. Magnetizing and subsequent washing and disposal of the beads were repeated three times. The respective anti-ASC primary antibodies (clones 6E10, AL177, D2W8U) were added to a final volume of 200 µl and the solution was again resuspended in PBS-T. After a rotation step for 10 min at room temperature (RT), the beads were magnetized and the supernatant was discarded. Another washing round with 1,000 µl PBS-T and resuspension followed, as well as repetitive magnetizing and discarding of the supernatant (3 times). Next, the cell lysate

containing 200 µg protein was added to the antibody solution and rotated for 1 h at RT. This was followed by magnetizing, discarding of the supernatant, washing with 1,000 µl PBS-T, resuspension, magnetizing and discarding of the supernatant (3 times). As final binding step, all tubes were spun down, magnetized once more and the residual buffer was aspirated from the tubes. For elution, 40 µl of Laemmli buffer was added and incubated for 10 min at 70 °C. The beads were magnetized and removed to a new vial.

The immunoprecipitates were analysed by immunoblotting as described above.

2.18 Statistical Analyses

Statistical analyses and graphs were generated using the Graph Pad Prism 7 and 9 software (San Diego, California). All quantitative results are presented as mean ± SEM. Immunohistochemical experiments were conducted on 44 mice in total, sub-divided into the different experimental groups, and also into two rounds of surgeries. Each dataset was analysed for Gaussian distribution. For statistical analysis, one-way ANOVA was used followed by the Tukey post hoc test. The differences were considered statistically significant if $p < 0.05$ and the levels of significance are indicated as follows: $^{*}p < 0.05$; $^{**}p < 0.01$; $^{***}p < 0.001$; $^{****}p < 0.0001$.

3. Results

3.1 Co-injection of Synthetic Amyloid β and ASC Induces Seeding and Spreading of Amyloid β in the Murine Hippocampus

As hypothesized, seeding and spreading of Aβ was detected following intrahippocampal injection of *APP/PS1*$^{wt/tg}$ brain homogenates in *wildtype* mice, which induced the formation of Aβ signals and clusters (Fig. 9a). No such effect was observed following injection of synthetic Aβ (Fig. 9b), or recombinant ASC alone (Fig. 9c). Interestingly, intrahippocampal co-injection of synthetic Aβ plus recombinant ASC increased Aβ signals (Fig. 9d), as detected by immunohistochemistry using the 6E10 antibody directed against Aβ.

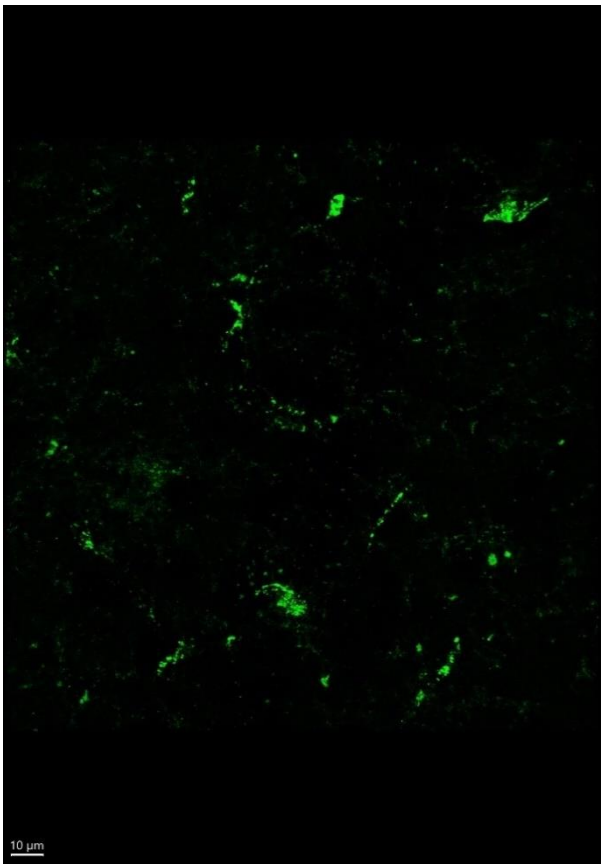

a

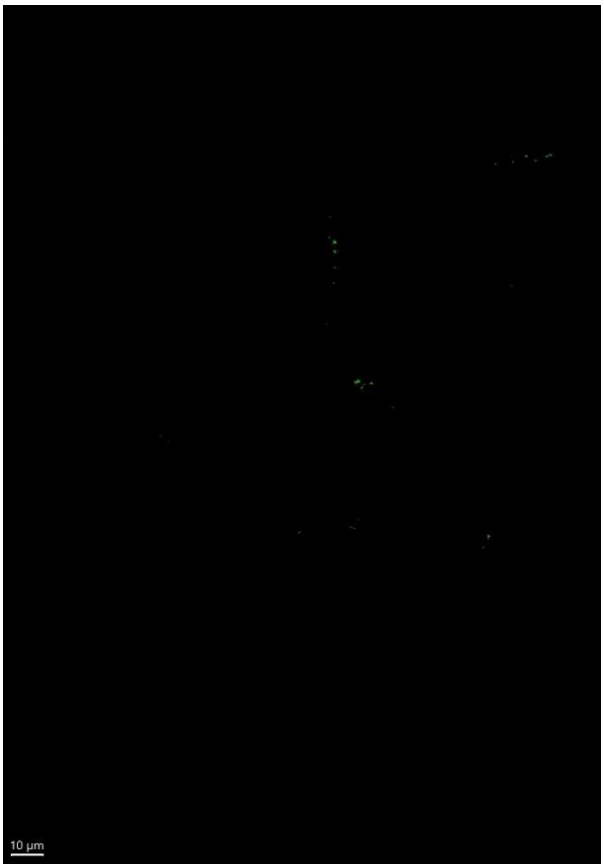

b

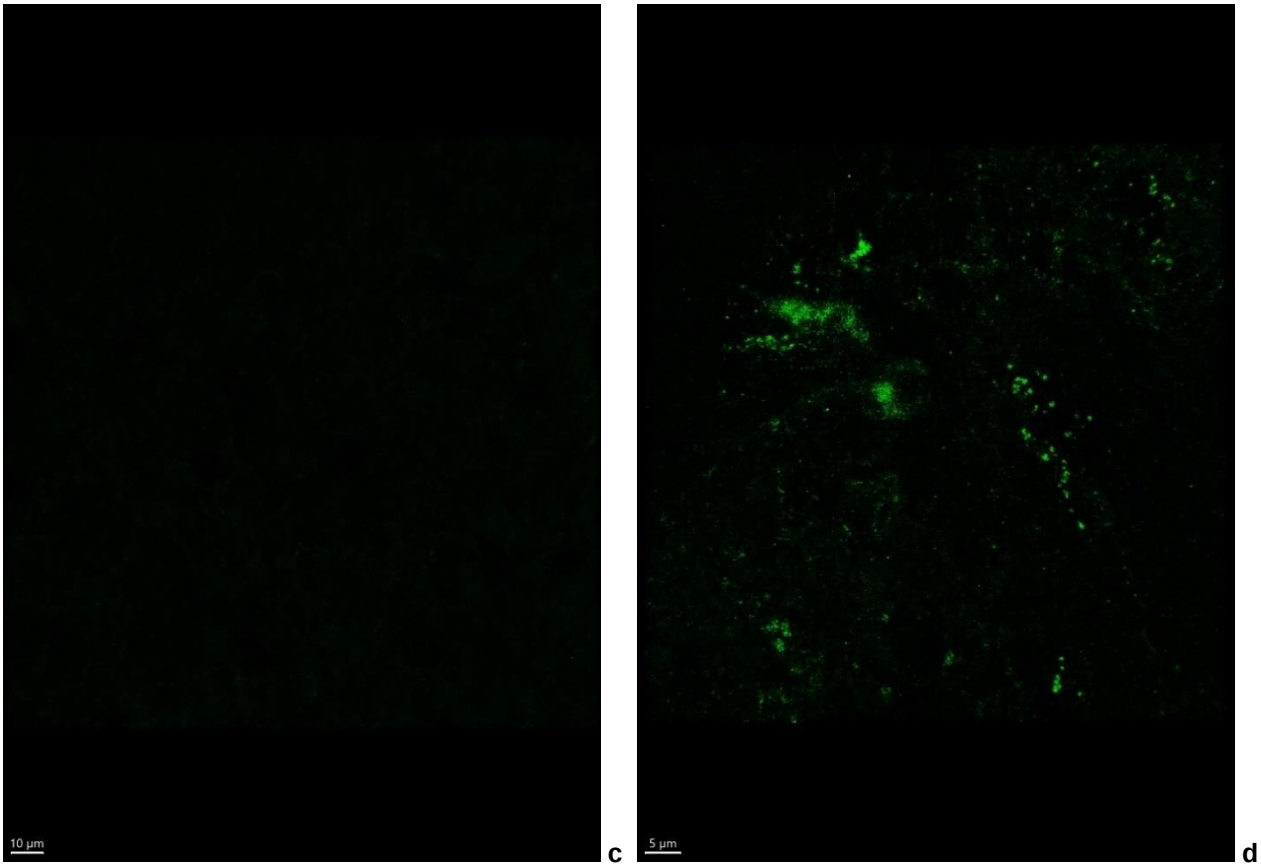

Fig. 9: Amyloid β Signals in Hippocampal Hemispheres of *Wildtype* Mice after Different Types of Intrahippocampal Injections. Staining of amyloid signals was conducted using clone 6E10 as primary antibody (green). Representative microphotographs are shown for each treatment group in the order of injection with *APP/PS1*$^{wt/tg}$ brain homogenate (a), synthetic Aβ (b), recombinant ASC (c), co-injection of ASC and Aβ (d). Small assemblies of Aβ signals can be seen in hemispheres after injection with either *APP/PS1*$^{wt/tg}$ brain homogenate or co-injection with ASC and synthetic Aβ (a, d). Due to the high sensitivity of the microscope for the detection of Aβ signals, certain background signals could not be avoided. Images were captured on an Olympus light microscope with a 63x oil objective, additional zoom applied (d).

Quantitative image analysis comparing homogenate/peptide injected hemispheres to sham-injected hemispheres confirmed a significant increase of Aβ signals in *APP/PS1*$^{wt/tg}$ homogenate-injected hippocampal hemispheres as well as in Aβ/ASC co-injected hemispheres (Fig. 10). In *APP/PS1*$^{wt/tg}$ homogenate-injected hemispheres (n = 8) 154.5 ± 25.9 Aβ signals/mm² (mean ± SEM) were detected. In Aβ/ASC co-injected hemispheres (n = 8) 136.3 ± 20.5 Aβ signals/mm² (mean ± SEM) were found. In contrast, hippocampal hemispheres injected with synthetic Aβ (55.4 ± 12.8 signals/mm², mean ± SEM, n = 6) or

recombinant ASC (46.6 ± 7.4 signals/mm², mean ± SEM, n = 7) similarly showed low numbers of Aβ signals as observed in all sham-injected hippocampal hemispheres (in total n = 28, 58.7 ± 4.9, mean ± SEM). Tissue sections from the negative control group (n = 4) were only incubated with secondary antibodies for immunohistochemistry and a mean of 52.6 ± 9.9 Aβ or rather background signals per mm² (mean ± SEM) were detected (Fig. 10). Certain background signals could not be avoided due to the highly adjusted sensitivity of the microscope to detect Aβ signals.

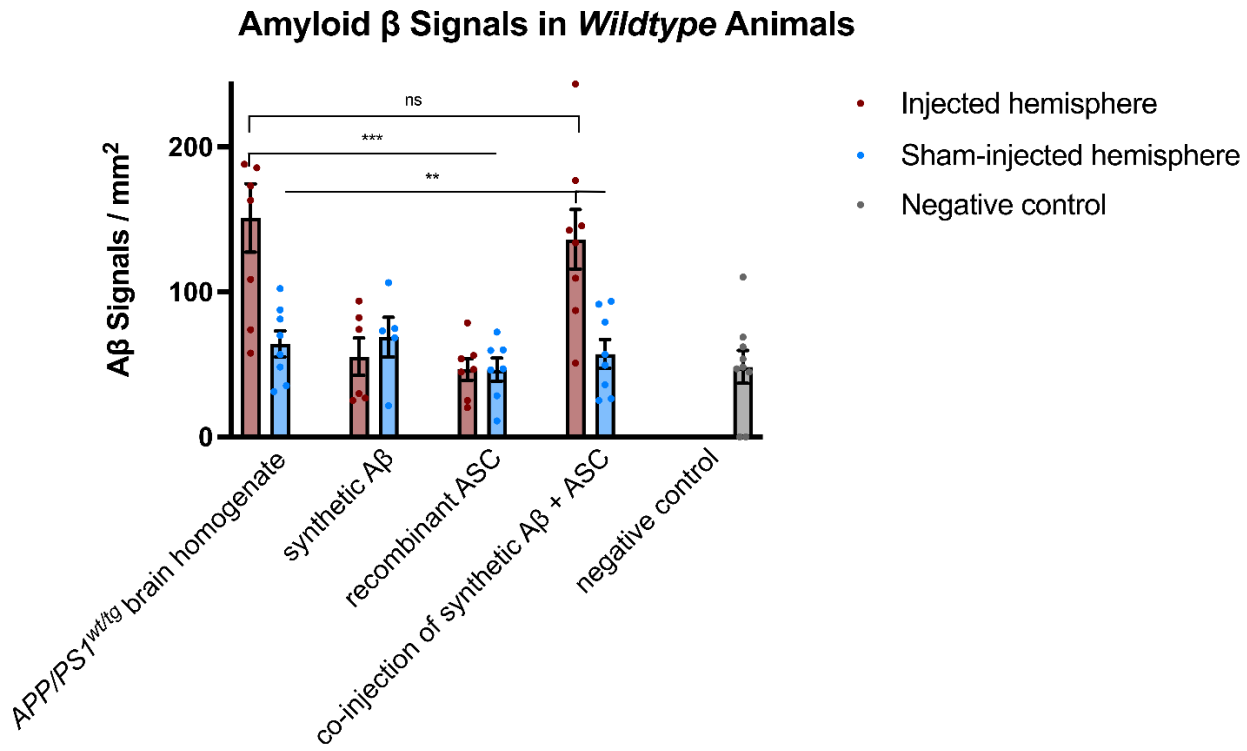

Fig. 10: Amyloid β Signals in *Wildtype* Animals. Total quantification of Aβ signals after intrahippocampal injection of *APP/PS1*$^{wt/tg}$ brain homogenate, synthetic Aβ, recombinant ASC or co-injection of synthetic Aβ and ASC. The left hemispheres of each animal (red bars) had been injected with one of the above-mentioned solutions, whereas the right hemispheres (blue bars) had been sham-injected with vehicle only. Negative control (grey bar) included immunohistochemical staining only with the secondary antibodies (n = 4). Each dot represents the mean absolute number of Aβ signals per mm² in one mouse. Significantly higher Aβ amplitudes can be seen in the experimental groups having received an injection of *APP/PS1*$^{wt/tg}$ brain homogenate (n = 8) or a co-injection of synthetic Aβ and ASC (n = 8). This difference was statistically significant by two-way ANOVA analysis with a Tukey post hoc test. It highlights the requirement of ASC for the spreading phenomenon of injected Aβ in the brain. Statistical significance is displayed as asterisks with **p < 0.01 and ***p < 0.001, vertical lines indicate the referral of the asterisk to one specific bar whereas horizontal lines without vertical offspring refer to all bars covered. Figure created with GraphPad Prism.

The comparison of groups having received an intrahippocampal injection of *APP/PS1*$^{wt/tg}$ brain homogenate and a co-injection of synthetic Aβ and ASC with their respective sham-injected hemisphere reached the predefined level of statistical significance (p = 0.0058 and p = 0.0052, respectively) (Tab. 3). In contrast, no statistically significant differences could be detected when comparing the groups injected either with synthetic Aβ (p = 0.5906) or recombinant ASC (p = 0.1055) alone with their respective sham-injected hemispheres (Tab. 3). Statistics were computed with ordinary one-way ANOVA.

Tab. 3: Ordinary One-way ANOVA of the Different Injection Groups in *Wildtype* Animals in Contrast to Respective Sham-injections. Comparisons of *wildtype* animals between the injected and respective sham-injected hemisphere and negative controls reveal significant differences in the groups injected with either *APP/PS1*$^{wt/tg}$ brain homogenate (p = 0,0058) or co-injected with synthetic Aβ and ASC (p = 0,0052), both groups highlighted with a red frame. Statistical significance is displayed as asterisks with **p < 0.01. Statistics computed with GraphPad Prism.

Ordinary one-way ANOVA	
wildtype animal injected with *APP/PS1*$^{wt/tg}$ brain homogenate, sham-injection and negative control	
ANOVA summary	
F	7.070
P value	0.0058
P value summary	**
Significant diff. among means (P < 0.05)?	Yes
R squared	0.4541

Ordinary one-way ANOVA	
wildtype animal injected with synthetic Aβ, sham-injection and negative control	
ANOVA summary	
F	0.5504
P value	0.5906
P value summary	Ns
Significant diff. among means (P < 0.05)?	No
R squared	0.08403

Ordinary one-way ANOVA	
wildtype animal injected with recombinant ASC, sham-injection and negative control	
ANOVA summary	
F	2.623
P value	0.1055
P value summary	ns
Significant diff. among means (P < 0.05)?	No
R squared	0.2591

Ordinary one-way ANOVA	
wildtype animal injected with synthetic Aβ and ASC, sham-injection and negative control	
ANOVA summary	
F	7.298
P value	0.0052
P value summary	**
Significant diff. among means (P < 0.05)?	Yes
R squared	0.4620

Next, the number of Aβ signals in the verum-injected hippocampal hemisphere was compared to signals observed in the groups that were injected with a different verum. In our experiments, verum groups were *APP/PS1*$^{wt/tg}$ brain homogenate, synthetic Aβ, recombinant ASC or the combination of synthetic Aβ and ASC. We found statistically significant differences between an injection of *APP/PS1*$^{wt/tg}$ brain homogenate and synthetic Aβ ($p = 0.0003$) as well as between *APP/PS1*$^{wt/tg}$ brain homogenate and recombinant ASC ($p < 0.0001$). Also, comparing the Aβ signals detected in mice after co-injection of synthetic Aβ and ASC against those detected after injection of synthetic Aβ alone, revealed a statistically significant difference ($p = 0.004$). Co-injection of synthetic Aβ and ASC induced significantly more Aβ signals than injection of recombinant ASC alone ($p = 0.0007$) (Tab. 4).

When comparing the number of Aβ signals in animals having received an injection of *APP/PS1*$^{wt/tg}$ brain homogenate to animals having received a co-injection of synthetic Aβ and ASC, no statistically significant difference was identified ($p = 0.8179$). This results indicates that the effect seen after intrahippocampal injection of brain homogenate can fully be recapitulated by co-injection of only ASC and synthetic Aβ. Likewise, there was no statistically significant quantitative difference between mice with an injection of either synthetic Aβ or recombinant ASC alone ($p = 0.9809$) (Fig. 10).

The numbers of Aβ signals observed in all sham-injected hippocampal hemispheres were very much alike, with p values between $p = 0.7931$ and $p = 0.9971$ in individual comparisons of each sham-injected experimental group (Fig. 10). Statistics were computed with Tukey's multiple comparisons test.

Tab. 4: Tukey's Multiple Comparisons Test Comparing All Verum-injected Groups in *Wildtype* Animals. Statistical analysis depicts significant differences concerning the Amyloid development comparing the injection of *APP/PS1*$^{wt/tg}$ brain homogenate to the injection of synthetic Aβ ($p = 0{,}0003$) or ASC ($p < 0{,}0001$) alone. Also, co-injection of synthetic Aβ and ASC leads to significantly more Aβ deposits than the injection of synthetic Aβ ($p = 0{,}004$) or ASC ($p = 0{,}0007$) alone. Statistical significance is displayed as asterisks with $^{**}p < 0.01$, $^{***}p < 0.001$ and $^{****}p < 0.0001$ and according groups are highlighted with red frames. Statistics were computed with GraphPad Prism.

Tukey's multiple Comparisons Test	Below threshold?	Summary	Adjusted P Value
injected hemispheres			
APP/PS1$^{wt/tg}$ brain homogenate vs. synthetic Aβ	Yes	***	0.0003
APP/PS1$^{wt/tg}$ brain homogenate vs. recombinant ASC	Yes	****	<0.0001
APP/PS1$^{wt/tg}$ brain homogenate vs. co-injection of synthetic Aβ + ASC	No	ns	0.8179
synthetic Aβ vs. recombinant ASC	No	ns	0.9809
synthetic Aβ vs. co-injection of synthetic Aβ + ASC	Yes	**	0.004
recombinant ASC vs. co-injection of synthetic Aβ + ASC	Yes	***	0.0007

3.2 Co-injection of Synthetic Amyloid β and Recombinant ASC Induces Formation of Amyloid β Aggregates Resembling a Precursor State of Amyloid β Plaques

At an age of 6 months transgenic *APP/PS1*$^{wt/tg}$ mice begin to form morphologically characteristic Aβ aggregates called plaques (The Jackson Laboratory, 2022). These plaques in mice with the overexpressed humanized Aβ sequence phenocopy those found in brains of patients with AD. Plaques can be detected by immunofluorescence, using an antibody against Aβ (6E10) on a confocal microscope (Fig. 11a), and for plaques additionally using the fluorescent dye Methoxy-X04 (Fig. 11b). 6E10 detects the residues 1-16 of Aβ with its epitope between the amino acids 3-8 of the peptide (BioLegend, 2021). Methoxy-X04 reacts to plaques, tangles and cerebrovascular amyloid as it specifically binds fibrillar β-sheet deposits (Abcam, 2023b). Three months following injection of brain homogenates from *APP/PS1*$^{wt/tg}$ mice into the hippocampus of *wildtype* mice the formation of Aβ aggregates was observed. These aggregates had a morphology distinct from the Aβ plaques found in transgenic *APP/PS1*$^{wt/tg}$ mice (Fig. 11c). Co-injection of synthetic Aβ plus recombinant ASC phenocopied the morphology of *APP/PS1*$^{wt/tg}$ brain homogenate-induced Aβ “pre-plaques” in *wildtype* animals (Fig. 9d). As expected, no such Aβ aggregates developed following injection of synthetic Aβ alone (Fig. 9b), recombinant ASC alone (Fig. 9c), or in sham-injected hippocampal hemispheres (Fig. 11c). We defined

these small aggregates, referred to as “pre-plaques”, as amyloid clusters exceeding the size of 0.003 px, which in the resolution of our microscopic images equalled approximately 0.8 µm. In contrast, classical amyloid plaques start at a size of 10 µm (Hall, 2016).

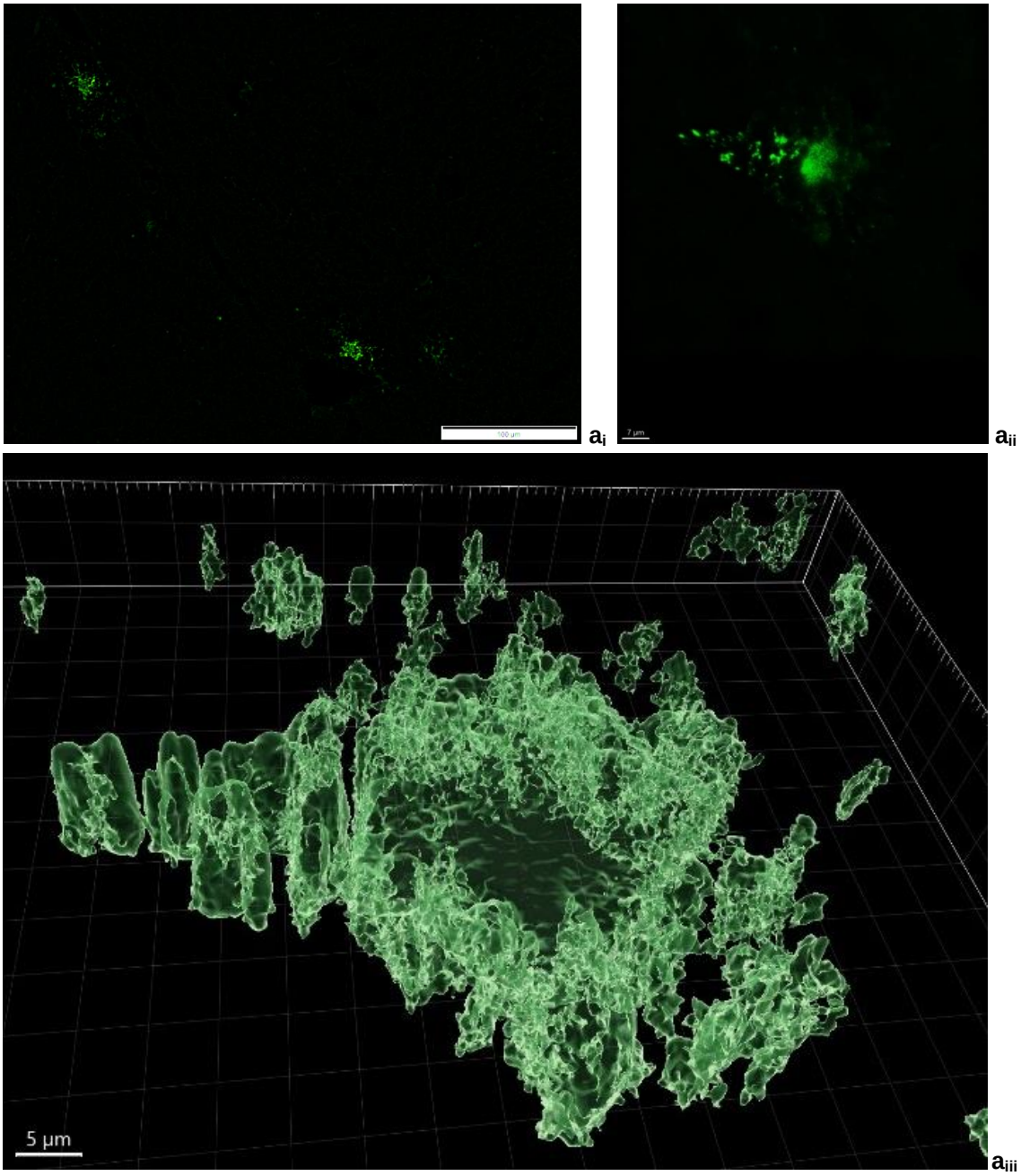

a$_{i}$ **a$_{ii}$** **a$_{iii}$**

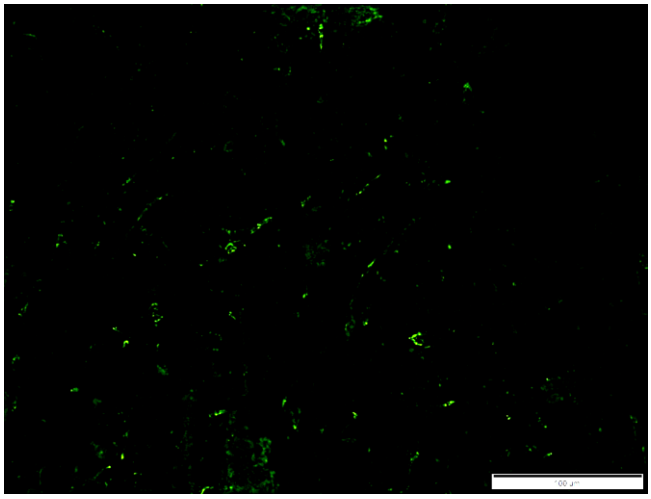

b_i

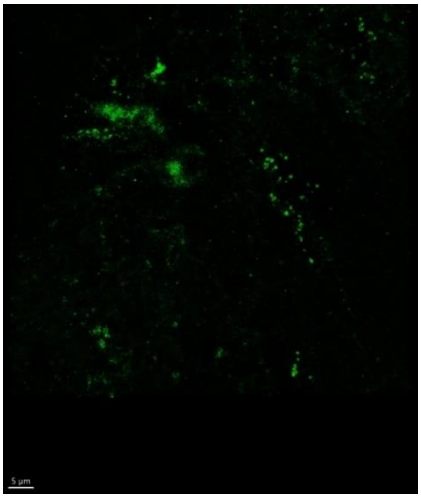

b_{ii}

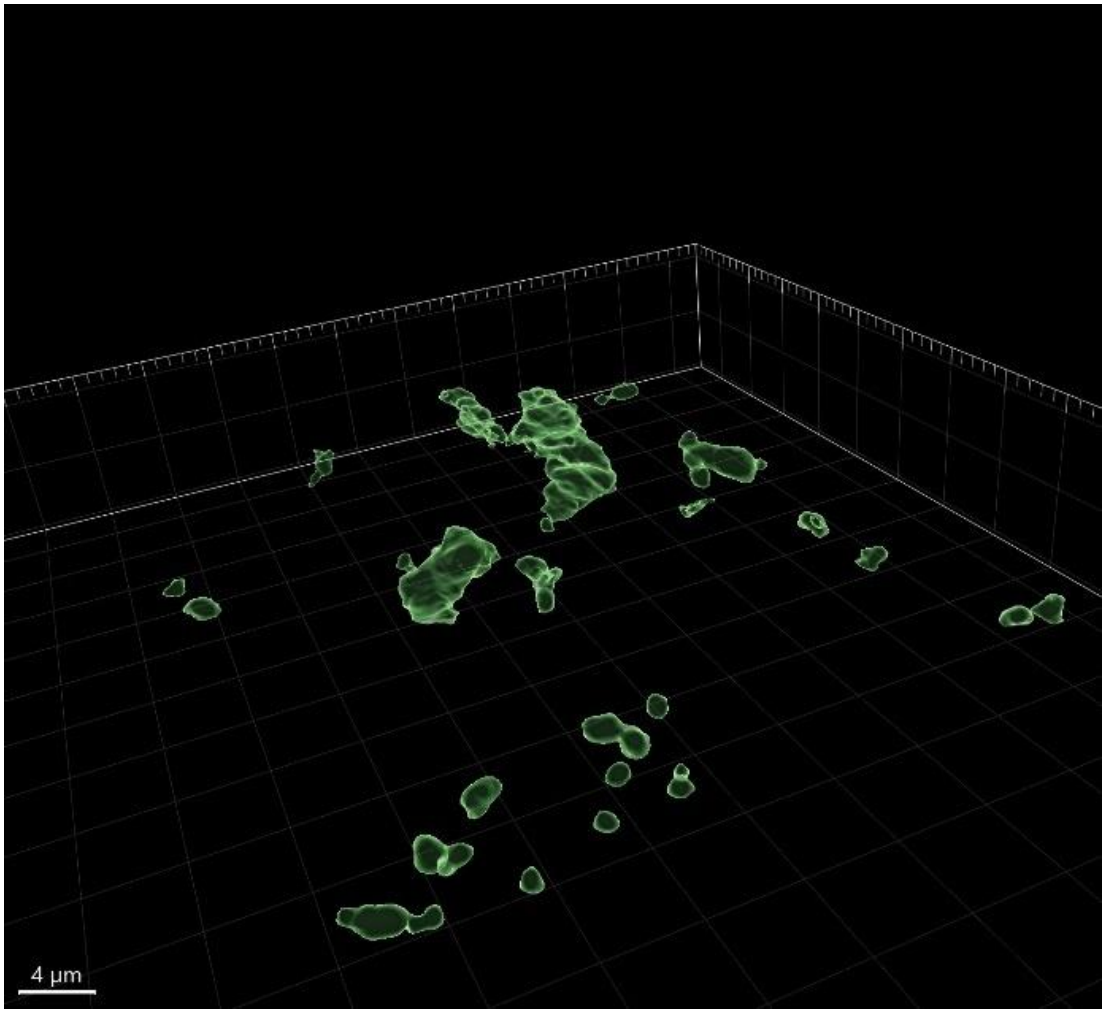

b_{iii}

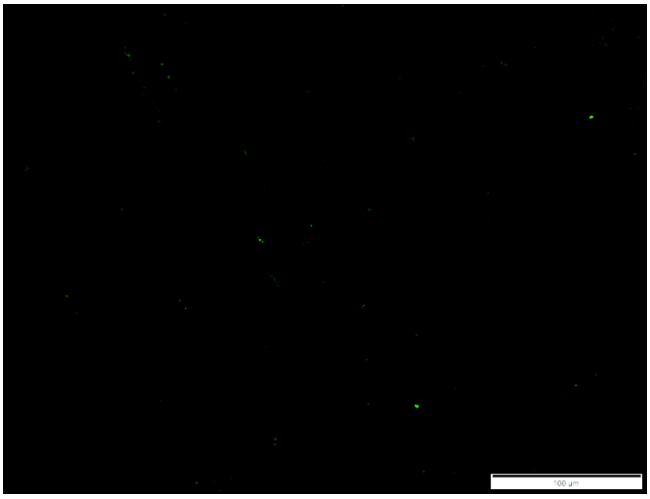

c

Fig. 11: Different Morphologies of Amyloid β Signals. Aβ signals detected in transgenic *APP/PS1*$^{wt/tg}$ animals accumulate in formations referred to as plaques. They can be detected using the primary antibody 6E10 (green) and are depicted here in two different magnifications, 20x (a_i) and 63x with oil (a_{ii}) and also as a 3D reconstruction model (a_{iii}). The induction of β-amyloid assemblies by intrahippocampal injection of either *APP/PS1*$^{wt/tg}$ brain homogenate or co-injection of ASC and synthetic Aβ in *wildtype* mice is a novel observation (b). In contrast to the plaque morphology seen in *APP/PS1*$^{wt/tg}$ mutated animals, amyloid β signals in *wildtype* animals are tiny, solitary illuminations (e.g., oligomers, fibrils) distributed throughout the brain with high affinity to the hippocampal area. 3D reconstruction (b_{iii}) of the different magnifications (b_i 20x, b_{ii} 63x with oil) allows detailed examination of the amyloid signals' morphology. 6E10 staining is very sensitive and detailed in mirroring amyloid β proteins. On the other hand, it has a higher susceptibility to errors. Some of those error-signals are depicted in sham-injected hemispheres after staining with 6E10 antibody (c). Images were captured on an Olympus and Leica microscope, with 20x and 63x objectives and partially zoomed in.

Quantifying the number of Aβ clusters by fluorescence microscopy revealed 81.9 ± 17.1 (mean ± SEM) Aβ "pre-plaques" per mm^2 following intrahippocampal injection of *APP/PS1*$^{wt/tg}$ brain homogenates (n = 8), and 65.0 ± 11.9 (mean ± SEM) Aβ "pre-plaques" following co-injection of synthetic Aβ plus recombinant ASC (n = 8). In contrast, only 23.9 ± 5.0 and 19.9 ± 2.6 (mean ± SEM) Aβ "pre-plaques" were observed in sections of hippocampal hemispheres injected with synthetic Aβ (n = 6) or recombinant ASC (n = 7) alone, respectively (Fig. 12). In these mice, formation of Aβ "pre-plaques" did not exceed the background level detected in non-injected hippocampal hemispheres stained exclusively with secondary antibodies (25.7 ± 3.1 (mean ± SEM) background signals resembling "pre-plaques" mm^2, n = 6 animals).

Comparing the Aβ cluster development of mice having been injected with brain homogenate of *APP/PS1*$^{wt/tg}$ mice (p = 0.0067) and of mice co-injected with synthetic Aβ and ASC (p = 0.006) revealed a statistically significant difference to their respective sham-injected hemispheres (Fig. 12). Neither the injection of synthetic Aβ nor of recombinant ASC alone led to significantly different amounts of cluster development as compared with their sham-injected hemispheres (p = 0.5337 and p = 0.3825).

The injection of brain homogenate from *APP/PS1*$^{wt/tg}$ mice induced significantly more Aβ clusters than the injection of synthetic Aβ (p = 0.0005) or recombinant ASC (p < 0.0001) alone. Corresponding trends were detected in the treatment group having received a co-injection of synthetic Aβ and ASC compared to the treatment groups having received an injection of synthetic Aβ (p = 0.0188) or recombinant ASC (p = 0.0055) alone (Fig. 12).

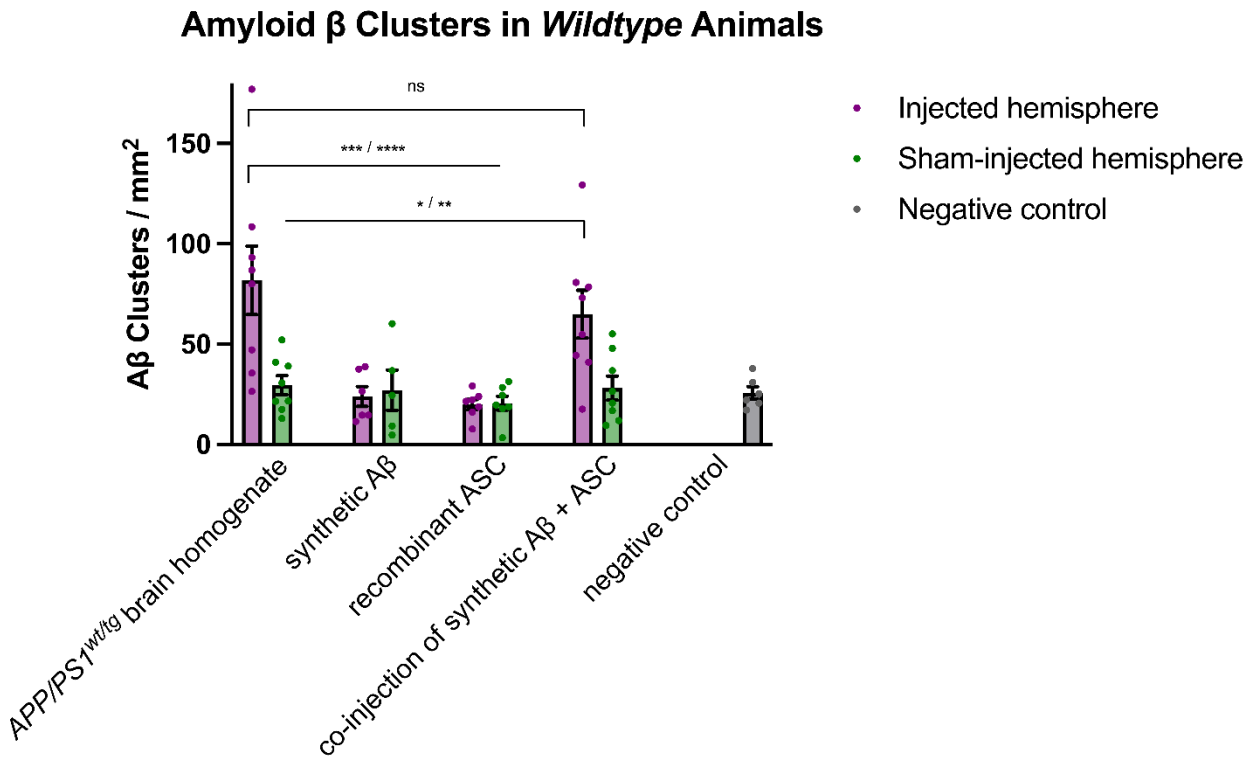

Fig. 12: Amyloid β Cluster Formation in *Wildtype* Animals. An amyloid cluster or "pre-plaque" was defined as an Aβ signal with a size larger than 0.003 px, equalling a size of 0.8 µm. Total quantification of the clusters after intrahippocampal injection of *APP/PS1*$^{wt/tg}$ brain homogenate, synthetic Aβ, recombinant ASC or co-injection of synthetic Aβ and ASC. The left hemispheres of each animal (purple bars) were injected with one of the above-mentioned solutions, the right hemispheres (green bars) were sham-injected with vehicle only. Negative controls (grey bar) were exclusively stained with secondary antibodies (n = 6). Each dot represents the mean absolute number of Aβ clusters per mm^2

in one mouse. Significantly more Aβ clusters can be seen in the experimental groups having received an injection of *APP/PS1*$^{wt/tg}$ brain homogenate (n = 8) or a co-injection of synthetic Aβ and ASC (n = 8). The numbers of clusters in these two groups were significantly higher than in negative controls or in mice injected with Aβ (n = 6) or ASC alone (n = 7) (*p < 0.05, **p < 0.01, ***p < 0.001 and ****p < 0.0001 by two-way ANOVA statistical analyses with a Tukey post hoc test). Vertical lines of the significance bars indicate the referral of the asterisk to one specific bar whereas horizontal lines without vertical offspring refer to all bars covered. Figure created with GraphPad Prism.

3.3 Amyloid β Aligns Parallel to Vessels

During microscopy we figured that the majority of Amyloid β signals detected in *wildtype* mice having been injected with either *APP/PS1*$^{wt/tg}$ brain homogenate or co-injected with synthetic Aβ and ASC visualized with anti-amyloid antibody 6E10 (green) were solitary signals distributed broadly throughout the hippocampal area, partly organised as clusters (Fig. 9 and 11b). By contrast, strikingly, at least a substantial part of amyloid signals was aligned in a row, one behind the other (Fig. 13 a_i, b_i). Additional use of DNA-binding DAPI fluorescent dye, especially binding to adenine and thymine-rich areas (Abcam, 2023a), as a detection method for endothelial cell nuclei (blue) and adding microglia staining Iba1 (red, 1:1000), which is a primary antibody against ionized calcium-binding adaptor molecule 1 (Chen et al., 2018), vessel-like shapes of some amyloid signals are visible (Fig. 13 a_{ii}, b_{ii}). Supporting this hypothesis, three-dimensional imaging and surface reconstruction via Imaris Software showed Aβ signals parallel to vessel walls (Fig. 13 c).

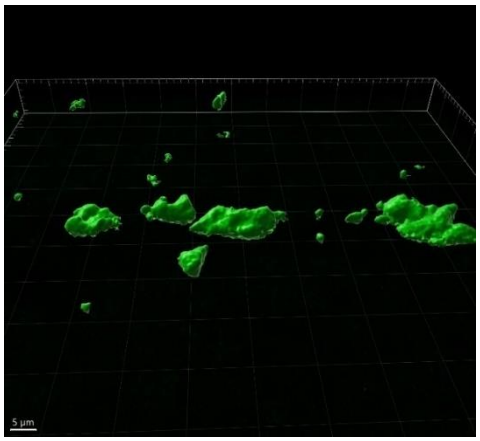

a_i

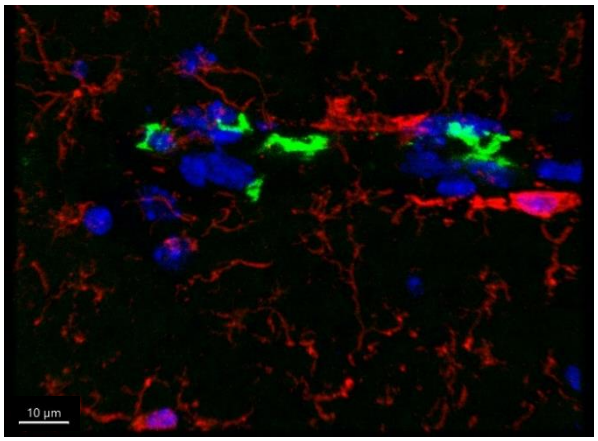

a_{ii}

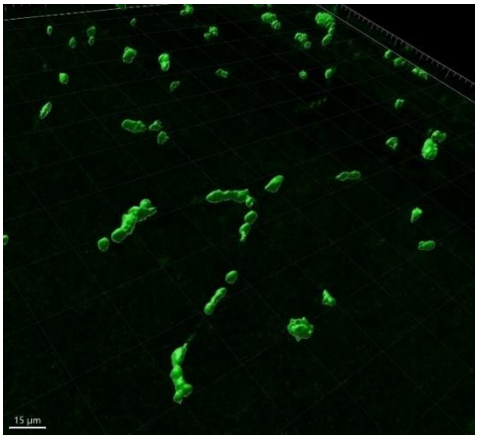

b$_i$

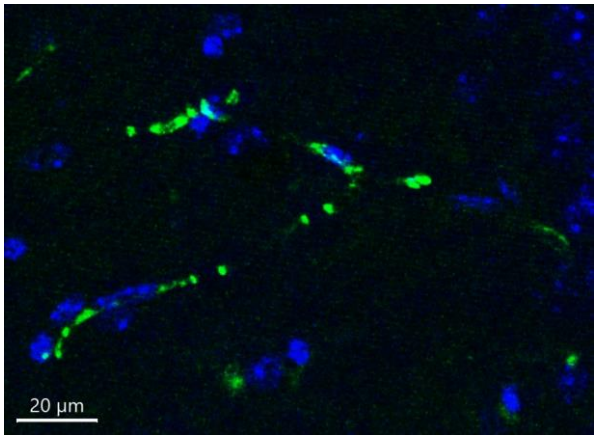

b$_{ii}$

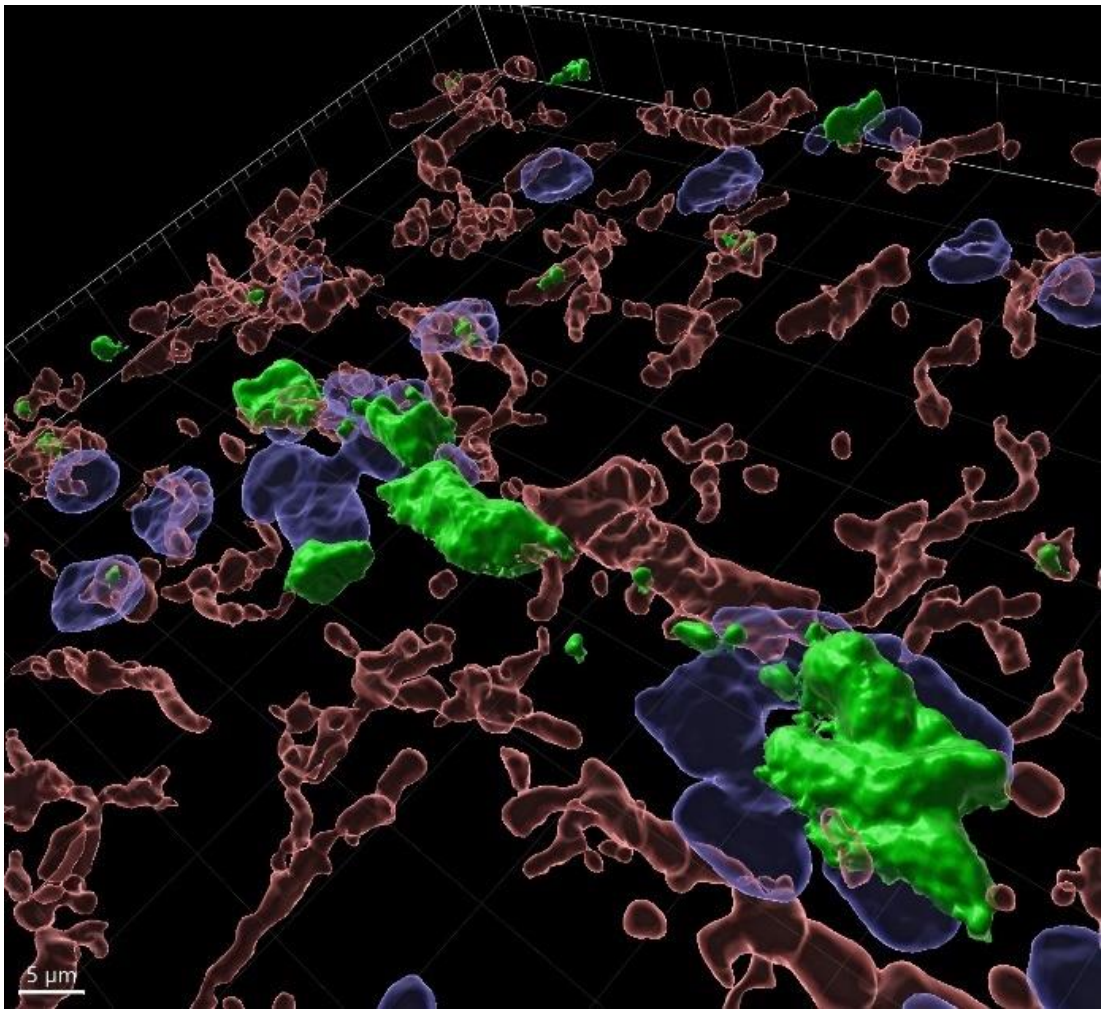

c

Fig. 13: Amyloid β Aligns Parallel to Vessels. Aβ signals detected in *wildtype* mice after intrahippocampal injection of either *APP/PS1$^{wt/tg}$* brain homogenate or co-injection of ASC and synthetic Aβ assemble in numerous configurations, mostly as solitary signals and small clusters (Fig. 9 and 11b). Yet a substantial part aligns in rows one behind another in shapes similar to vessels. Applying the primary antibody 6E10 (green) against Aβ, the in-row alignment can be visualized with 20x and 63x oil objectives (a_i and b_i). A vessel-like arrangement of Aβ signals demarcates more noticeable after including DAPI

fluorescent dye and anti-Iba1 antibody (a_{ii}, b_{ii}). DAPI (blue) serves as a detection method for cell bodies, including endothelia, and anti-Iba1 (red) for microglial cells. Three-dimensional surface reconstruction of the fluorescence signals underlines parallel alignment of Aβ, endothelial and microglial cells (c). Images were captured on a Leica microscope with 20x and 63x oil objectives. 3D reconstruction was performed with Imaris software.

3.4 Amyloid β Accumulates In- and Outside of Microglia

Three-dimensional imaging of brain slices of *wildtype* mice co-injected with ASC and synthetic Aβ served to reconstruct the interaction of microglia and amyloid protein aggregates. Interestingly, Aβ accumulates both inside and outside of microglial cells in injected *wildtype* mice (Fig. 14). This strikes a contrast to amyloid plaques in mice from an *APP/PS1*$^{wt/tg}$ background: classical amyloid plaques localise extracellular. However, also in *APP/PS1*$^{wt/tg}$ transgenic mice, smaller aggregates of amyloid (monomers, oligomers, fibrils) assemble inside microglial cells. Microglia might unsuccessfully try to eliminate Aβ and subsequently this failure could be the fundamental prerequisite for the amyloid spreading.

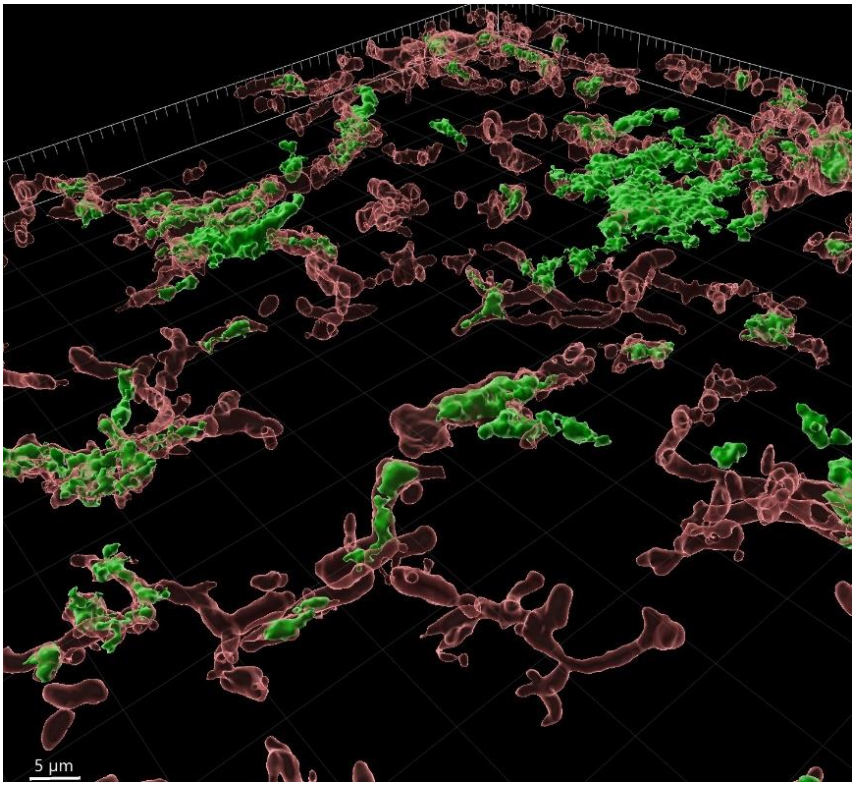

a

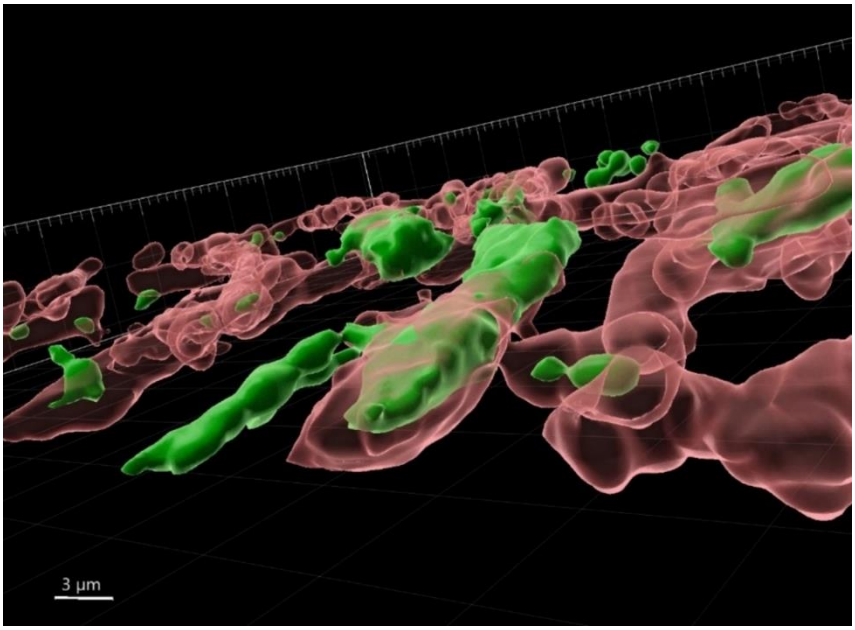

b

Fig. 14: Amyloid β Accumulates In- and Outside of Microglia. Close-up three-dimensional reconstruction of Aβ signals (green) in *wildtype* mice having been co-injected with ASC and synthetic Aβ reveals extracellular amyloid assemblies, but on the other side also shows Aβ assemblies inside microglia (red). This ambilateral positioning is seen in an overview cell reconstruction image (a) as well as in a close-up image (b). Both intra- and extracellular amyloid positioning in injected *wildtype* mice contrast with the extracellular positioning of amyloid plaques in mice from an *APP/PS1*$^{wt/tg}$ background. Images were captured on a Leica microscope with 20x and 63x oil objectives. 3D reconstruction was performed with Imaris software.

3.5 Phenotypic Characterization of Microglia Following Intrahippocampal Injection of *APP/PS1*$^{wt/tg}$ Brain Homogenate, Amyloid β and ASC

To study by immunohistochemistry the distribution and morphology of microglia, Iba1 was applied. Microglial cells are omnipresent throughout the brain. Since higher expression of Iba1 occurs in activated microglia, they are particularly visible in the presence of amyloid plaques as seen in *APP/PS1*$^{wt/tg}$ animals, where they assemble in close proximity (Fig. 15).

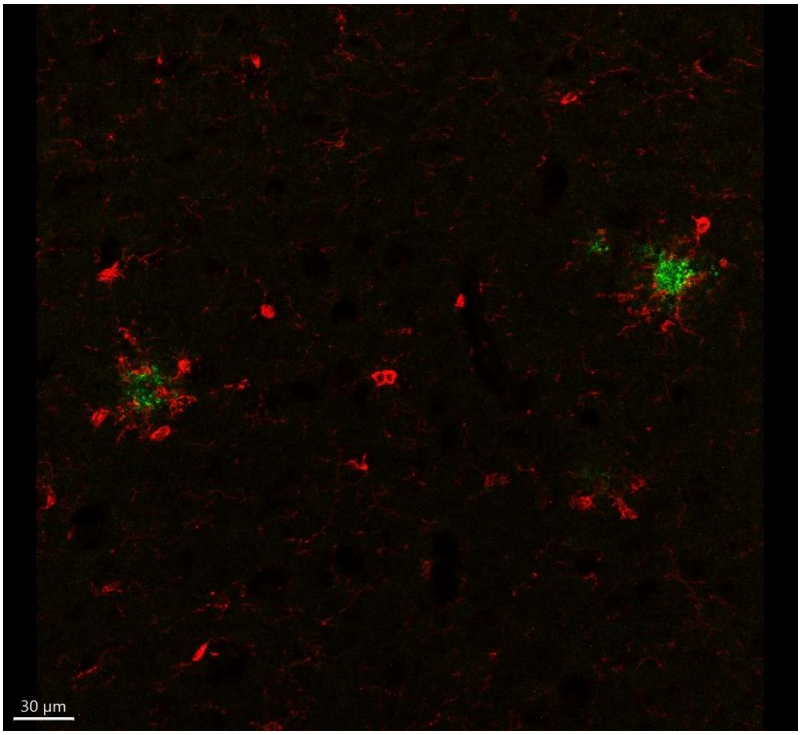

a

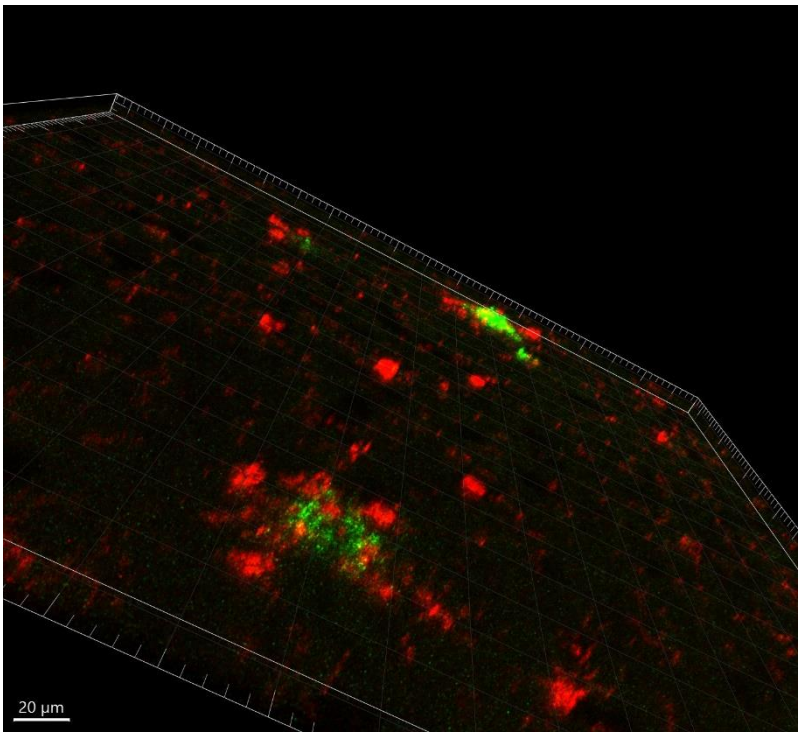

b

Fig. 15: Iba-1 Staining of an *APP/PS1*$^{wt/tg}$ Animal. Microphotograph taken after immunohistochemical staining with 6E10 (green) and anti-Iba1 (red). Microglial cells play a major role in the aggregating process of amyloid and accumulate in close proximity to the plaques. Image captured on a Leica microscope with a 20x objective.

113.5 ± 2.2 Iba1-positive microglial cells (mean ± SEM, n = 8 animals) per mm² were detected following co-injection of Aβ plus ASC (Fig. 16). This compared to 142.6 ± 6.7 microglial cells/mm² (mean ± SEM, n = 8), 118.5 ± 2.0 microglial cells/mm² (mean ± SEM, n = 7), and 111.2 ± 2.9 microglial cells/mm² (mean ± SEM, n = 7) following injection of brain homogenate of *APP/PS1*$^{wt/tg}$ mice, synthetic Aβ or recombinant ASC, respectively. Considering all sham-injections together (n = 28), 117.8 ± 1.0 (mean ± SEM) microglial signals per mm² were detected. Hence, there were no significant differences in the quantity of microglial cells between those four animal groups (*APP/PS1*$^{wt/tg}$ brain homogenate, synthetic Aβ, ASC, co-injection of ASC and synthetic Aβ) or sham-injected mice (p = 0.9323, p = 0.9940, p = 0.9530 and p = 0.4198). The signals detected in the negative control group only incubated with the secondary antibody differed significantly from all other injection groups. Those background signals are confined to 36.0 ± 8.9 (mean ± SEM, n = 5) microglial signals/mm² that have been detected (Fig. 16).

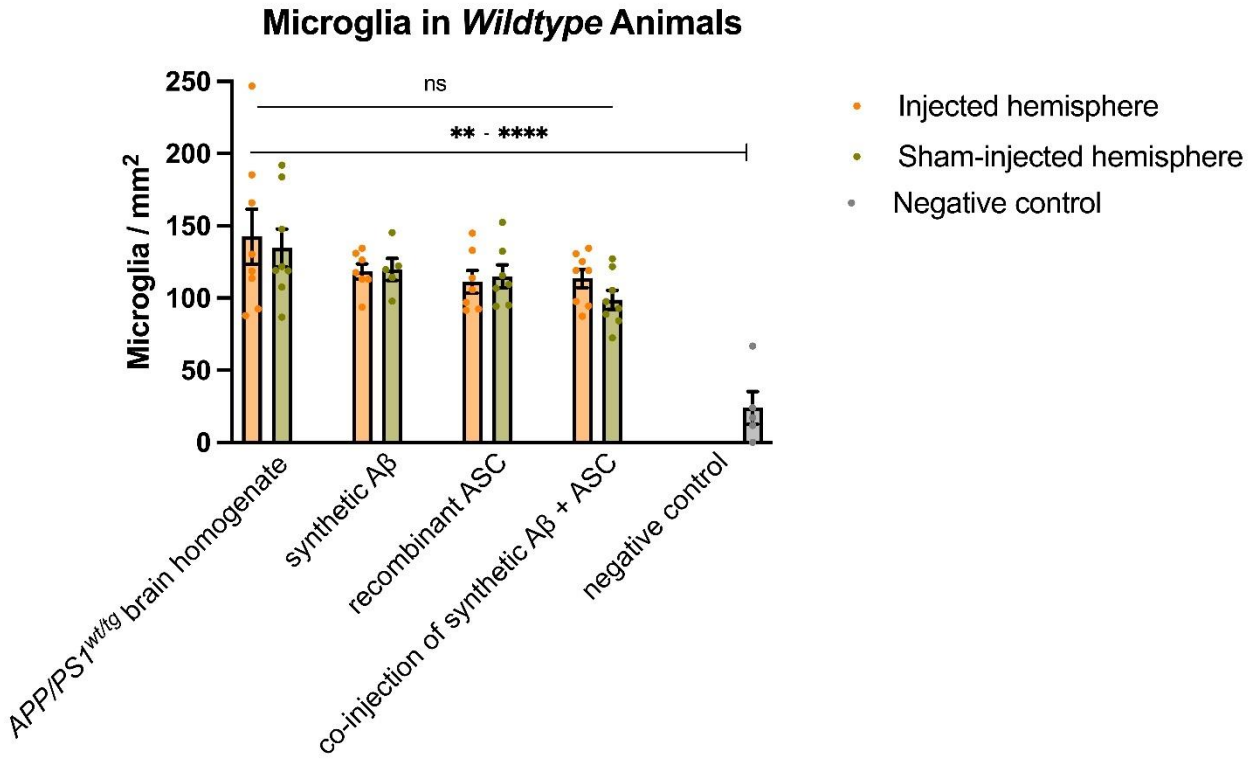

Fig. 16: Quantification of Microglial Cells in *Wildtype* Animals. Quantification of microglial somata after intrahippocampal injections of *APP/PS1*$^{wt/tg}$ brain homogenate (n = 8), synthetic Aβ (n = 7), recombinant ASC (n = 7) or co-injection of synthetic Aβ and ASC (n = 8). The left hemispheres of each animal (orange bars) had been injected with one of the above-mentioned solutions, the right hemispheres (olive green bars) had been sham-injected with vehicle only. Brain section stained only with the secondary antibody are

included as negative control for background fluorescence (grey bar). Each dot represents the mean absolute number of microglial somata per mm^2 in one mouse. Comparable numbers of microglial perikarya were observed, signifying a similar level of neuroinflammation across all experimental groups. In all injected and sham-injected groups significantly higher amounts of microglia were detected as compared to the negative control group (n = 5). Differences between groups were compared using two-way ANOVA analysis with a Tukey post hoc test (**p < 0.01, ***p < 0.001 and ****p < 0.0001). Vertical lines of the significance bars indicate the referral of the asterisk to one specific bar whereas horizontal lines without vertical offspring refer to all bars covered. Figure created with GraphPad Prism.

Analysing the size of the microglial somata revealed no significant differences between the individual injection groups with p values ranging from p = 0.9733 to p = 0.9999 (Fig. 17). In each ROI the sizes of all detected microglial perikarya were measured, and the mean value was calculated representing the average size of one microglial cell per mouse. The injection of brain homogenate of *APP/PS1*$^{wt/tg}$ mice led to average sized microglia of 8.53 ± 0.50 µm (mean ± SEM, n = 8), which was similar to the corresponding sham-injected hemisphere depicting microglia of an average size of 8.31 ± 0.54 µm (mean ± SEM, n = 8). The average sizes of microglial perikarya after the injection of synthetic Aβ and recombinant ASC alone amounted 8.41 ± 0.54 µm (mean ± SEM, n = 6) and 8.24 ± 0.41 µm (mean ± SEM, n = 7). The average microglial sizes in the respective sham-injected hemispheres were 8.27 ± 0.66 µm (mean ± SEM, n = 5) and 8.06 ± 0.39 µm (mean ± SEM, n = 7). Following co-injection of ASC with synthetic Aβ the average sized microglia was 8.29 ± 0.41 µm (mean ± SEM, n = 8), which compared to the somata in sham-injected hemispheres of 8.16 ± 0.37 µm (mean ± SEM, n = 8). The specificity of these stains over background fluorescence was confirmed by a statistically higher ($p \leq 0.005$) mean microglial size than in negative controls only stained with the secondary antibody (Fig. 17).

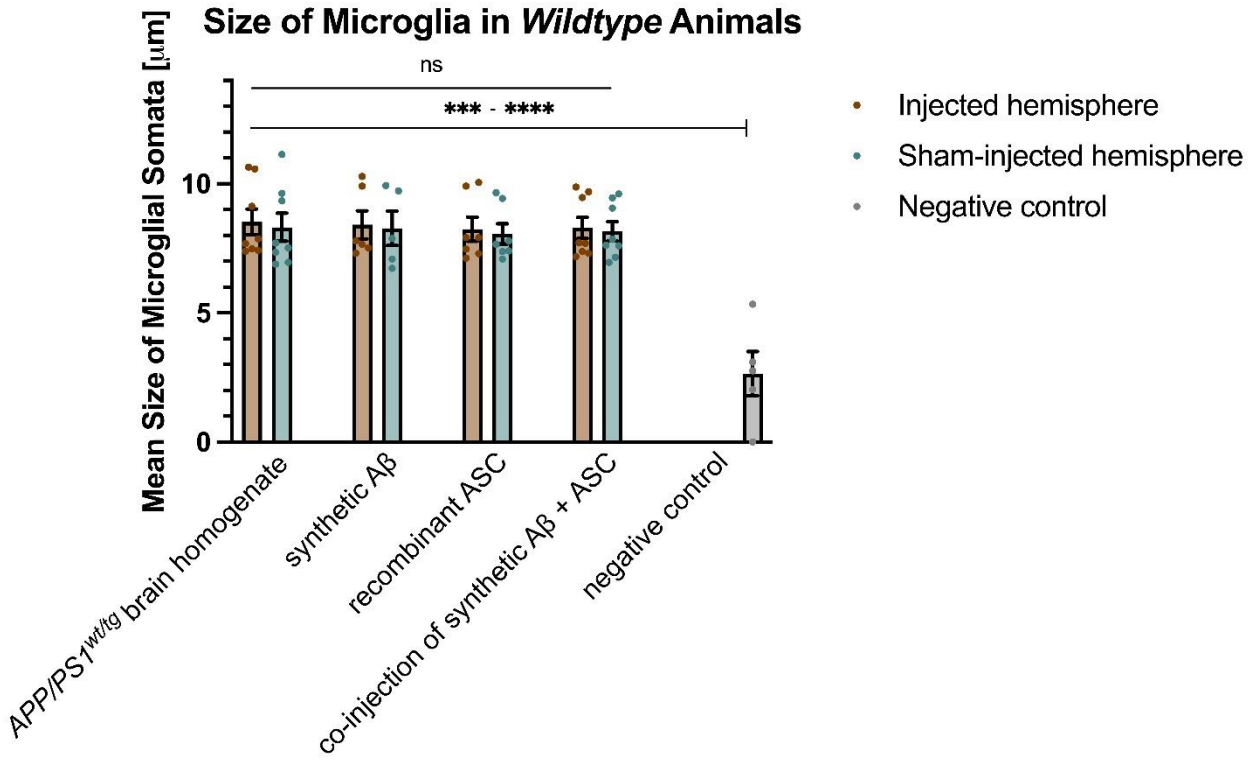

Fig. 17: Average Size of Microglial Perikarya in *Wildtype* Animals. The size of individual microglial perikarya was measured per ROI and converted to mm, and an average size per microglia was defined for each mouse, represented by one dot. The mice were grouped according to their experimental setting of intrahippocampal injection with either *APP/PS1*$^{wt/tg}$ brain homogenate (n = 8), synthetic Aβ (n = 6), recombinant ASC (n = 7), co-injection of synthetic Aβ and ASC (n = 8), and the respective sham-injected hemispheres. Left hemispheres of each animal (brown bars) had been injected with one of the above-mentioned solutions, right hemispheres (blue bars) had been sham-injected with vehicle only. Sections exclusively stained with the secondary antibody (n = 5) were included as negative controls of background fluorescence (grey bar). Independently of the experimental treatment, microglial perikarya were of similar size (ns); signifying a similar level of neuroinflammation induced by all experimental injections. In all injected and sham-injected groups significantly larger-sized signals were detected as compared to the negative control group. Experimental groups were compared using two-way ANOVA statistical analysis with a Tukey post hoc test (***$p < 0.001$ and ****$p < 0.0001$). Vertical lines of the significance bars indicate the referral of the asterisk to one specific bar whereas horizontal lines without vertical offspring refer to all bars covered. Figure created with GraphPad Prism.

3.6 Ambiguous Specificity of Anti-ASC Antibodies

ASC protein and specks locate in close proximity to amyloid signals (Friker et al., 2020). Particularly in *APP/PS1*$^{wt/tg}$ mice, ASC proteins cluster in the centre of β-amyloid plaques

(Venegas et al., 2017). The recombinant ASC protein used for intrahippocampal injection in mice was expressed from a human ASC cDNA. In theory, this setting could allow to differentiate clusters that contain exogenously injected human ASC from clusters that are exclusively formed with endogenous murine ASC. To this end, the following primary anti-ASC antibodies were applied for immunohistochemical studies: Antibody AL177 (Adipogen) and 10500-1-AP (Proteintech) cross-react with human and murine ASC, antibody D2W8U (Cell Signaling Technology) detects only murine ASC, and antibody E1E3I (Cell Signaling Technology) detects only human ASC.

Physiologically, endogenous ASC protein is omnipresent throughout the entire murine brain and becomes more detectable in neuroinflammation sites. With the help of the primary antibody AL177, ASC was detected in immunohistochemistry of injected *wildtype* mice (Fig. 18).

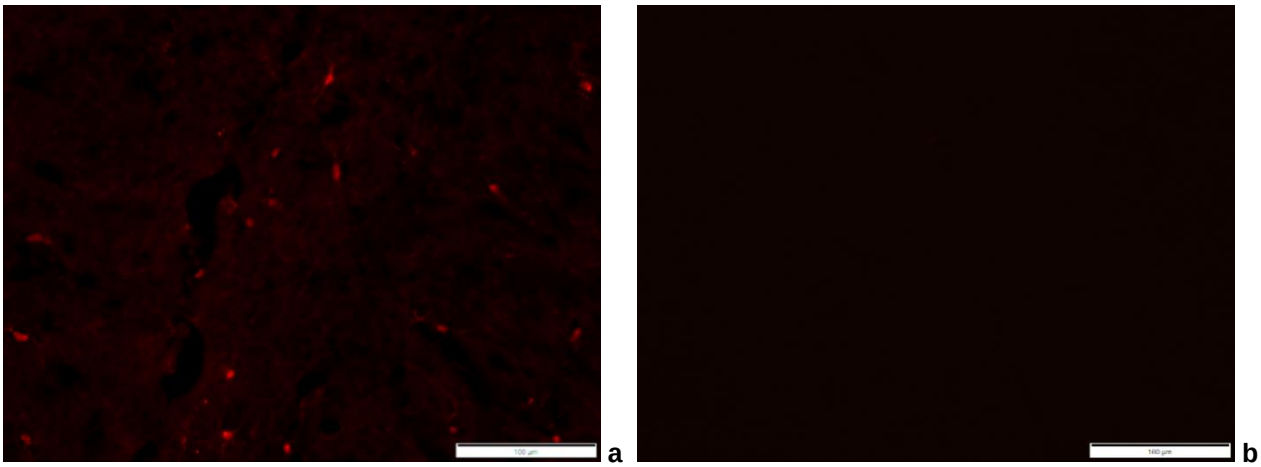

Fig. 18: Endogenous ASC Protein is Omnipresent in the Murine Brain. Staining brains of *wildtype* mice having received an injection of recombinant ASC protein with AL177 anti-ASC antibody reveals a broad distribution of ASC signals (a, red). In contrast to this, the negative control, which consists of the application of AL177 antibody on ASC *knockout (ko)* tissue (b), does not show any ASC. Images were captured on an Olympus microscope with a 20x objective.

However, further application of AL177 anti-ASC antibody on more brain slides raised doubts on its specificity. ASC is supposed to also be located in the core of Aβ plaques, yet in our stainings we only found ASC signals (red) surrounding the green plaques (Fig.

19a). Three-dimensional computer reconstruction of Z-stack images of the Aβ plaques and ASC confirmed this positioning towards each other (Fig. 19b).

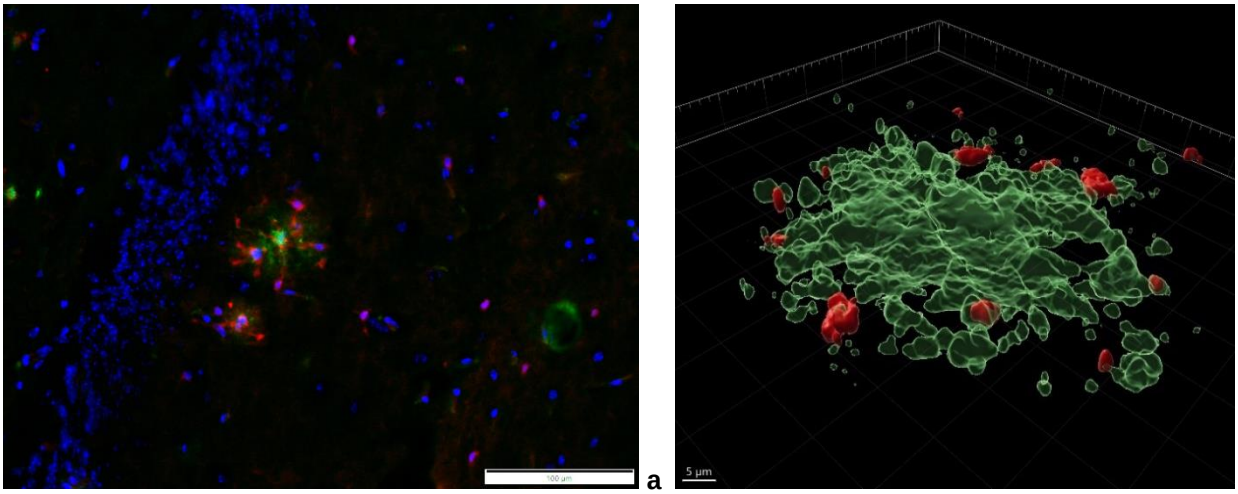

Fig. 19: Amyloid β Plaque Surrounded by ASC Specks, Stained with AL177 anti-ASC Antibody. Immunofluorescent microphotographs after application of the anti-ASC antibody AL177 (red), the anti-6E10 antibody (green) and the DNA dye DAPI (blue). The stained brain tissue originates from *APP/PS1*$^{wt/tg}$ mice. Cell nuclei (blue) in close proximity to the amyloid plaque (green) are accompanied by ASC specks (red) (a). ASC specks are essential co-factors of the β-amyloid pathology. Close-up three-dimensional reconstruction of an amyloid plaque (b) leads to the identical conclusion of ASC proteins assembling in peripheral areas of the plaque. Images captured on Olympus and Leica microscopes with 20x and 63x oil objectives.

Staining brains of mice from an *APP/PS1*$^{wt/tg}$ genetic background with a different anti-ASC antibody results in similar findings: The application of 10500-1-AP (Proteintech) anti-ASC antibody shows ASC signals (magenta) assembling outside of amyloid (green). Microglial cell bodies (red), stained with anti-Cd11b antibody, occur in close proximity to Aβ signals.

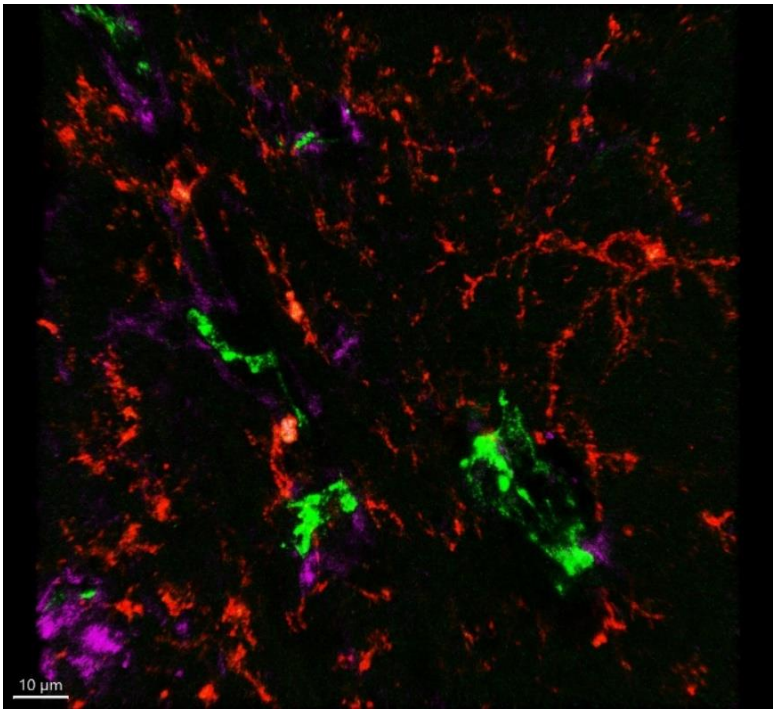

Fig. 20: Amyloid Signals Surrounded by ASC Specks, Stained with 10500-1-AP anti-ASC antibody. Application of a different anti-ASC antibody (10500-1-AP) reveals ASC signals (magenta) in the periphery of Aβ (green). The microphotograph further contains a microglial staining with anti-Cd11b antibody (red). Images were captured on a Leica microscope with a 63x oil objective.

Closely zooming in on the “ASC” signals (red) reveals their morphology: A circular main part of the signal can be differentiated from weaker ramifications. These characterised immunohistochemical signals rather indicate that the present batch of AL177 anti-ASC antibody is not specific for extracellular ASC protein only but also detects ASC specks within microglial cells.

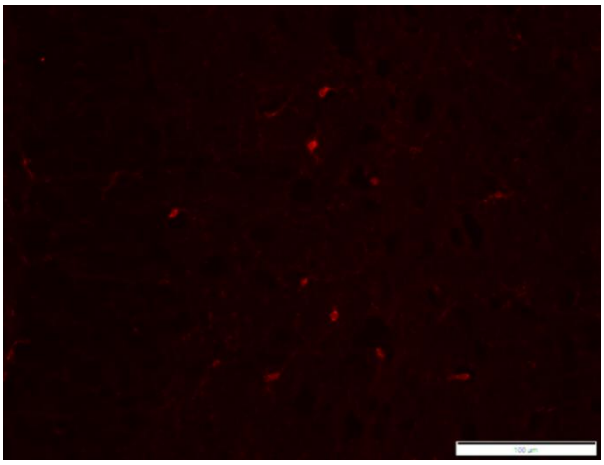
a

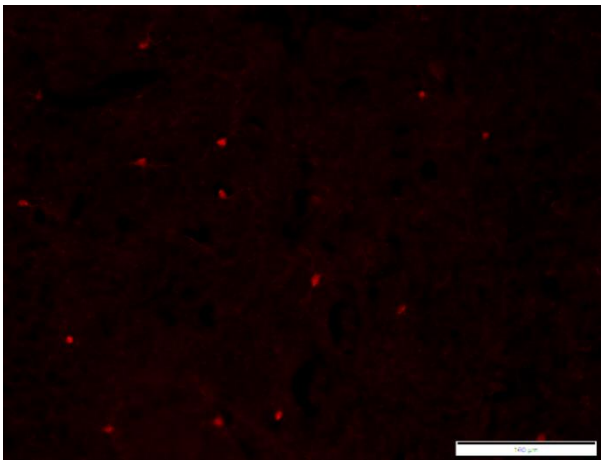
b

Fig. 21: AL177 anti-ASC Antibody Detects Extracellular ASC Protein and ASC Specks within Microglia. Representative microphotographs of *wildtype* mice having been injected with ASC (a) and *APP/PS1*$^{wt/tg}$ brain homogenate (b) and stained with AL177 anti-ASC antibody. Once taking a closer look at the detailed shape of the ASC signals (red), they remind of microglia with their huge cell body and thin ramifications. Images captured on an Olympus microscope with a 20x objective.

Despite exploring a wide range of experimental conditions (dilutions of primary and secondary antibodies, buffer conditions, incubation periods), we were unable to detect the exogenously injected human ASC using the anti-human ASC-specific primary antibody E1E3I (Fig. 22). The aim was to differentiate the injected ASC from the mouse-endogenous ASC. No signals were detectable in immunofluorescence microscopy.

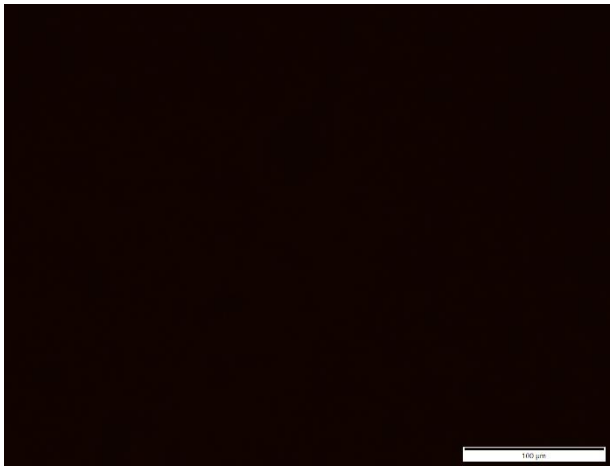

Fig. 22: No ASC Signals Definable after Staining with E1E3I anti-ASC Antibody. Application of a further anti-ASC antibody (E1E3I) failed in staining ASC proteins. No Signals are detectable after the staining. Image captured on an Olympus microscope with a 20x objective.

As a detection method of endogenous murine ASC, D2W8U anti-ASC antibody was tested on *APP/PS1*$^{wt/tg}$ animals. This antibody was compared to the signals obtained after application of AL177 anti-ASC antibody. When taking into account Aβ plaques of comparable size and shape, the portrayed inflammatory reaction surrounding the plaque was larger when stained with AL177 than with D2W8U anti-ASC antibody: more ASC signals were detectable distributed over a larger surface area (Fig. 23).

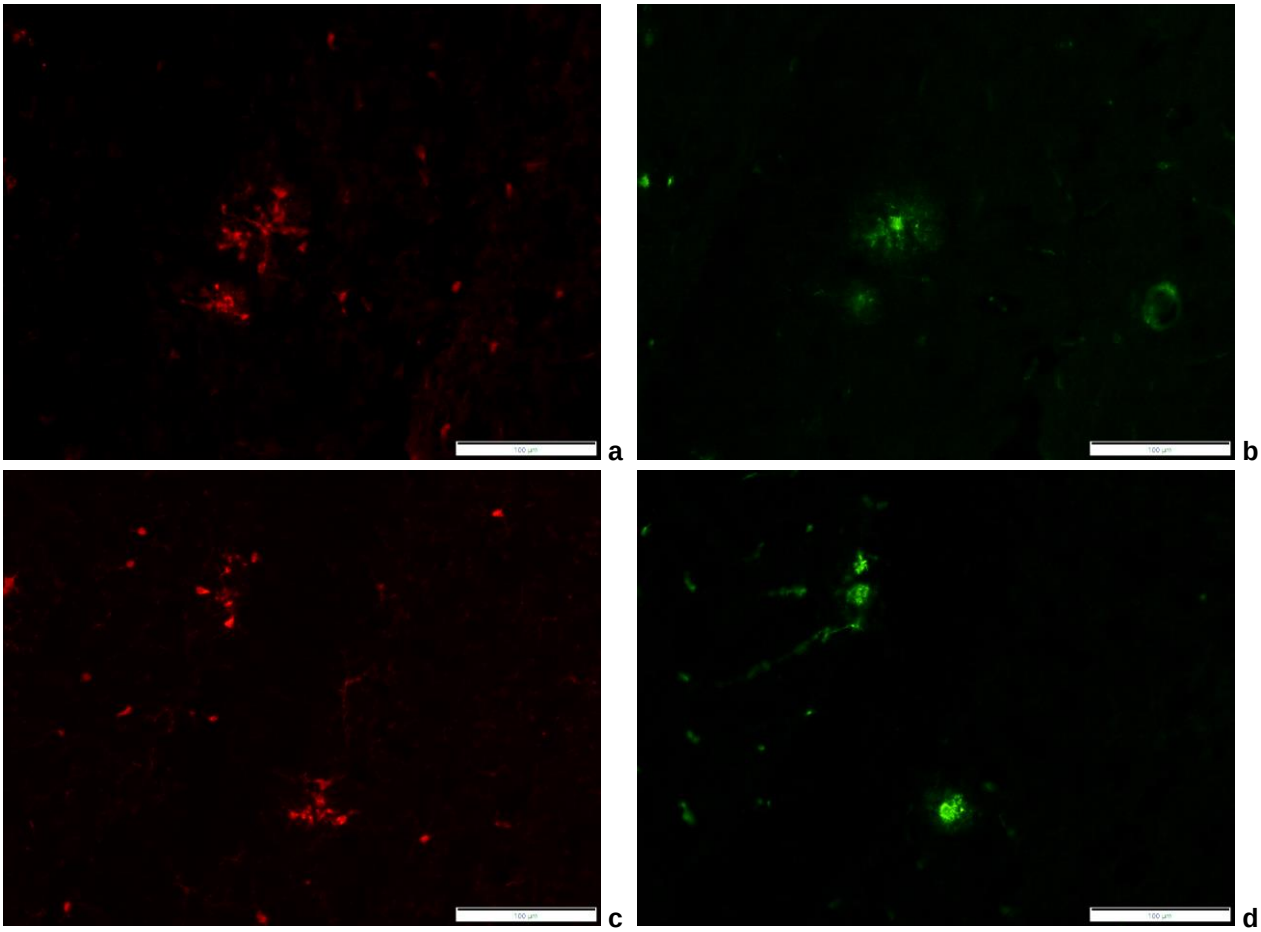

Fig. 23: Direct Comparison of the Anti-ASC Primary Antibodies AL177 and D2W8U. Hippocampal tissue sections from *APP/PS1*$^{wt/tg}$ mice developing amyloid plaques (green) similar in size and shape after intrahippocampal co-injection of ASC and Aβ were stained using the antibodies 6E10 (Aβ, green, b and d) and two anti-ASC antibodies (red, a and c). In theory, the antibody AL177 (a) detects murine as well as injected human ASC. The antibody D2W8U (c) specifically detects murine ASC as part of the NLRP3 inflammasome. Representative images covering the identical ROIs of the exact same mouse, yet the microscopic immunofluorescent channels differ. Following incubation with the anti-ASC primary antibodies, ASC specks (red) are detected as clusters in close proximity to amyloid plaques (green). Using the D2W8U primary antibody (c, only detecting endogenous, murine ASC) results in a reduced ASC speck signal in proximity to the Aβ plaques, as compared to the images acquired with AL177 primary antibody (a, detecting human and murine ASC). Representative images captured on an Olympus light microscope with a 20x objective.

3.7 Heterogeneity of ASC Signals in Relation to Intrahippocampal Treatment in *APP/PS1$^{wt/tg}$* Mice

Comparing ASC stainings in differently injected *wildtype* mice, the development of different morphologies of ASC-containing clusters was observed by immunofluorescence analysis of hippocampal sections from *APP/PS1$^{wt/tg}$* animals using the primary anti-ASC antibody AL177. Since applying the identical antibody on differently injected brains, direct comparability is given. Increased quantity and fluorescence intensity of ASC signals was observed in brain sections from mice having received injections including recombinant human ASC (Fig. 24). In a representative measurement (n = 1), 55 ASC signals with a mean raw integrated intensity (RawIntDen) of 0.16 / nm per ROI were observed in an *APP/PS1$^{wt/tg}$* mouse injected with recombinant ASC alone. In contrast, a total of 29 ASC signals with a mean RawIntDen of 0.24 / nm were detected in another mouse being co-injected with recombinant ASC and synthetic Aβ. A representative *APP/PS1$^{wt/tg}$* mouse injected with brain homogenate from an *APP/PS1$^{wt/tg}$* mouse exhibited 20 ASC signals with a mean RawIntDen of 0.14 / nm per ROI.

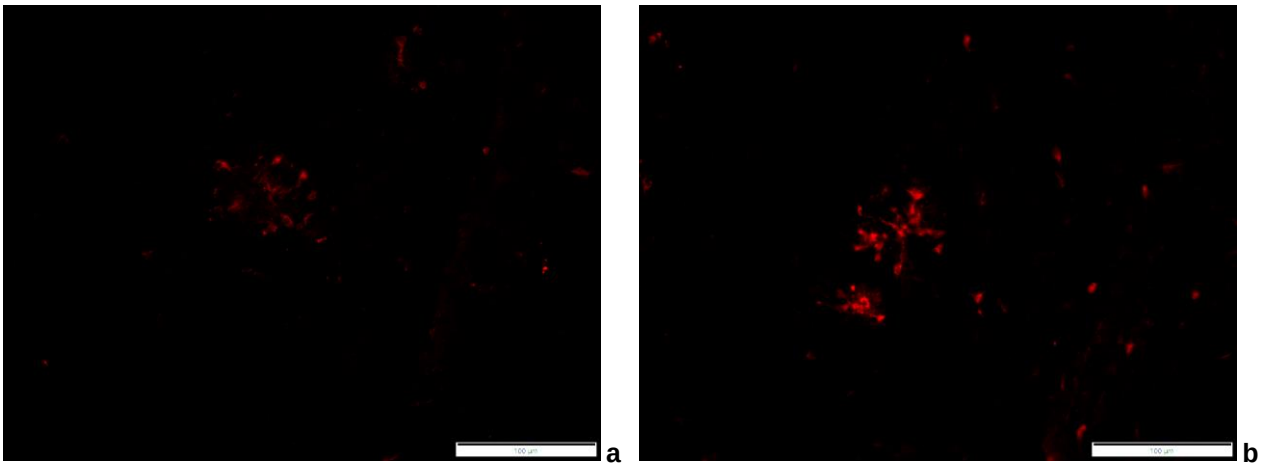

a **b**

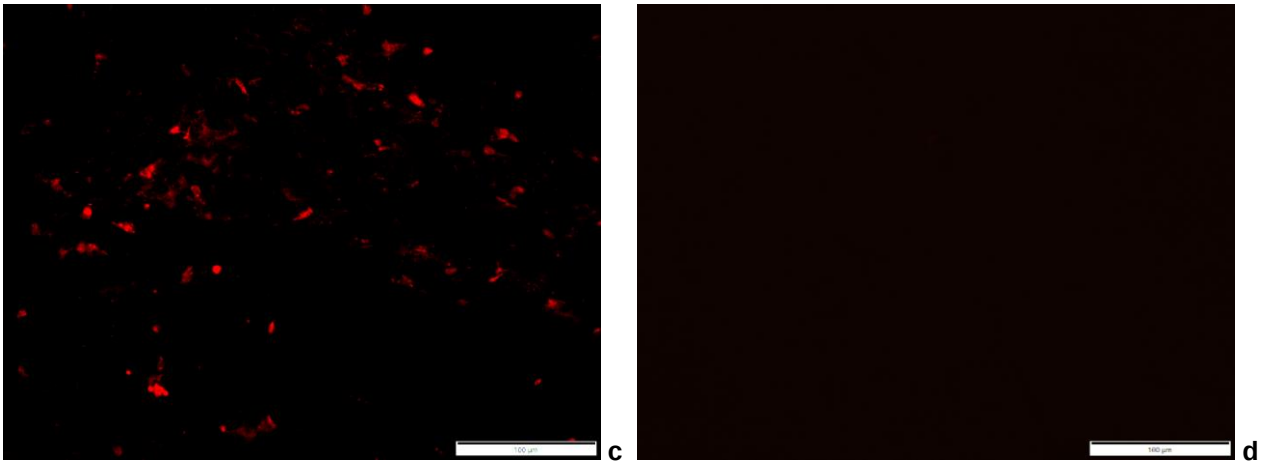

c d

Fig. 24: Heterogeneity of ASC Signals in Relation to Intrahippocampal Treatment in *APP/PS1*$^{wt/tg}$ Mice. Representative microphotographs of tissue sections from *APP/PS1*$^{wt/tg}$ mice injected with *APP/PS1*$^{wt/tg}$ brain homogenate (a), recombinant human ASC (b), or co-injected with recombinant ASC plus synthetic amyloid β (c). ASC-containing clusters (red) were detected by immunofluorescence using the primary anti-ASC (murine/human) antibody AL177. The quantity and intensity of ASC signals is higher in brains that have received an injection including recombinant ASC (b, c). Applying all three anti-ASC antibodies (AL177, D2W8U, E1E3I) no ASC signals were detected in tissue sections from an ASC *knockout (ko)* mouse serving as negative control (d). Representative images were captured on an Olympus light microscope with a 20x objective.

3.8 Orthogonal Biochemical Approach to Detect Amyloid β Signals and ASC-Amyloid β Composites

The induction of ASC-Aβ complexes by intrahippocampal co-injection of recombinant ASC plus Aβ or by *APP/PS1*$^{wt/tg}$ brain homogenate (positive control), but not by ASC alone or Aβ alone, was reproducibly detected using established immunofluorescence microscopy. In order to orthogonally validate the induction of complex formation we explored the utility of co-immunoprecipitation. Brain tissue homogenates from *wildtype* mice injected with *APP/PS1*$^{wt/tg}$ brain homogenate (n = 2), synthetic Aβ (n = 2), recombinant ASC (n = 3), or co-injected with synthetic Aβ and ASC were prepared (n = 2). For immunoprecipitation we used the primary anti-ASC antibody AL177, since it proved to be the most sensitive antibody at immunohistochemistry. After pulldown of AL177-bound protein complexes, we tried to detect Aβ (using the primary antibody 6E10) and human recombinant ASC (using the primary antibody D2W8U) by immunoblotting. Special attention was paid to signals occurring at a molecular weight of approx. 17 kDa, around which range Aβ oligomers can be located (Friker et al., 2020).

In the group having received intrahippocampal co-injection of synthetic Aβ and ASC we detected an increased intensity of the amyloid signals after immunoblotting with 6E10 antibody (Fig. 25a). This finding supports the hypothesis, that higher amount of Aβ, especially in formations of oligomers at around 17 kDa, developed in hippocampal lysates after co-injection of ASC and synthetic Aβ in comparison to after injection of recombinant ASC or synthetic Aβ alone.

Specifying the amount of ASC protein in the brain homogenates with AL177 antibody, no differences were detected between the injection groups. Amyloid seems to mainly be present in the brain lysates as homologous aggregates rather than as heterogenous clusters as in ASC-Aβ clusters.

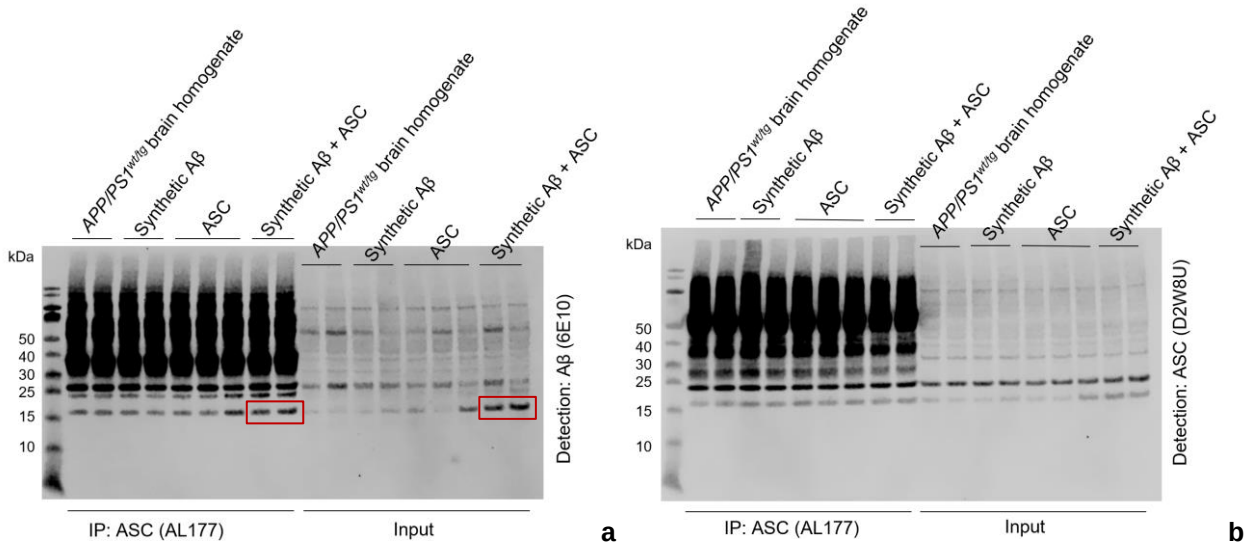

Fig. 25: Co-Immunoprecipitation of Differently Injected Brain Lysates lead to an Increase of Aβ Signal Intensity after Co-Injection of ASC and Aβ. Immunoprecipitation was performed with AL177 anti-ASC antibody on hippocampal lysates of *wildtype* mice having been injected with either brain homogenate of *APP/PS1*$^{wt/tg}$ mice (n = 2), synthetic Aβ (n = 2), recombinant ASC (n = 3) or co-injected with recombinant ASC plus synthetic Aβ (n = 2). As a detection method, anti-amyloid antibody 6E10 (a) and anti-ASC antibody D2W8U (b) were chosen. A higher intensity of Aβ signals can be detected in hippocampal brain lysates having been co-injected with ASC and Aβ, represented by an intensified band around 17 kDa (a, red box). Highest amounts of amyloid aggregates, especially as oligomers, are present in the brain lysates after co-injection of recombinant ASC and synthetic Aβ. Similar amounts of ASC and amyloid protein were detected in the other experimental groups.

Immunoblotting was performed on differently injected hippocampal lysates applying 6E10 anti-amyloid and D2W8U anti-ASC antibodies. Each row represents the amount of Aβ or, respectively, ASC in one mouse. Both blots revealed intensified signals around a molecular weight of 17 kDa in the group of mice having been co-injected with ASC and Aβ (Fig. 26, red and blue boxes, n = 5). Zooming in on the marked red areas (Fig. 26a) revealed a further but less bright band at around 25 kDa, representing also a higher prevalence of slightly larger amyloid aggregates after co-injection of ASC and synthetic Aβ. Not every single mouse demonstrated this correlation, though the majority of the injected mice (3 out of 5) confirmed the hypothesis that co-injection of ASC and synthetic Aβ leads to enhanced Aβ (Fig. 26a) and also ASC (Fig. 26b) development as compared to the remaining injection groups.

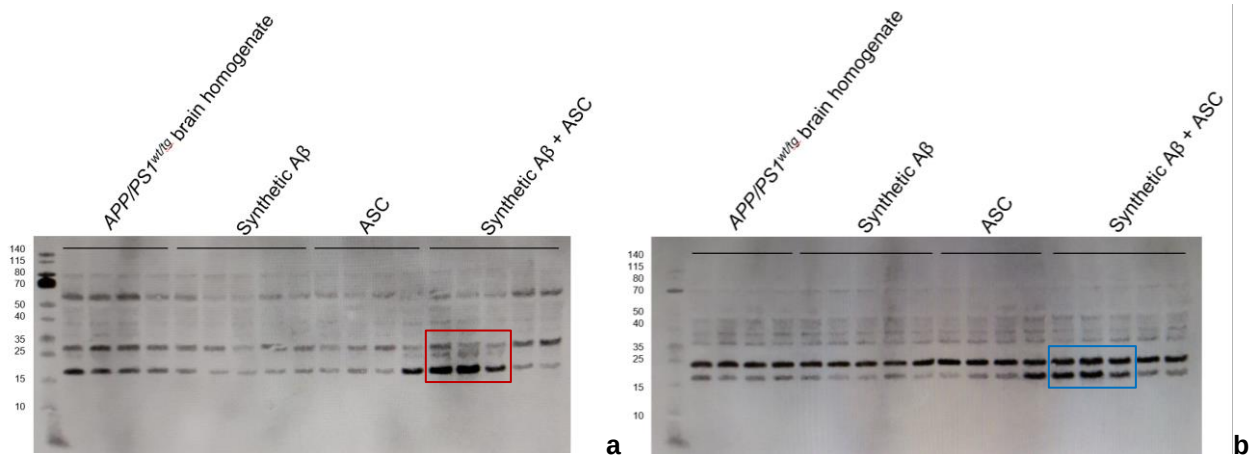

Fig. 26: Western Blots of Differently Injected Brain Lysates Revealed an Increase of Aβ and ASC Signals after Co-Injection of ASC and Synthetic Aβ. Immunoblotting was performed with 6E10 anti-Aβ antibody (a) and with D2W8U anti-ASC antibody (b) on hippocampal lysates of *wildtype* mice having been injected with either brain homogenate of *APP/PS1*$^{wt/tg}$ mice (n = 4), synthetic Aβ (n = 5), recombinant ASC (n = 4) or co-injected with recombinant ASC plus synthetic Aβ (n = 5). At molecular sizes of around 17 and 25 kDa enhanced Aβ signals were revealed after co-injection of ASC with synthetic Aβ (red box, a). Comparably, intensified ASC signals became visible in the co-injection group after immunoblotting with anti-ASC antibody (blue box, b). Similar amounts of amyloid and ASC protein were detected in all other experimental groups.

3.9 No Gender Differences were detected in Amyloid Stainings of *Wildtype* Mice

Each group contained mice from mixed gender, comprising a total of 13 female (Fig. 27, ochre bars) and 16 male (Fig. 27, blue bars) mice distributed over the different injection

groups for immunohistochemical staining. There were 3 female and 5 male mice in the group having been injected with brain homogenate of *APP/PS1*$^{wt/tg}$ mice. Comparing the number of Aβ signals/mm^2 in this group revealed almost no difference between females and males with a p-value of > 0.9999: 156.6 ± 24.4 (mean ± SEM) in female (n = 3) and 153.2 ± 41.2 (mean ± SEM) in male (n = 5) mice. There was only n = 1 female mouse having received an injection of synthetic Aβ alone, which showed 29.9 Aβ signals/mm^2, whereas the mean value of Aβ signals/mm^2 in the male group (n = 5) was 60.5 ± 14.4 (mean ± SEM). The p-value of 0.9795 reveals no statistical significance between the genders in this injection group either. In a total of 3 female and 4 male mice 59.8 ± 9.7 (mean ± SEM) and respective 36.7 ± 8.4 (mean ± SEM) Aβ signals/mm^2 were found after the injection of recombinant ASC alone (p = 0.9728). Female mice co-injected with ASC and synthetic Aβ counted up to 143.8 ± 21.9 (mean ± SEM, n = 6) Aβ signals/mm^2 and 114.0 ± 63.0 (mean ± SEM, n = 2) Aβ signals/mm^2 in the corresponding male group (p = 0.9473).

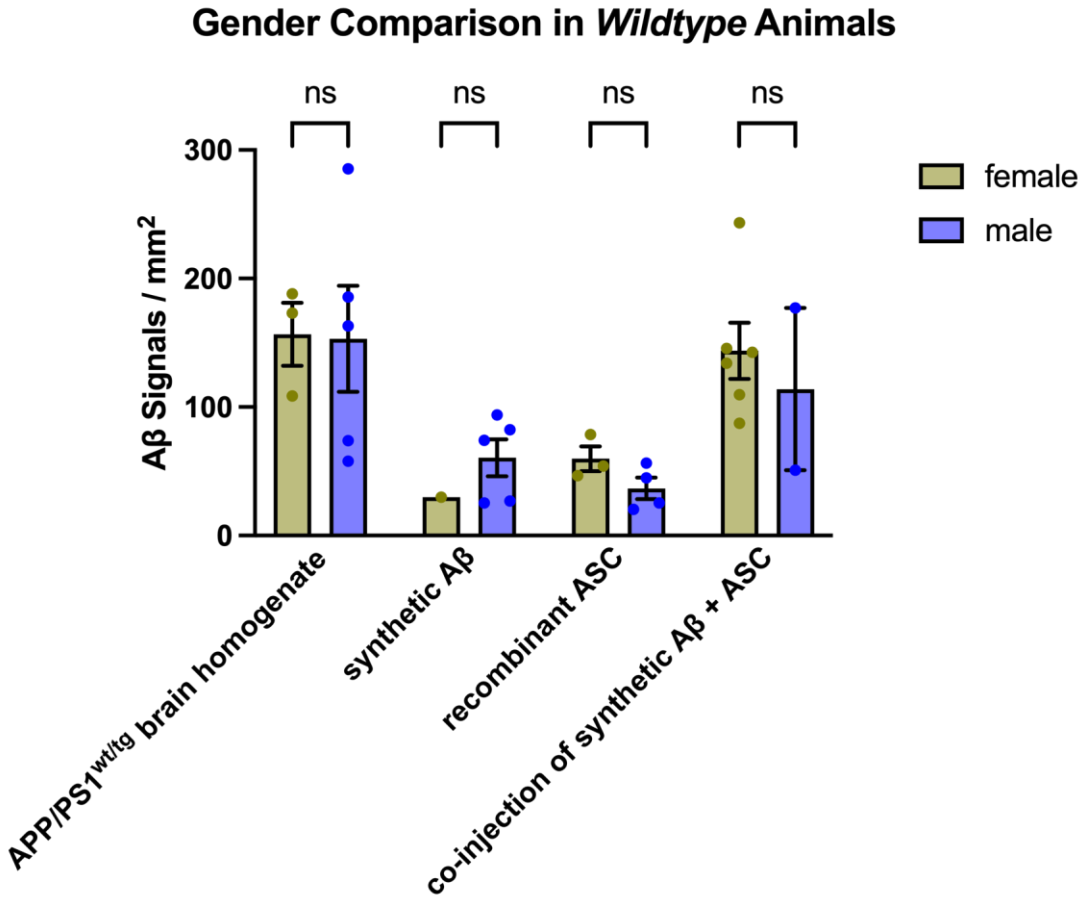

Fig. 27: Gender Comparison in *Wildtype* Animals. Distribution of the counted Aβ signals/mm^2 between a total of 13 female (ochre bars) and 16 male (blue bars) mice in the different injection groups for immunohistochemical staining of *wildtype* mice. 3 female and 5 male mice were injected with brain homogenate of *APP/PS1$^{wt/tg}$* mice, whereas the injection group with synthetic Aβ alone comprised 1 female and 5 male mice. Recombinant ASC was injected into 3 female and 4 male animals and the group co-injected with ASC and synthetic Aβ consisted of most animals: 6 female and 2 male mice. Independently of the type of injection, no statistically significant gender differences were elaborated (p-values between $p = 0.9473$ and $p > 0.9999$). Differences between groups were compared using two-way ANOVA analysis with a Tukey post hoc test. Vertical lines of the significance bars indicate the referral to one specific bar. Figure created with GraphPad Prism.

4. Discussion

Understanding the molecular pathophysiology of AD holds promise to identify rational approaches for targeted treatments of this devastating disease. Since AD is characterized by the extracellular deposition of Aβ fibrils and plaques, these were the first to be selected as a therapeutic target for antibody treatment. Several anti-amyloid antibodies (e.g. crenezumab, solanezumab) have been studied in large clinical trials, which failed in terms of detectable clinical efficacy (Huang et al., 2020). Only recently, the monoclonal antibody lecanemab was the first to demonstrate moderate efficacy in terms of delaying the decline of cognitive functioning in patients with early stage AD (van Dyck et al., 2023). While this first success certainly spurs optimism, there still is much room for further developments.

An alternative strategy to antibody treatment of Aβ plaques/fibrils themselves is to target pathophysiological processes that are essentially involved in formation of AD plaques. Observations from experimental AD models as well as correlative analyses in biospecimens from AD patients strongly suggest a central role for inflammatory signalling in AD pathophysiology. In particular, the formation of the NLRP3 inflammasome was identified as an essential step in triggering signalling, that results in more rapid Aβ seeding and spreading. Accordingly, essential components of the NLRP3 inflammasome may serve as molecular targets for rational development of therapies aiming at reduction (or even prevention) of the chronic neuroinflammation and subsequent formation of Aβ plaques in AD.

Given this background, this thesis aimed to systematically explore the contribution of ASC, an essential component of the NLRP3 inflammasome, to the development of early pathology in an established murine model of the amyloid pathology. In addition to ASC, the NLRP3 inflammasome is composed of NLRP3 and pro-caspase-1. ASC serves as an adaptor for the recruitment of pro-caspase-1 into the inflammasome, in which the latter is activated and cleaves inflammatory cytokines into their active products.

Using intrahippocampal injections in *wildtype* mice, we found that co-injection of recombinant ASC and synthetic Aβ was able to induce the formation of Aβ “pre-plaques”. These were indistinguishable from Aβ “pre-plaques” induced by the injection of brain homogenates from *APP/PS1*$^{wt/tg}$ mice serving as positive control. Intrahippocampal

injection of synthetic Aβ alone, or ASC alone, were unable to induce this specific pathology. From this original finding it can be concluded that ASC is an essential co-factor in the induction of an early step in AD pathophysiology. Interestingly, the induction of Aβ “pre-plaques” occurred independently of a detectable increase in recruitment of microglial cells. This may point towards the activation of pathological signalling without the necessity to attract a much larger quantity of additional immune cells to the sites of plaque formation. Alternatively, this observation may result from the experimental setting. Stereotactic intrahippocampal injection of exogenous proteins or tissue homogenates themselves may induce such a strong inflammatory reaction that no further recruitment of microglial cells is triggered by the co-injected ASC plus Aβ. Also, since the analysed images were two-dimensional or have a third (z) dimension with a maximal thickness of 8-10 µm, imaged microglial somata might have been cut at the margin and not in the position of the largest diameter.

Interestingly, in immunohistochemistry experiments, great versatility of amyloid accumulation was identified: Aβ assembled as extracellular clusters, as described above, and parallel to as well as inside of blood vessels and inside of microglial cells. Soluble amyloid proteins are transported between the interstitium of the brain and systemic blood stream via endothelial cells. This pathophysiologic traverse of Aβ across the blood brain barrier (Prakash et al., 2021; Hampel et al., 2021) was seen in our microscopic analysis (Fig. 13). In order to combat the pathogen Aβ through phagocytosis, microglial uptake occurs (Gallego Villarejo et al., 2022), which sporadically leads to an intramicroglial location of Aβ (Fig. 14).

Reliable staining protocols as with anti-Iba1 (microglial) or anti-6E10 (amyloid) antibodies are not yet established and the antibodies’ specificities are under debate. Additional antigen retrieval might be necessary to visualize ASC protein and specks also inside the core of the amyloid plaques. The non-detection of human ASC after application of E1E3I anti-ASC antibody (human) might be explained by the insufficient sensitivity of immunofluorescence microscopy to detect the relatively small amount of recombinant ASC that was stereotactically injected into the hippocampal regions of our experimental animals.

Female mice of an *APP/PS1*$^{wt/tg}$ genetic background develop more amyloid plaques than their male litter mates (The Jackson Laboratory, 2022). Nonetheless, in our *wildtype* mice having been injected with *APP/PS1*$^{wt/tg}$ brain homogenate, synthetic Aβ, ASC or co-injected with synthetic Aβ and ASC no statistically significant Aβ quantity could be detected between the two genders. After all, gender-wise division of the groups decreased total quantity of mice per group and therefore diminishes its informative value. Further, the gender disparity in β-amyloid burden becomes relevant between 6 and 15 months of age (The Jackson Laboratory, 2022), signifying our mice might have developed further gender differences at a later timepoint. Also, literature references account for mice of an *APP/PS1*$^{wt/tg}$ genetic background, whereas our experiments mainly were performed on *wildtype* mice.

The strength of this work is the convincing demonstration of an essential role of ASC in the induction of early amyloid pathology in an injected *wildtype* mouse model. The validity of this observation is supported by the application of extensive positive and negative controls as well as complementing approaches to image analysis. The potential weakness of this work lies in the insignificant demonstration of the formation of complexes containing the exogenously injected ASC and Aβ by orthogonal biochemical assays. The majority of analysed brain homogenates revealed intensified Aβ signals aggregated to formations of oligomers supporting the results obtained in immunohistochemical analyses. However, this trend was not confirmed in every single mouse and therefore not considered as statistically significant. This may be inherent to the low quantity of analysed brain homogenates and to the relative discrete pathology induced in this model representing an early step in AD pathophysiology, at which preliminary stages of Aβ aggregates like clusters of amyloid monomers, oligomers and fibrils occur.

Nevertheless, the original results obtained in this thesis using relevant animal models of AD strongly support the idea that ASC is an essential contributor to AD pathophysiology. Clinically, this early disease stage described in our model may be particularly promising for early therapeutic interventions. Hence, ASC may serve as target for novel drug development approaches towards negatively modulating Aβ seeding and spreading in early-stage AD. As ASC behaves intra- and extracellularly, a straightforward antibody approach is a possible mean to attack this inflammasome-related protein. However,

further potential pharmacotherapeutic strategies might include antisense or shRNA approaches to also deplete endogenous ASC, or small, cell-permeable molecules that interfere with protein-protein interactions of ASC that are essential steps in formation of the NLRP3 inflammasome complex.

As innate inflammatory signalling serves a purpose in defending the host against various pathogens, the therapeutic window of such anti-inflammatory treatment strategies of AD will have to be carefully defined. Alternatively, a regional drug delivery approach to the cerebrospinal fluid could be explored, which may result in highest drug levels and thus activity in the brain, the most relevant organ of AD pathophysiology, while drug levels in the periphery remain lower to prevent systemic adverse events along with immune suppression.

Before the findings from this thesis can be translated into therapeutic strategies, confirmatory studies should be considered. These could include co-injection experiments of synthetic Aβ plus additional components of the NLRP3 inflammasome to explore whether ASC is the sole potential therapeutic target. Further relevant injection experiments would be brain homogenate of *APP/PS1*$^{wt/tg}$ mice and co-injection of ASC and synthetic Aβ along with an anti-ASC antibody. Importantly, alternative experimental approaches should be undertaken to confirm that exogenous ASC in fact triggers a specific effect and is integrated into inflammatory complexes with endogenous proteins. As conventional western blotting seems to lack the sensitivity that is required to detect exogenous ASC in such native complexes, mass spectrometry and/or radiolabelling might serve this purpose. The dissection of the mouse brains could be modified in a way that not the whole hippocampus but the region immediately surrounding the injection site is harvested for molecular analyses. This effort to reduce background signal might enhance the sensitivity of the assays. Alternatively, the injection of larger volumes or higher peptide concentrations into the mouse brains could be considered. However, this could have adverse effects on the experimental mice during the monthlong incubation period. A longer incubation time of 5 up to 7 months after intrahippocampal injection may be another way to generate enhanced pathology that can be detected by biochemical or other assays. For the purpose of examining phenotypic differences between all eight experimental

groups, animal behaviour experiments could be performed with experimental mice of the different injection groups.

In summary, this thesis work has provided evidence in murine AD models that ASC may be an essential factor in the early steps of Aβ plaque formation, a key feature of AD. It is hoped that these findings may contribute to a more precise understanding of AD pathophysiology, which may ultimately support the development of effective prevention and treatment strategies of this terrible disease.

5. Summary

Histopathologically and molecularly, AD is characterized by the deposition of extracellular amyloid β (Aβ) fibrils and plaques as well as intraneuronal aggregation of neurofibrillary tau tangles in the brain. Recent studies suggest a pivotal role of neuroinflammation, particularly activated innate immunity signalling, in AD pathophysiology. At a molecular level this is initiated by the formation of supramolecular complexes called inflammasomes. The NACHT-, LRR-, and pyrin domain (PYD)-containing protein 3 (NLRP3) inflammasome complex is formed by NLRP3, caspase-1 and apoptosis-associated speck-like protein containing a CARD (ASC). Recently, the NLRP3 inflammasome has been implicated as central regulator of Aβ-induced pathology of AD. In AD, amyloid begins to accumulate in the hippocampal area and afterwards spreads throughout the entire brain following specific trajectories. In experimental models the injection of synthetic Aβ into the hippocampi of *wildtype* mice failed to seed and therefore did not lead to spreading of amyloid with the subsequent development of AD pathologies. From this observation it was concluded that additional factor(s) are required to trigger Aβ-seeding and inflammation-dependent spreading events. Recent work from our group has described a central role of ASC in NLRP3 activation in microglial cells *in vitro*. The aim of this thesis was to investigate *in vivo* whether ASC aggregates, called ASC specks, are necessary and sufficient co-factors to induce seeding and spreading of synthetic Aβ injected in murine brains.

Towards this end, *wildtype* (C57/BL6 strain) and transgenic *APP/PS1*$^{wt/tg}$ mice were treated by stereotactic intrahippocampal injections of synthetic Aβ, ASC, or co-injection of ASC and synthetic Aβ. As positive control we injected *APP/PS1*$^{wt/tg}$ brain homogenate. Readout systems for the presence or absence of seeding and spreading were histopathological and biochemical analyses of the hippocampi three months after the injections. By fluorescence immunohistochemistry we found a statistically significant increase of Aβ signals in *wildtype* animals co-injected with ASC and synthetic Aβ. Only upon co-injection of Aβ and ASC, but not upon injection of Aβ or ASC alone, we observed the formation of amyloid composites. These aggregates differed morphologically from the classical amyloid plaques developing in *APP/PS1*$^{wt/tg}$ mice. However, co-injection of ASC and Aβ fully reproduced the phenotype induced by intrahippocampal injection of brain

homogenates from *APP/PS1*$^{wt/tg}$ mice as demonstrated by automated image analyses. These “pre-plaques” most likely represent an early stage of plaque formation in AD pathophysiology. Microglial cells were recruited to the injection sites independently of the respective treatment group. In biochemical assays we could orthogonally confirm the enhancement of Aβ and recombinant ASC in hippocampal cell homogenates, but without statistical significance due to limitations in sensitivity of biochemical assays.

In summary, we have demonstrated a role of ASC specks as essential co-factor in early Aβ-induced AD pathophysiology *in vivo*. This supports a potential relevance of ASC as therapeutic target for novel approaches to treatment of this devastating neurodegenerative disease.

6. Supplementary Data

6.1 Direct Comparison of Amyloid β Signals in Verum-injected and Sham-injected Hemispheres

The data already described under “3.1 Results” and in Fig. 10 is repeated, each separate graph representing one injected substance with its respective sham-injection (Fig. A1). In this presentation asterisks clearly show a significant increase of Aβ signals in *APP/PS1*$^{wt/tg}$ homogenate-injected hippocampal hemispheres as well as in Aβ/ASC co-injected hemispheres as compared to their sham-injected hemispheres. Statistical significance is displayed as asterisks with *$p < 0.05$, **$p < 0.01$ and ns standing for not significant (Fig. A1). In n = 8 *APP/PS1*$^{wt/tg}$ homogenate-injected hemispheres a mean of 154.5 ± 25.9 Aβ signals/mm² (mean ± SEM) were detected (Fig. A1a). In n = 8 Aβ/ASC co-injected hemispheres averagely 136.3 ± 20.5 Aβ signals/mm² (mean ± SEM) were found (Fig. A1d). In contrast, hippocampal hemispheres injected with synthetic Aβ (55.4 ± 12.8 signals/mm², mean ± SEM, n = 6 (Fig. A1b)) or recombinant ASC (46.6 ± 7.4 signals/mm², mean ± SEM, n = 7 (Fig A1c)) showed similar mean numbers of Aβ signals as observed in all sham-injected hippocampal hemispheres (in total n = 28, 58.7 ± 4.9, mean ± SEM). The negative control group was treated only with secondary antibodies in immunohistochemical experiments and in n = 4 probes a mean of 52.6 ± 4.3 Aβ or rather background signals/mm² (mean ± SEM) were detected (Fig. A1).

The comparison of groups having received an intrahippocampal injection of *APP/PS1*$^{wt/tg}$ brain homogenate and a co-injection of synthetic Aβ and ASC with their respective sham-injected hemisphere reached statistical significance with a p value of $p = 0.0058$ and the latter of $p = 0.0052$, respectively (Tab. A1). In contrast, no statistically significant differences could be detected when comparing the groups having received an injection of either synthetic Aβ ($p = 0.5906$) or recombinant ASC ($p = 0.1055$) with their respective sham-injected hemispheres (Tab. A1). Statistics were computed with ordinary one-way ANOVA.

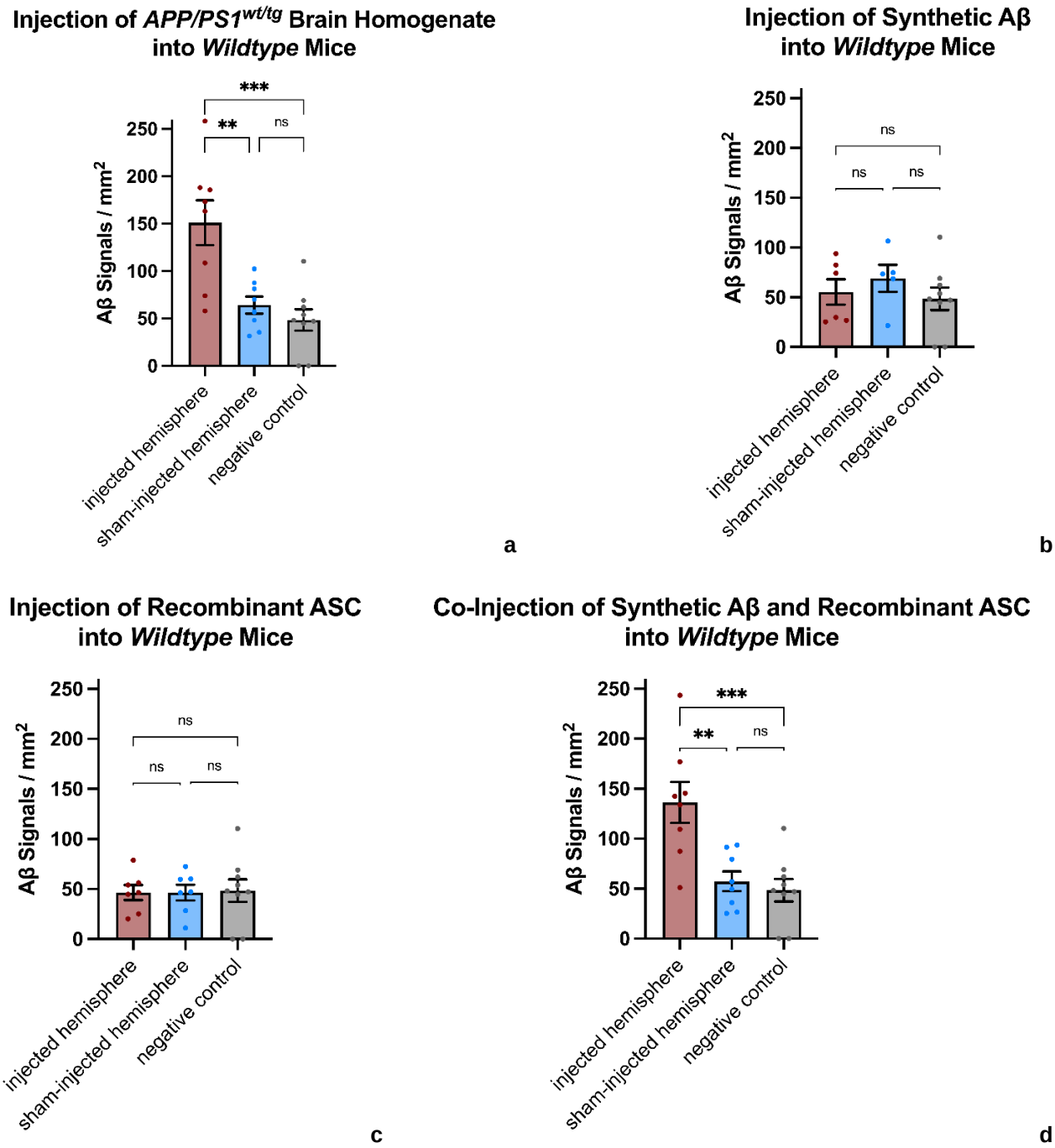

Fig. A1: Direct Comparison of Amyloid β Quantity in Injected Hemispheres with Corresponding Sham-injected Hemispheres. Significant differences between injected (red bars) and sham-injected (blue bars) hemispheres regarding the number of Aβ signals in *wildtype* animals can be seen in two groups: intrahippocampal injection of *APP/PS1*$^{wt/tg}$ brain homogenate (n = 8, p = 0.0058, Fig. A1a) and co-injection of ASC and Aβ (n = 8, p = 0.0052, Fig. A1d) lead to significantly more Aβ signals in contrast to their respective sham-injected hemispheres after ordinary one-way ANOVA statistical analysis. Statistical significance is displayed as asterisks with *p < 0.05 and **p < 0.01, ns standing for not significant. Figure created with GraphPad Prism.

Tab. A1: Ordinary One-way ANOVA of the Different Injection Groups in *Wildtype* Animals in Contrast to Respective Sham-injections. Comparisons of *wildtype* animals between the injected and respective sham-injected hemisphere and negative controls reveal significant differences in the groups injected with either *APP/PS1*$^{wt/tg}$ brain homogenate (p = 0,0058) or co-injected with synthetic Aβ and ASC (p = 0,0052), both groups highlighted with a red frame. Statistical significance is displayed as asterisks with **p < 0.01. Statistics computed with GraphPad Prism.

Ordinary one-way ANOVA	
wildtype animal injected with *APP/PS1*$^{wt/tg}$ brain homogenate, sham-injection and negative control	
ANOVA summary	
F	7.070
P value	0.0058
P value summary	**
Significant diff. among means (P < 0.05)?	Yes
R squared	0.4541

Ordinary one-way ANOVA	
wildtype animal injected with synthetic Aβ, sham-injection and negative control	
ANOVA summary	
F	0.5504
P value	0.5906
P value summary	Ns
Significant diff. among means (P < 0.05)?	No
R squared	0.08403

Ordinary one-way ANOVA	
wildtype animal injected with recombinant ASC, sham-injection and negative control	
ANOVA summary	
F	2.623
P value	0.1055
P value summary	ns
Significant diff. among means (P < 0.05)?	No
R squared	0.2591

Ordinary one-way ANOVA	
wildtype animal injected with synthetic Aβ and ASC, sham-injection and negative control	
ANOVA summary	
F	7.298
P value	0.0052
P value summary	**
Significant diff. among means (P < 0.05)?	Yes
R squared	0.4620

6.2 Representative Microphotographs of Hippocampal Sections from Treatment Groups and Controls in *Wildtype* Mice

Direct confrontation of exemplary microscopic images for each injection group visualises the development of comparable widely-distributed small Aβ assemblies in the left hemispheres having received an injection of either brain homogenate from *APP/PS1*$^{wt/tg}$ mice or a co-injection of recombinant ASC and synthetic Aβ (Fig. A2). This overview simplifies the evaluation of the Aβ signals' morphology, with particular emphasis on the contrast between Aβ assemblies developed in *wildtype* animals (as stated just above) and

in the positive control. The exemplary positive control image is a microscopic image of a mouse from an *APP/PS1*$^{wt/tg}$ genotype visualizing AD-typical Aβ plaques. Plaques are larger assemblies of Aβ, yet restricted to fewer loci than the Aβ signals detected after injections into *wildtype* animals. Aβ signals in left hemispheres having been injected with synthetic Aβ or recombinant ASC alone, in all sham-injected right hemispheres and in the negative control image can be described as unsteady background signals. The negative control images a brain slice of an injected mouse treated with secondary antibody only (Fig. A2).

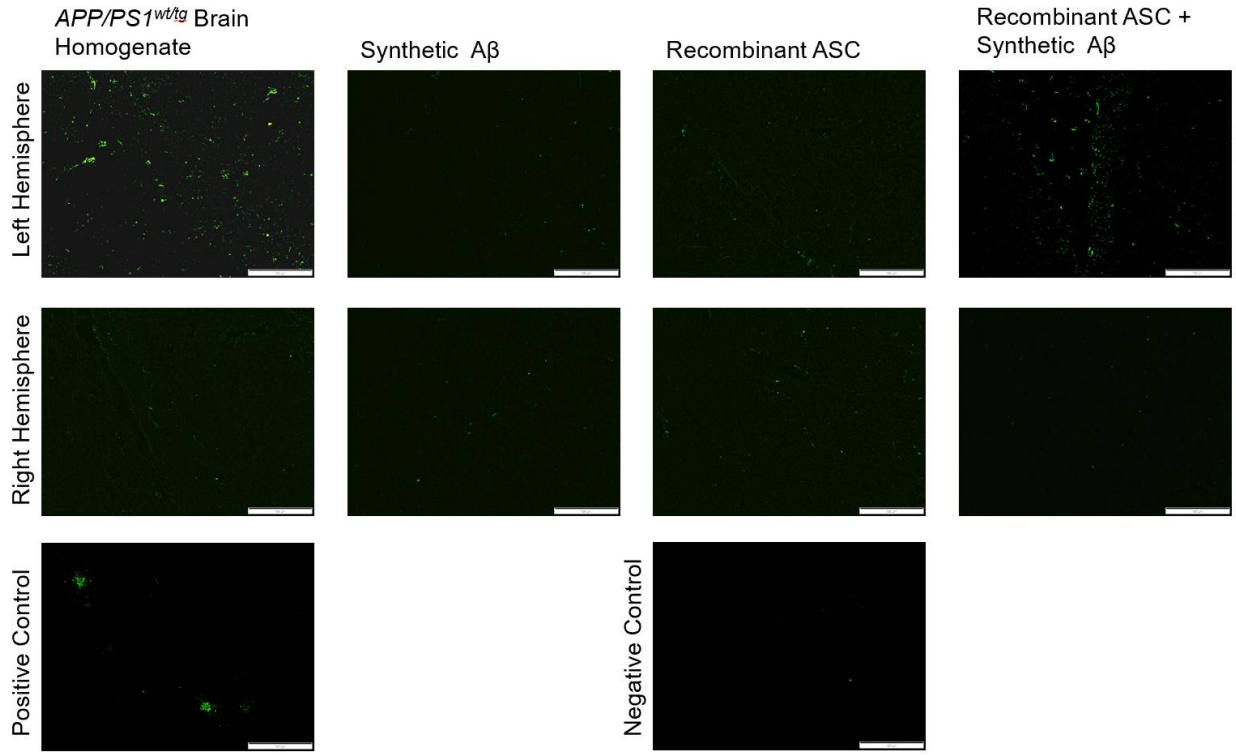

Fig. A2: Visualization of Amyloid β Signals in *Wildtype* Mice After Different Types of Intrahippocampal Injections. Reliable amyloid signals (green, 6E10) can be demarcated in *wildtype* animals after intrahippocampal injection of either *APP/PS1*$^{wt/tg}$ brain homogenate or after co-injection of ASC and synthetic Aβ, as well as in the positive control image. The exemplary positive control image is a microscopic image of a mouse from an *APP/PS1*$^{wt/tg}$ genotype clearly showing two AD-typical Aβ plaques. Plaques differ in terms of size and distribution of the Aβ signals from the signals developing in *wildtype* animals. All right hemispheres have been sham-injected with carrier solution, which did not induce spreading of amyloid signals. Negative control images a brain slice having been treated with secondary antibody only. Images captured on an Olympus light microscope with a 20x objective.

6.3 Amyloid β Signals After Intrahippocampal Injection of Brain Homogenate or Synthetic Peptides in *APP/PS1$^{wt/tg}$* Animals

Intrahippocampal injections were also performed on mice from an *APP/PS1$^{wt/tg}$* genetic background. The experimental groups consisted of 3 mice per injected substance having received identical substances as the *wildtype* animals: injection of brain homogenate from an *APP/PS1$^{wt/tg}$* mice, synthetic Aβ, recombinant ASC or co-injection of synthetic Aβ and ASC, all groups including sham-injections of respective carrier solutions in right brain hemispheres. Absolute numbers of *APP/PS1$^{wt/tg}$* mice per injection group are smaller with n = 3 than investigated injected groups of *wildtype* animals (approx. n = 8).

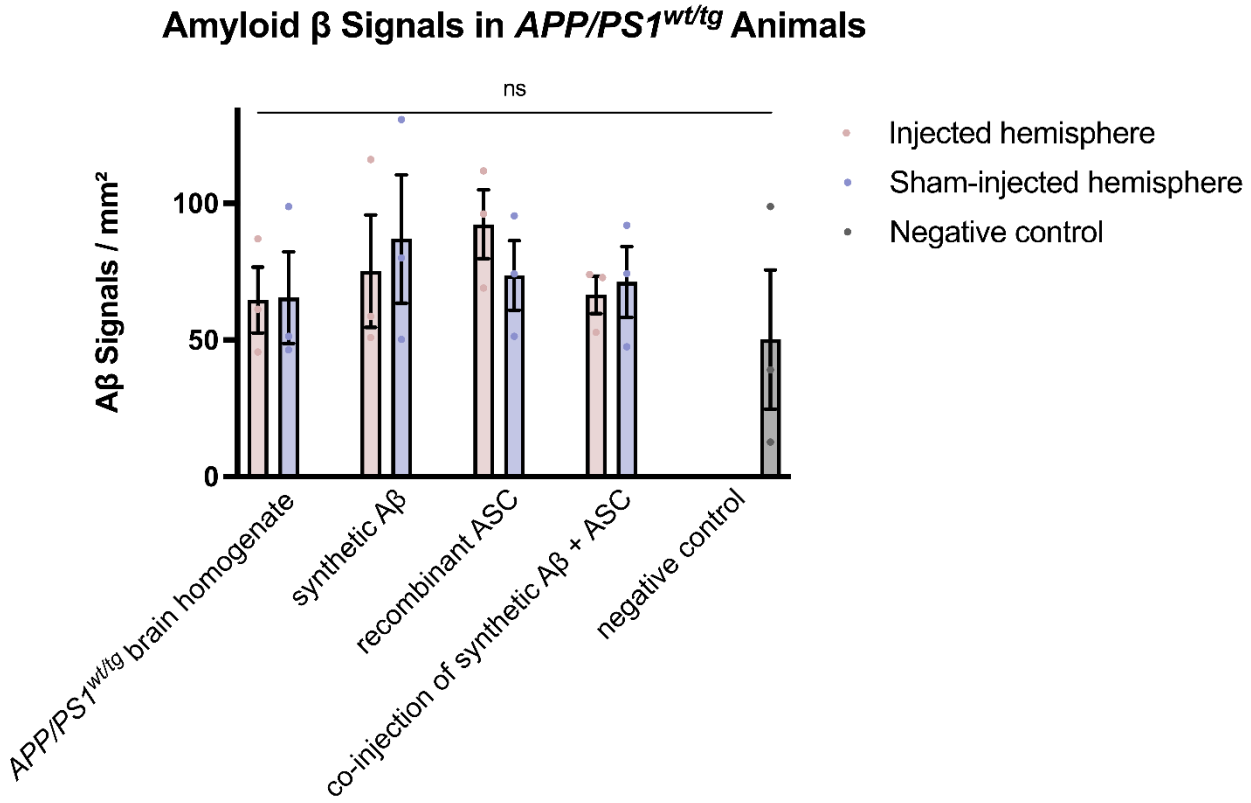

Fig. A3: Amyloid β Signals in *APP/PS1$^{wt/tg}$* Animals. Total quantification of Aβ signals after intrahippocampal injection of *APP/PS1$^{wt/tg}$* brain homogenate (n = 3), synthetic Aβ (n = 3), recombinant ASC (n = 3) or co-injection of synthetic Aβ and ASC (n = 3) into *APP/PS1$^{wt/tg}$* animals. The left hemispheres of each animal (rose bars) have been injected with one of the above-mentioned solutions, whereas right hemispheres (lavender bars) have been sham-injected with vehicle only. Negative control (grey bar) includes immunohistochemical staining only with secondary antibody (n = 3). Each dot represents the mean absolute number of Aβ signals per ROI (0.145 mm^2) in one mouse. Independently of the injected or sham-injected substance, similar absolute numbers of Aβ signals can be detected, signifying the absence of any significant differences between the

groups. This was analysed applying two-way ANOVA with a Tukey post hoc test. Ns stands for not significant. Figure created with GraphPad Prism.

Quantitative image analyses did not result in significantly different amounts of Aβ signals between different injection groups. In n = 3 *APP/PS1*$^{wt/tg}$ homogenate-injected hemispheres 64.6 ± 12.2 Aβ signals/mm² (mean ± SEM) were detected. Hippocampal hemispheres injected with synthetic Aβ (n = 3) showed 75.2 ± 20.6 Aβ signals/mm² (mean ± SEM) and the injection of recombinant ASC (n = 3) resulted in 92.3 ± 12.5 Aβ signals/mm² (mean ± SEM). In n = 3 Aβ/ASC co-injected hemispheres 66.5 ± 6.8 Aβ signals/mm² (mean ± SEM) were found (Fig. A3). All sham-injected hemispheres lead to similar numbers of Aβ signals, wherefore the values were summarized: in a total of n = 12 sham-injected right brain hemispheres 74.0 ± 7.7 Aβ signals/mm² (mean ± SEM) were detected. Negative control groups were treated with secondary antibody only and in n = 3 probes 50.2 ± 25.5 Aβ or rather background signals/mm² (mean ± SEM) were detected. Due to the small number of mice per injection group, the mouse-individual values per group and accordingly the SEMs differ substantially.

Ordinary one-way ANOVA performed between differently injected brain hemispheres and their respective sham-injected hemisphere did not lead to significant differences concerning the absolute number of Aβ signals. The group having received an intrahippocampal injection of *APP/PS1*$^{wt/tg}$ brain homogenate states no significant difference with a p value of p = 0.8535 as compared to the sham-injected and negative control hemispheres. Neither injections of synthetic Aβ (p = 0.5544) nor of recombinant ASC (p = 0.3212) result in Aβ signals significantly varying from Aβ signals depicted in respective sham-injected or negative control hemispheres. Quantity of Aβ signals visualized in hemispheres after co-injection of ASC and synthetic Aβ are similar (p = 0.6723) to signals after respective sham-injection or to negative control images (Tab A2).

Tab. A2: Ordinary One-way ANOVA of the Different Injection Groups in *APP/PS1$^{wt/tg}$* Animals in Contrast to Respective Sham-injections. Comparisons between the injected and respective sham-injected hemispheres as well as between negative controls do not reveal significant differences between any groups with p values ranging from p = 0.3212 up to p = 0.8353. Ns stands for not significant. Statistics computed with GraphPad Prism.

Ordinary one-way ANOVA			**Ordinary one-way ANOVA**	
APP/PS1$^{wt/tg}$ animal injected with *APP/PS1$^{wt/tg}$* brain homogenate, sham-injection and negative control			*APP/PS1$^{wt/tg}$* animal injected with synthetic Aβ, sham-injection and negative control	
ANOVA summary			ANOVA summary	
F	0.1854		F	0.652
P value	0.8353		P value	0.5544
P value summary	ns		P value summary	ns
Significant diff. among means (P < 0.05)?	no		Significant diff. among means (P < 0.05)?	no
R squared	0.05821		R squared	0.1785
Ordinary one-way ANOVA			**Ordinary one-way ANOVA**	
APP/PS1$^{wt/tg}$ animal injected with recombinant ASC, sham-injection and negative control			*APP/PS1$^{wt/tg}$* animal injected with synthetic Aβ and ASC, sham-injection and negative control	
ANOVA summary			ANOVA summary	
F	1.38		F	0.4246
P value	0.3212		P value	0.6723
P value summary	ns		P value summary	ns
Significant diff. among means (P < 0.05)?	no		Significant diff. among means (P < 0.05)?	no
R squared	0.3151		R squared	0.124

Multiple comparisons between all verum-injected hemispheres with the groups having been injected with a different verum in Tukey's test reveal no significant differences between the injection groups. Comparing an injection with *APP/PS1$^{wt/tg}$* brain homogenate to an injection with synthetic Aβ, recombinant ASC or to a co-injection of synthetic Aβ and ASC similar absolute numbers of Aβ signals result in all groups with p values of p = 0.9626, p = 0.6039 and p = 0.9998, respectively. Likewise, co-injection of synthetic Aβ and ASC compared to injections of synthetic Aβ or recombinant ASC alone measure no significant differences with p values of p = 0.9787 and p = 0.6555. Aβ signals found in hemispheres having been injected with synthetic Aβ are nearly alike (p = 0.8651) with signals developed after injection with recombinant ASC (Tab. A3).

Tab. A3: Tukey's Multiple Comparisons Test Between the Differently Verum-injected Hemispheres in *APP/PS1$^{wt/tg}$* Animals. All verum-injected hemispheres develop similar absolute numbers of Aβ signals, since no significant differences can be revealed after comparing all injection groups to each other. P values range from p = 0.6039 up to p = 0.9998. Ns stands for not significant. Statistics computed with GraphPad Prism.

Tukey's multiple Comparisons Test	Below threshold?	Summary	Adjusted p value
injected hemispheres			
APP/PS1$^{wt/tg}$ brain homogenate vs. synthetic Aβ	no	ns	0.9626
APP/PS1$^{wt/tg}$ brain homogenate vs. recombinant ASC	no	ns	0.6039
APP/PS1$^{wt/tg}$ brain homogenate vs. co-injection of synthetic Aβ + ASC	no	ns	0.9998
synthetic Aβ vs. recombinant ASC	no	ns	0.8651
synthetic Aβ vs. co-injection of synthetic Aβ + ASC	no	ns	0.9787
recombinant ASC vs. co-injection of synthetic Aβ + ASC	no	ns	0.6555

6.4 Co-localization of Microglia and Amyloid Plaques

The appearance and morphology of microglial cells varies depending on their state of activation. Once the brain-resident innate immune system is activated, microglia move around towards the loci of inflammation. The development of an amyloid plaque is a typical neuroinflammatory reaction in AD and comprises the presence of microglial cells (cf. 1.5 Microglia). In immunohistochemical stainings of *APP/PS1$^{wt/tg}$* mice showing Aβ plaques, microglia are localised in close proximity to the plaque.

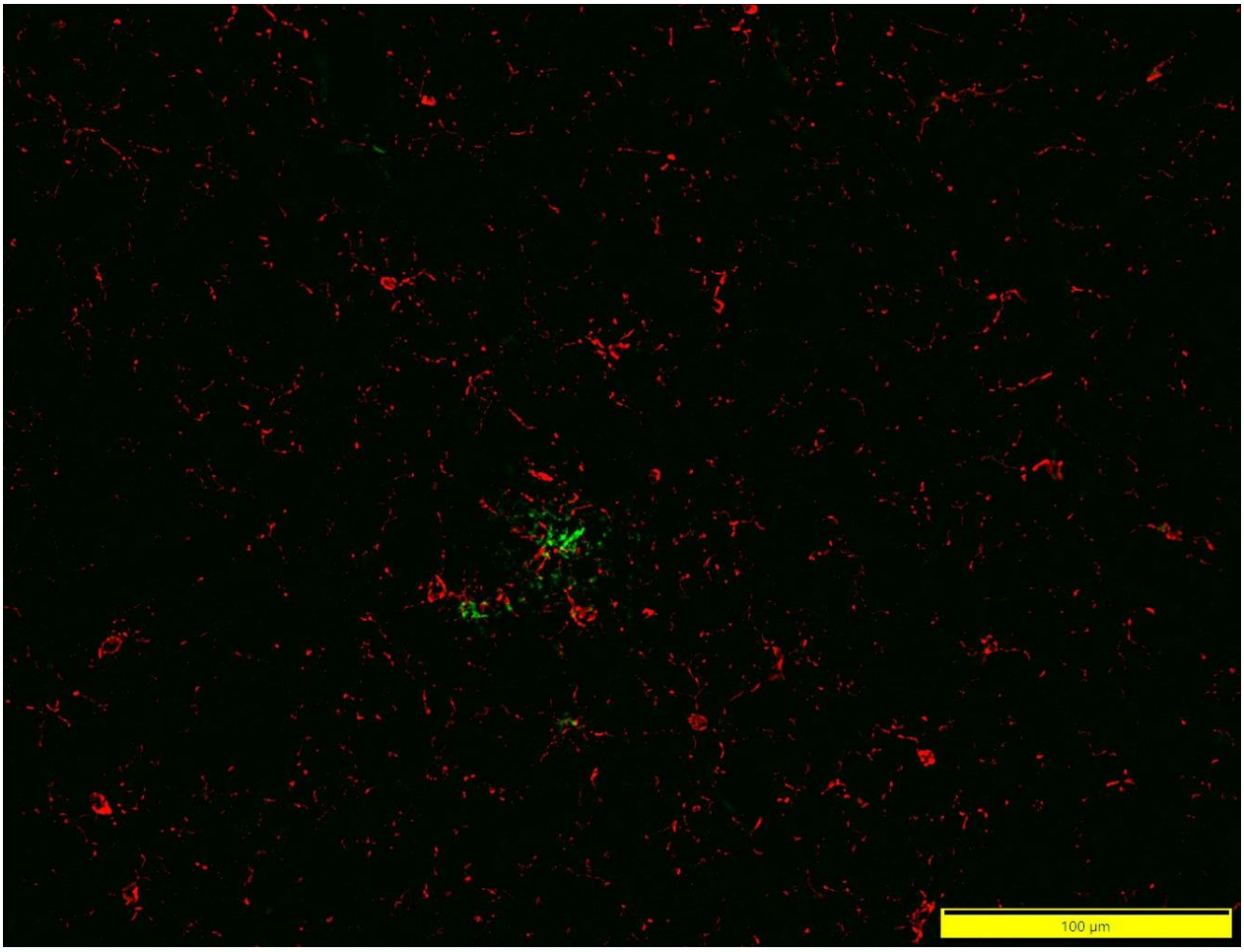

Fig. A4: Microglial Cells in Close Proximity to an Amyloid β Plaque. Microscopic image of an *APP/PS1*$^{wt/tg}$ mouse expressing Aβ plaques (6E10, green). Microglia (Iba-1, red) are co-localized with the β-amyloid, visible clearly as 3 innate immune cells are directly attached to the plaque with several more microglia in the immediate surrounding. Their morphology seems to have reached ameboid state with a convoluting morphology and short branches. Image captured on an Olympus light microscope with a 20x objective.

7. List of Figures

8. List of Tables

9. References

Abcam. 2023a. DAPI Staining Solution. Verfügbar unter https://www.abcam.com/en-lu/products/assay-kits/dapi-staining-solution-ab228549#datasheet (Zugriffsdatum: 23.09.2023)

Abcam. 2023b. Methoxy-X04, amyloid beta fluorescent marker. Verfügbar unter https://www.abcam.com/en-lu/products/biochemicals/methoxy-x04-amyloid-beta-fluorescent-marker-ab142818#datasheet (Zugriffsdatum: 23.09.2023)

BioLegend. 2021. Purified anti-β-Amyloid, 1-16 Antibody. Verfügbar unter https://www.biolegend.com/en-us/products/purified-anti-beta-amyloid-1-16-antibody-11228?GroupID=BLG15648 (Zugriffsdatum: 23.09.2023)

Bio-Rad. 2023. Protocol: Immunoprecipitation with SureBeads Protein A/G Magnetic Beads. Verfügbar unter https://www.bio-rad-antibodies.com/immunoprecipitation-surebeads-protocol.html (Zugriffsdatum: 30.05.2022)

Braak B. Neuropathological stageing of Alzheimer-related changes. Acta Neuropathologica 1991; 82: 239–259

Braak H, Thal DR, Ghebremedhin E, Del Tredici K. Stages of the pathologic process in Alzheimer disease: age categories from 1 to 100 years. Journal of neuropathology and experimental neurology 2011; 70: 960–969

Castro-Gomez S, Binder J, Heneka MT. Neuroinflammation als Motor der Alzheimer-Erkrankung. Der Nervenarzt 2019; 90: 898–906

Chen Y-J, Nguyen HM, Maezawa I, Jin L-W, Wulff H. A microglial marker - Anti Iba1 antibody series. Annals of clinical and translational neurology 2018; 5: 147–161

Dickson JR, Yoon H, Frosch MP, Hyman BT. Cytoplasmic Mislocalization of RNA Polymerase II Subunit RPB1 in Alzheimer Disease Is Linked to Pathologic Tau. Journal of neuropathology and experimental neurology 2021; 80: 530–540

Friker LL, Scheiblich H, Hochheiser IV, Brinkschulte R, Riedel D, Latz E, Geyer M, Heneka MT. β-Amyloid Clustering around ASC Fibrils Boosts Its Toxicity in Microglia. Cell reports 2020; 30: 3743-3754.e6

Fusco R, Siracusa R, Genovese T, Cuzzocrea S, Di Paola R. Focus on the Role of NLRP3 Inflammasome in Diseases. International Journal of Molecular Sciences 2020; 21: 4223

Gallego Villarejo L, Bachmann L, Marks D, Brachthäuser M, Geidies A, Müller T. Role of Intracellular Amyloid β as Pathway Modulator, Biomarker, and Therapy Target. International Journal of Molecular Sciences 2022; 23: 4656

Hall JE. States of Brain Activity—Sleep, Brain Waves, Epilepsy, Psychoses - The Nervous System: C. Motor and Integrative Neurophysiology - Guyton and Hall Textbook of Medical Physiology: Elsevier Health Sciences 2016

Hampel H, Hardy J, Blennow K, Chen C, Perry G, Kim SH, Villemagne VL, Aisen P, Vendruscolo M, Iwatsubo T, Masters CL, Cho M, Lannfelt L, Cummings JL, Vergallo A. The Amyloid-β Pathway in Alzheimer's Disease. Mol Psychiatry 2021; 26: 5481–5503

Han C, Yang Y, Guan Q, Zhang X, Shen H, Sheng Y, Wang J, Zhou X, Li W, Guo L, Jiao Q. New mechanism of nerve injury in Alzheimer's disease: β-amyloid-induced neuronal pyroptosis. Journal of cellular and molecular medicine 2020; 24: 8078–8090

Heneka MT, Carson MJ, Khoury JE, Landreth GE, Brosseron F, Feinstein DL, Jacobs AH, Wyss-Coray T, Vitorica J, Ransohoff RM, Herrup K, Frautschy SA, Finsen B, Brown GC, Verkhratsky A, Yamanaka K, Koistinaho J, Latz E, Halle A, Petzold GC, Town T, Morgan D, Shinohara ML, Perry VH, Holmes C, Bazan NG, Brooks DJ, Hunot S, Joseph B, Deigendesch N, Garaschuk O, Boddeke E, Dinarello CA, Breitner JC, Cole GM, Golenbock DT, Kummer MP. Neuroinflammation in Alzheimer's disease. The Lancet Neurology 2015; 14: 388–405

Hochheiser IV, Behrmann H, Hagelueken G, Rodríguez-Alcázar JF, Kopp A, Latz E, Behrmann E, Geyer M. Directionality of PYD filament growth determined by the transition of NLRP3 nucleation seeds to ASC elongation. Science Advances 2022; 8: eabn7583

Huang L-K, Chao S-P, Hu C-J. Clinical trials of new drugs for Alzheimer disease. Journal of biomedical science 2020; 27: 18

Ising C, Venegas C, Zhang S, Scheiblich H, Schmidt SV, Vieira-Saecker A, Schwartz S, Albasset S, McManus RM, Tejera D, Griep A, Santarelli F, Brosseron F, Opitz S, Stunden J, Merten M, Kayed R, Golenbock DT, Blum D, Latz E, Buée L, Heneka MT. NLRP3 inflammasome activation drives tau pathology. Nature 2019; 575: 669–673

Kelley N, Jeltema D, Duan Y, He Y. The NLRP3 Inflammasome: An Overview of Mechanisms of Activation and Regulation. International Journal of Molecular Sciences 2019; 20: 3328

Koenig LN, Day GS, Salter A, Keefe S, Marple LM, Long J, LaMontagne P, Massoumzadeh P, Snider BJ, Kanthamneni M, Raji CA, Ghoshal N, Gordon BA, Miller-Thomas M, Morris JC, Shimony JS, Benzinger TLS. Select Atrophied Regions in Alzheimer disease (SARA): An improved volumetric model for identifying Alzheimer disease dementia. NeuroImage. Clinical 2020; 26: 102248

Labzin LI, Heneka MT, Latz E. Innate Immunity and Neurodegeneration. Annual review of medicine 2018; 69: 437–449

Long JM, Holtzman DM. Alzheimer Disease: An Update on Pathobiology and Treatment Strategies. Cell 2019; 179: 312–339

Manabe T, Rácz I, Schwartz S, Oberle L, Santarelli F, Emmrich JV, Neher JJ, Heneka MT. Systemic inflammation induced the delayed reduction of excitatory synapses in the CA3 during ageing. Journal of Neurochemistry 2021; 159: 525–542

Marzesco A-M, Flötenmeyer M, Bühler A, Obermüller U, Staufenbiel M, Jucker M, Baumann F. Highly potent intracellular membrane-associated Aβ seeds. Scientific reports 2016; 6: 28125

Paxinos G, Franklin KBJ. The mouse brain in stereotaxic coordinates. London: Academic Press 2013

Pini L, Pievani M, Bocchetta M, Altomare D, Bosco P, Cavedo E, Galluzzi S, Marizzoni M, Frisoni GB. Brain atrophy in Alzheimer's Disease and aging. Ageing research reviews 2016; 30: 25–48

Prakash P, Jethava KP, Korte N, Izquierdo P, Favuzzi E, Rose IVL, Guttenplan KA, Manchanda P, Dutta S, Rochet J-C, Fishell G, Liddelow SA, Attwell D, Chopra G. Monitoring phagocytic uptake of amyloid β into glial cell lysosomes in real time. Chemical Science 2021; 12: 10901–10918

Ravichandran KA, Heneka MT. Inflammasome activation in neurodegenerative diseases. Essays in biochemistry 2021; 65: 885–904

Ravichandran KA, Heneka MT. Inflammasome and neurodegenerative diseases. In: Ravichandran KA, Heneka MT, Hrsg. Inflammasome Biology: Elsevier, 2023: 291–326

Reitz C, Mayeux R. Alzheimer disease: epidemiology, diagnostic criteria, risk factors and biomarkers. Biochemical Pharmacology 2014; 88: 640–651

Ryman DC, Acosta-Baena N, Aisen PS, Bird T, Danek A, Fox NC, Goate A, Frommelt P, Ghetti B, Langbaum JBS, Lopera F, Martins R, Masters CL, Mayeux RP, McDade E,

Moreno S, Reiman EM, Ringman JM, Salloway S, Schofield PR, Sperling R, Tariot PN, Xiong C, Morris JC, Bateman RJ. Symptom onset in autosomal dominant Alzheimer disease: a systematic review and meta-analysis. Neurology 2014; 83: 253–260

Sahillioglu AC, Sumbul F, Ozoren N, Haliloglu T. Structural and dynamics aspects of ASC speck assembly. Structure (London, England : 1993) 2014; 22: 1722–1734

Sarlus H, Heneka MT. Microglia in Alzheimer's disease. The Journal of clinical investigation 2017; 127: 3240–3249

Shao B-Z, Xu Z-Q, Han B-Z, Su D-F, Liu C. NLRP3 inflammasome and its inhibitors: a review. Frontiers in Pharmacology 2015; 6: 262

Soria Lopez JA, González HM, Léger GC. Alzheimer's disease. Handbook of Clinical Neurology: Elsevier 2019; 231–255

Tejera D, Mercan D, Sanchez-Caro JM, Hanan M, Greenberg D, Soreq H, Latz E, Golenbock D, Heneka MT. Systemic inflammation impairs microglial Aβ clearance through NLRP3 inflammasome. The EMBO journal 2019; 38: e101064

The Jackson Laboratory. 2022. B6.Cg-Tg(APPswe,PSEN1dE9)85Dbo/Mmjax. Verfügbar unter https://www.jax.org/strain/005864 (Zugriffsdatum: 24.09.2023)

van Dyck CH, Swanson CJ, Aisen P, Bateman RJ, Chen C, Gee M, Kanekiyo M, Li D, Reyderman L, Cohen S, Froelich L, Katayama S, Sabbagh M, Vellas B, Watson D, Dhadda S, Irizarry M, Kramer LD, Iwatsubo T. Lecanemab in Early Alzheimer's Disease. The New England journal of medicine 2023; 388: 9–21

Venegas C, Kumar S, Franklin BS, Dierkes T, Brinkschulte R, Tejera D, Vieira-Saecker A, Schwartz S, Santarelli F, Kummer MP, Griep A, Gelpi E, Beilharz M, Riedel D, Golenbock DT, Geyer M, Walter J, Latz E, Heneka MT. Microglia-derived ASC specks cross-seed amyloid-β in Alzheimer's disease. Nature 2017; 552: 355–361

Vogel JW, Young AL, Oxtoby NP, Smith R, Ossenkoppele R, Strandberg OT, La Joie R, Aksman LM, Grothe MJ, Iturria-Medina Y, Pontecorvo MJ, Devous MD, Rabinovici GD, Alexander DC, Lyoo CH, Evans AC, Hansson O. Four distinct trajectories of tau deposition identified in Alzheimer's disease. Nature medicine 2021; 27: 871–881

Ye L, Rasmussen J, Kaeser SA, Marzesco A-M, Obermüller U, Mahler J, Schelle J, Odenthal J, Krüger C, Fritschi SK, Walker LC, Staufenbiel M, Baumann F, Jucker M. Aβ seeding potency peaks in the early stages of cerebral β-amyloidosis. EMBO reports 2017; 18: 1536–1544

10. Acknowledgments

I would like to thank my supervisor Prof Michael Heneka for his supervision and continued support with the project. I would furthermore like to thank PD Dr Ildiko Racz and Stephanie Schwartz for providing help during the experiments in the laboratory in Bonn. Many thanks are also owed to Dr Arnaud Mary and Adrien Rauh for their support and time enabling my final week of experiments in Luxembourg. Lastly, I would like to thank my boyfriend Max and especially my father for proofreading the thesis and also my mother, sister, grandparents and friends for constantly encouraging me to further advance the project.